Theoretical investigation of the interaction of a polymer film with a nanoparticle

Dissertation

zur Erlangung des Grades
„Doktor der Naturwissenschaften“

am Fachbereich Physik
der Johannes Gutenberg-Universität in Mainz

vorgelegt von

Juan G. Díaz Ochoa

geboren in Bogotá

Mainz 2005

Abstract

The fundamental aim in our investigation of the interaction of a polymer film with a nanoparticle is the extraction of information on the dynamics of the liquid using a single tracking particle. In this work two theoretical methods were used: one passive, where the motion of the particle measures the dynamics of the liquid, one active, where perturbations in the system are introduced through the particle. In the first part of this investigation a thin polymeric film on a substrate is studied using molecular dynamics simulations. The polymer is modeled via a *bead spring* model. The particle is spheric and non structured and is able to interact with the monomers via a Lennard Jones potential. The system is micro-canonical and simulations were performed for average temperatures between the glass transition temperature T_g of the film and its dewetting temperature.

It is shown that the stability of the nanoparticle on the polymer film in the absence of gravity depends strongly on the form of the chosen interaction potential between nanoparticle and polymer. The relative position of the tracking particle to the liquid vapor interface of the polymer film shows the glass transition of the latter. The velocity correlation function and the mean square displacement of the particle has shown that it is caged when the temperature is close to the glass transition temperature T_g. The analysis of the dynamics at long times shows the coupling of the nanoparticle to the center of mass of the polymer chains. The use of the Stokes-Einstein formula, which relates the diffusion coefficient to the viscosity, permits to use the nanoparticle as a probe for the determination of the bulk viscosity of the melt, the so called 'microrheology'. It is shown that for low frequencies the result obtained using microrheology coincides with the results of the Rouse model applied to the polymer dynamics.

In the second part of this investigation the equations of Linear Hydrodynamics are solved for a nanoparticle oscillating above the film. It is shown that compressible liquids have mechanical response to external perturbations induced with the nanoparticle. These solutions show strong velocity and pressure profiles of the liquid near the interface, as well as a mechanical response of the liquid-vapor interface. The results obtained with this calculations can be employed for the interpretation of experimental results of non contact AFM microscopy.

Zusammenfassung

In dieser Arbeit wird die Wechselwirkung zwischen einem Polymerfilm und einem Nanoteilchen untersucht. Die grundlegende Idee dabei ist, Information über die Dynamik der Flüssigkeit mittels der Information über die Dynamik des Teilchens zu bekommen. Zwei Untersuchungsmethoden sind benutzt worden: eine sogenannte passive Methode, bei der die Bewegung des Teilchens die Dynamik der Monomere im Film misst, und eine aktive, bei der kleine Störungen in der Flüssigkeit durch das Teilchen bewirkt werden.

In diesen Untersuchungen eines Polymerfilms auf einem Substrat wird mit Molekulardynamik-Methoden simuliert. Das Polymer wird mit dem sogenannten '*bead spring*' Modell dargestellt. Das Teilchen ist nicht strukturiert und wechselwirkt mit der Monomeren durch ein Lennard-Jones-Potential. Das System ist mikrokanonisch und die Simulationen werden ohne Schwerkraft im Temperaturbereich zwischen Glasübergangstemperatur und der Verdampfungstemperatur durchgeführt.

Die Ergebnisse dieser Untersuchungen zeigen, dass die Stabilität des Teilchens in der Flüssigkeit von der Form des Wechselwirkungspotentials abhängt. Die Position des Nanoteilchens bezüglich der Grenzfläche des Films zeigt den Glasübergang der Grenzfläche. Die Geschwindigkeitskorrelationsfunktion und das Mittlere Verschiebungsquadrat zeigen für Temperaturen in der Nähe des Glasübergangs, dass es einen Käfigeffekt für das Teilchen gibt. Die Ergebnisse dieser Untersuchungen zeigen also, dass die Bewegung des Teilchens an die Bewegung der Polymerschwerpunkte gekoppelt ist. Durch die Stokes-Einstein-Gleichung, die eine Verbindung zwischen dem Diffusionskoeffizient und der Viskosität herstellt, ist es möglich, Information über die Viskosität der Flüssigkeit mit Hilfe des Nanoteilchens zu erhalten. Diese Methode wird 'Mikrorheologie' genannt. Die Ergebnisse zeigen, dass nur für kleine Frequenzen die Mikrorheologie mit dem Rouse-Modell übereinstimmt.

Im zweiten Teil dieser Arbeit sind die Gleichungen der linearisierten Hydrodynamik für das System eines Nanoteilchens mit kleiner Oszillation auf einem flüssigen Film gelöst worden. Die Ergebnisse zeigen, dass nur kompressible Flüssigkeiten eine mechanische Antwort zeigen. In diesem Fall sind der Druck und das Geschwindigkeitsprofil in der Nähe der Grenzfläche größer als innerhalb des Films. Die Grenzfläche zeigt also eine mechanische Antwort. Die Ergebnisse aus diesen Rechnungen können für die Interpretation experimenteller Ergebnisse aus der Rasterkraftmikroskopie benutzt werden.

Contents

Nomenclature

Definitions	**Meaning**
LJ	Designation for Lennard Jones potential
$FENE$	Designation for Finite Extendable non Elastic potential
PCA	Predictor Corrector Algorithm
NVE	Ensemble with constant number of particles, volume and energy
NVT	Ensemble with constant number of particles, volume and temperature
VV	Velocity Verlet algorithm
MD	Molecular dynamics
MC	Monte Carlo
RGA	Recoil growth algorithm
FCF	Force correlation function
MCT	Mode coupling theory
NS	Navier Stokes equations
VCF	Velocity correlation function
MSD	Mean square displacement
FT	Fourier transform

Symbol	**Meaning**
k_B	Boltzmann constant
ε_{ij}	Interaction particle-particle
ε_{pi}	Interaction nanoparticle-fluid
σ	Collision parameter of LJ potentials
r	Separation particle-particle
R_0	Radius of the hard core of the particle
R_{eff}	Effective Radius of the particle
R_l	Thickness of the liquid layer on the nanoparticle
$H = \epsilon_H$	Hammaker constant (chapter 2)
k	Parameter of the FENE potential
μ_{coex}	Coexistence chemical potential
q_i	Elements of the covariant coordinate system
Vol	Volume.
N_p	Number of particles in the melt
N	Number of monomers in the chain
$X_p(t)$	Rouse modes
A_1	Exponent of the polynomial fit for MSD
$\Psi(t)$	Designation of the function for VCF
Δr^2	Designation of the function for MSD

$D(t)$	Diffusion coefficient
G^*	Complex shear modulus
$G\prime$	Real part of the complex shear modulus (Elasticity)
$G"$	Complex part of the complex shear modulus (Loss modulus)
$\phi\prime(\omega)$	Real part of the FT of the velocity
$\phi"(\omega)$	Complex part of the FT of VCF
$H_0 = H_{0\Gamma}$	Thickness of the film in equilibrium
$H_\Gamma(r,t)$	Thickness of the film
$\delta H_\Gamma(r,t)$	Small oscillation of the film thickness
$\overline{H_0}$	Perturbation amplitude of the interaction potential of the nanoparticle
$\left\{v^r, v^\theta, v^z\right\}$	Components of the velocity fields in cylindrical coordinates
v_Γ^i	Velocity of the interface projected on i axis
S_Γ	Curvature of the interface
γ_Γ	Surface tension
$\Pr(t,r,z)$	Function of the pressure
$f_m(t)$	Temporal function of the velocity on r axis
$g_m(t)$	Temporal function of the velocity on z axis
$A_m(t)$	Temporal function of the pressure
$f_m^D(t)$	Temporal function of the velocity in the vapor phase on r axis
$g_m^D(t)$	Temporal function of the velocity in vapor phase on z axis
$A_m^D(t)$	Temporal function of the pressure in vapor phase
$J_m(r)$	Bessel function of order m
$\phi(r,z,t)$	External potential
$H_\nu(r,m)$	Hankel transformation of $\overline{H_0}(r,m)$
K_η	Bulk modulus
K_ξ	Shear modulus
C_T	Isothermal bulk modulus in the liquid
C_T^D	Isothermal bulk modulus in the vapor phase
B_{nm}	Expansion coefficients of the potential of the particle in the liquid phase

List of Figures

1 Introduction

1.1 Brownian motion in nanoscales

One hundred years ago Einstein presented his three seminal papers about the photoelectric effect, the theory of relativity and the Brownian motion. These three papers appear as three problems on different scales[2]. At first glance, there is no relation between these papers, but in a sense all of these three works are in a profound way interconnected. The first one sets the limit of the Maxwell equations and shows the quantum nature of light; the second was basically motivated by a research for alternatives to the equations of Maxwell and their relation with the concept of ether, giving as principal result a new dynamics[1] and the third is an investigation on the connection between the atomistic dynamics of liquids and the motion of mesoscopic particles. This last work shows no apparent connection with the other two; but the statistical nature of this phenomenon, where Einstein's interpretation as collisions between the particle and the liquid particles is a fundamental element of this theory, shows Einstein's deep interest in statistical physics and has opened the way to a wide application of stochastic ideas in physics in different scales, even in the quantum regime;[2] therefore the quantum phenomena can also be viewed as stochastic phenomena. The meaning of Brownian motion extends not only to the theoretical, but also the practical fields and its concepts permeate other neighboring disciplines. The concepts derived from the theory about Brownian motion do not only explain fundamental phenomena in small space scales (and intermediary and long time scales), but also help to understand the emergence of complex phenomena in systems with many simple constituents.

One important part of the present work is devoted to the understanding of Brownian motion in nanoscales and in presence of a complex fluid; therefore the following questions are addressed: What is the difference between classical Brownian motion and the dynamics of a single nanoparticle? Which information of the fluid can be obtained by making an analysis of the dynamics of this nanoparticle? From this last question, the nanoparticle can be called as a "tracking particle" or alternatively as a "nanoprobe" (and in a short definition as a probe).

[1] therefore the research on the nature of light was the starting point for the formulation of both works

[2] A kind of unification of both works was developed in recent years, by means a stochastic formulation of quantum theory is proposed; in the former case the quantum description of a particle is derived by modifying the classical description solely by the addition of a universal Brownian motion, which satisfies certain properties [7].

As was mentioned previously, the milestone of the Brownian motion is the concept of thermal fluctuations, which can be classified in soft matter as $k_BT \simeq 1$ (in hard matter as $k_BT \to 0$), where the energy scale of the system is based on the intrinsic energy scale ($k_BT = 1$). Such fluctuations can be represented, from the point of view of the kinetic theory, as small particles colliding with a tracking particle in suspension. From the theory of statistical mechanics, the dynamics of the particle is represented as the equilibrium between a diffusion and a drift current; in this case some aspects of the dynamics of the fluctuations are independent of the intrinsic details of the dynamic of the microscopic processes, implying that the measurements are made in a time scale where all of such processes are uncorrelated. As a main result an expression which connects two mean microscopical equations is obtained: the Stokes equation, which describes overdamped fluids, and the diffusion equation, $D = \frac{k_BT}{\varsigma}$, where ς is a friction coefficient. The meaning of this equation (which was of revolutionary character) is the connection of the macroscopic with the microscopic phenomena through the Boltzmann constant; such relation was later developed in the so called Green-Kubo relations for other transport coefficients (for example viscosity in liquids). In the present case, it is possible to measure the diffusion coefficient by making an analysis of the displacement of the particle, the so called self diffusion constant. On the other hand, each polymer chain also diffuses in the polymer liquid; the fundamental question is in this case: if the particle has a size equivalent to the gyration radius of a single polymer chain,[3] is there some relation between the self diffusion constant of a single big nanoparticle and the diffusion of the particles in the fluid?

The previous theory is also the starting point for the so called "microrheology", which consists in the use of a nanoparticle, called again tracking particle, that can be used as a non invasive technique for the measurement of transport coefficients by making an analysis of its Brownian motion. The advantage of this technique is, for example, the possibility to use it in measurements "*in vivo*" of biological materials. This technique has been used in experimental situations for the measurement of the complex shear modulus in polymeric networks, for example actin, where entanglement of the polymer chains is observed. In this work the question is, if this technique can be used in dense polymer melts, in the Rouse regime (see fig. 1.1) and adsorbed on a substrate, for the measurement of local bulk viscosity.

For short and intermediary time scales it is unclear if the so called anomalous diffusion is found, when the fluid is a complex one with long spatial and temporal correlations; in this sense the tracking particle is also a sensor, of the complex character of the fluid. For high fluid densities and temperatures near the glass transition temperature T_g, it is quite evident that in intermediate times, after a short ballistic regime, that the particle is trapped locally in a cage that prevents the normal diffusion of the probe. The relaxation time required for the particle to leave the cage, the time where the system reorganizes, is the so called α relaxation

[3]The gyration radius is defined via the second central moment of the mass distribution of the molecule

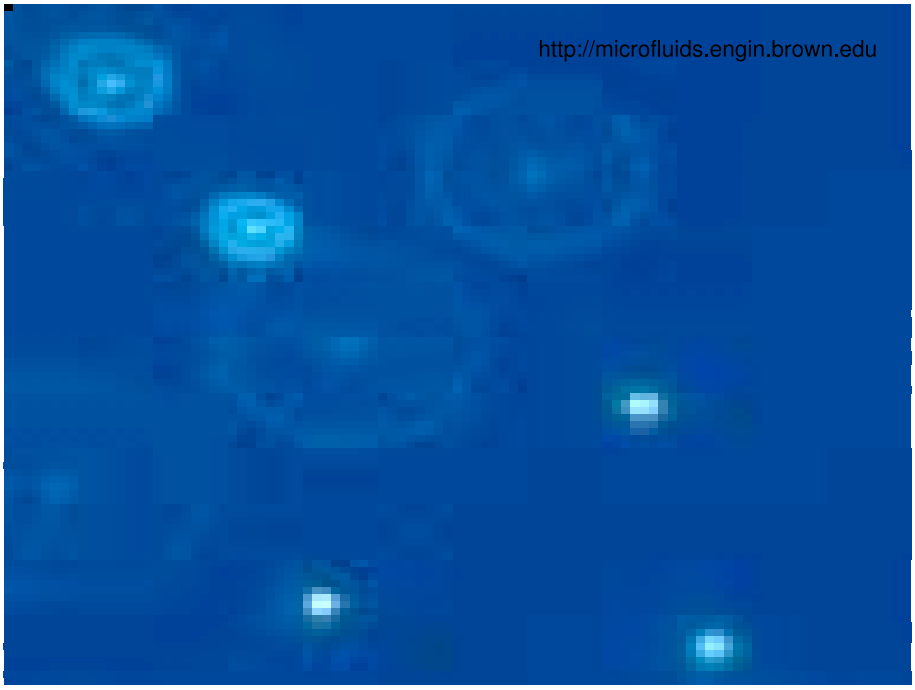

Figure 1.1: In this image a nanoparticle in a complex liquid is shown using confocal microscopy. The information about the displacement of tracking particles is related to the complex shear modulus of the liquid [8].

time. The recognition and measurement of this dynamics is also a relevant part of this work, where the dynamics of the single tracking particle is connected with the dynamics of single monomers as well as the center of mass of the chains. The fundamental idea is to test if the nanoparticle can act also as a sensor for the dynamics of the single monomers and polymer chains.

The definition of a fluid film has a particular meaning for this work: this is the confrontation of the dynamics of the single nanoparticle not only to the dynamics of the particles in the fluid but also to the dynamics of the liquid-vapor interface. The main question is: is there a remarkable influence of the free interface on the glass transition of the film? In order to answer this question the distribution of the nanoparticle will be used as a test of the state of the interface; in this sense the dynamics of the interface and the "wettability" of the particle are two main information sources that allow to find an answer to this question. The interface has not only an influence on the statics but also on the dynamics of the nanoparticle; this object is a fluctuating manifold associated with different modes of oscillation, the so called capillary waves. So, it is relevant to ask: is there some influence of the interface, and its dynamics, on the dynamics of the nanoprobe?

Regarding the simulation technique, this simple formulation of a single particle in a liquid is an alternative for conventional simulation problems, where the perturbation is introduced in the fluid using an additional wall in order to obtain information

of the transport as well as the dynamics of the fluid. Due to the novelty of this system some technical aspects are important to be considered: the definition of the interaction potential of the particle with the fluid, the correct simulation protocol and the selection of the algorithm.

1.2 Force spectroscopy and beyond

It was shown that the nanoparticle can be used as a probe for the polymeric fluid and its interface. What happen if a force is applied through the nanoparticle, when it is situated at the interface? This question is motivated experimentally by Atomic Force Microscopy (AFM); in which case a small particle, called tip of the AFM, is attached to a cantilever and approaches to the surface of the liquid. If the tip is in contact with the surface of the liquid film, the so called tipping mode, it is possible either to measure the thermal fluctuations of the liquid or to introduce a force on the liquid and then, observe the response by the deflection of the cantilever. A diagram of this technique is shown in fig. 1.2.

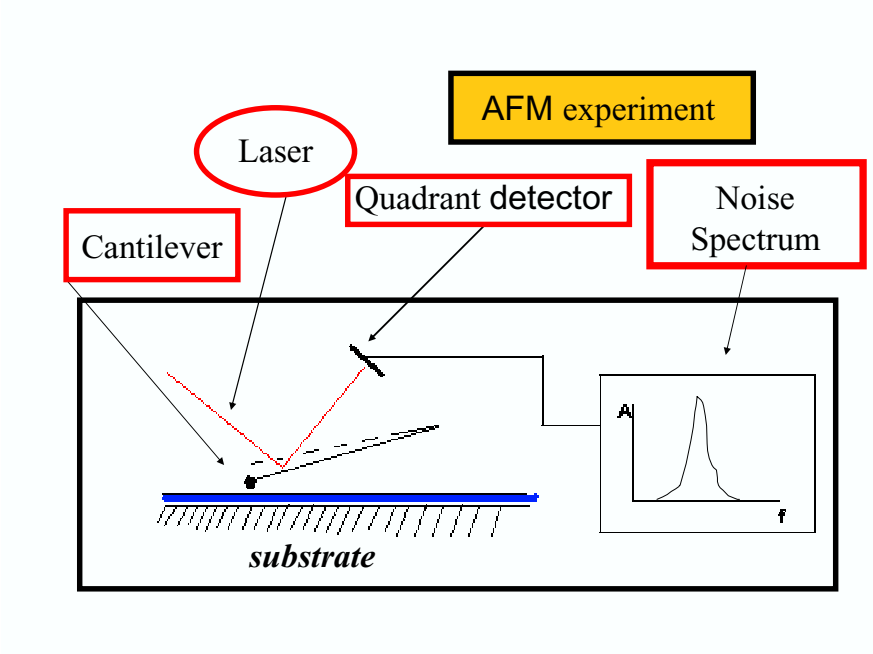

Figure 1.2: Diagram showing the main elements of an AFM. An small tip is attached to a cantilever and interacts with the particles in the vicinity. The forces on the tip provoke a deflection in the cantilever; this deflection is detected with a LASER and processed.

This work is performed under the supposition that the fluid can be described using the Navier Stokes (NS) equations. Then it is possible to ask: how is the response of a liquid when a single LJ particle (without cantilever) introduces a perturbation?

In order to answer this question it will be supposed that the liquid is at rest; the liquid can be simple as well as complex, i.e. has a complex time dependent relaxation module. This last supposition implies that the liquid has memory effects; this means that the liquid does not loss information of its initial conditions. The NS equations will be solved for incompressible fluids, i.e. the density remains always constant, as well as for compressible ones.

The understanding of this kind of systems can be useful for the solution of a variety of problems in different technological branches and in general, due to its typical lenght scale in the nanometer range, could have implications in nanotechnology, which is called a global technological promise.[4]

One example is the storage of information on surfaces of melts near the glass transition. The AFM information storage technology utilises the application of force on a polymer melt through a tip of an AFM in order to form a "hole" on the surface which represents a bit of information.[5] This hole-information can be read with an array of AFMs, and the information can be easily erased and stored by repetition of this procedure. The advantage of this alternative technology is that the information can be stored and erased very quickly and is not sensible to magnetic fields in contrast to conventional technologies.[6] For such kind of systems the comprehension of phenomena of the liquid-vapor interface is of reveled importance in order to understand the stability of the hole and its dynamics dependending on the temperature of the system.[7] Another possible aplication of the results of this investigation is the comprehension of the dynamics of the signaling in biofilms (For a short report see [3] and [4]); this information could carried serious consequences in healt (sterilization of surfaces) and industry (for example corrosion).

Another example is related to the construction of nanomachines. A nanobuoy (a tracking particle can be also considered as a nanobuoy) is one of the simplest kind of those machines. Actually many researchers try to construct nanoboats and nanosubmarines that are able to swim, and eventually to be directed, applied for example to the delivery of some drug into a specific target in the human or animal organism. The design of those nanorobots implies the knowledge of the environment where they habit. For this reason, to obtain information from computer simulations of the tracking particle is fundamental for the design of optimal nanorobots; further developments require the use of computer simulations of nanorobots in nanoscales that resemble the macroscopic counterparts, with nanogears and complex nanome-

[4]See for example "Nanotech promise for global poor", BBC News, 11 April, 2005. [5]

[5]An electric current flowing through the tip increases its temperature and therefore the temperature of the melt. Thereafter it is possible to form a tiny hole with the same tip, taking care to leave the melt to reach again the glass transition temperature. Each hole represents a bit of information; a big amount of information of course is represented by an array of holes

[6]For a complete review of this technique see [1]

[7]Then we must switch off the particle (for example by making its potential equal zero) and follow the hole (no particle position), for example using the nearest particles from the no-particle. On the oder hand this procedure shows the possibility to produce this holes on the melt using free colloidal particles; so, the presence of a colloid on the interface corresponds to a bit of information.

chanical parts. [6]

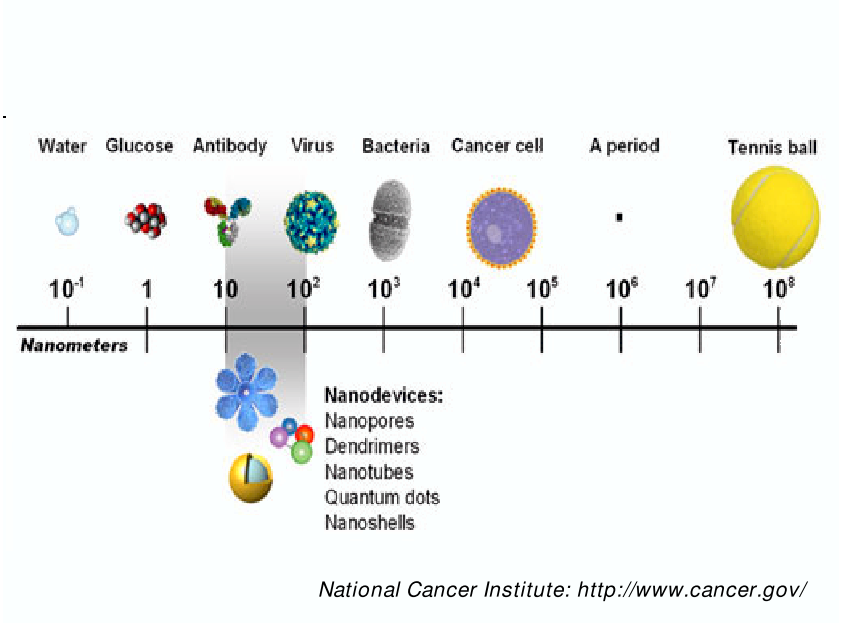

Figure 1.3: Comparison of different objects in nanoscales (National Institute of Cancer, USA).

1.3 Organization of the work

This work contains four chapters, that explain the results obtained by means of the computer simulations and a fifth chapter dedicated to analytical calculations.

In Chapter two an explanation about the technical details of computer simulations is given. In particular, the aspects taken into account for the selection of the potential of the particle are analyzed. Chapter three is dedicated to the discussion of the statics of the tracking particle and its relation to the glass transition of the melt, with special emphasis on the glass transition at the interface of the film. In chapter four the dynamics of the particle in the melt, and its coupling with the dynamics of the fluid particles, is analyzed. Finally, in chapter five the NS equations are solved for a liquid thin film in the presence of a nanoparticle, defined as a LJ particle, for both simple and complex liquids, considering incompressible as well as compressible liquids.

In appendix A a discussion about the influence of the interface on the dynamics of the nanoparticle is made. Appendix B pressents a discussion about the diffusion constant in bulk and in films at $T \sim T_g$. In appendix C an alternative method for the computation of the shear modulus is shown. In appendix D a short explanation about Rouse modes is given. These first four appendices are concerned to the simulations. The next set of appendix are for the analytical solutions of the NS

equations. In appendix E the formulation of the Navier Stokes equations is made and in appendix F different differential operators in cylindrical coordinates are explained. In appendix G an alternative potential is developed in order to facilitate the Bessel-Fourier-Bessel transformation of the external potential. In appendix H the solutions of the NS equations for incompressible fluids are shown. In appendix I a conversion table of some constants is shown and in appendix J the solution of the NS equations for complex liquids in frequency domain is done.

2 Discussion of technical details

2.1 Introduction

The aim of this work is to understand the dynamics of a single probe particle in a complex fluid using a Molecular Dynamics (MD) method. In the present section the problems related with this simulation, the selection of the algorithms and potentials for the modeling of the polymer chains and substrate are discussed. As starting ansatz the interaction potential between probe particle and liquid will be defined as a LJ one; but such definition carries out many problems related to the stability of the nanoparticle at the interface of the fluid film (stable or metastable vertical distribution of the nanoparticle); for this reason an alternative definition for such potential is proposed in order to improve the vertical distribution of the nanoparticle in the liquid.

This chapter is divided in three parts. In the first part the choice of algorithm and the method of iteration is discussed. In the second part the potentials for the interaction monomer-monomer, chain-chain and monomer-substrate, are introduced; thereafter the problems that a single LJ potential presents for the description of the probe particle are shown and it is discussed, why in this simulation one is forced to define an alternative potential for the probe particle. Finally the simulation protocol is commented as well as the problems and the details of the construction of the present simulation.

2.2 Algorithm

2.2.1 Selection of the algorithm

The description of the dynamics of a dense polymeric melt and the particle can be modeled using for example Monte Carlo (MC) [26], Lattice Boltzmann Gas or Molecular Dynamics. Monte Carlo methods consider only configuration space and eliminate the momentum in the phase space; for such reason it is valid for the modeling of systems in thermodynamical equilibrium, although dynamical processes can be analyzed in different equilibrium states. The main problem of the system tracking particle-polymer melt is that it is a complex system with a complex relaxation behavior inside the liquid as well as at the interface of the film, where the particle is able to couple it to capillary waves [83]. Only after very long times the system can reach an equilibrium state. In the present project it is necessary to extract information of short as well as long time scales, because each time scale contains

fundamental information of many dynamical processes; for this reason it is necessary to use a method (different to MC) that can take account those different time regimes.

One alternative simulation method (that can represent many time regimes) is the Lattice Boltzmann gas (or lattice gas automata)[79]. In this method identical particles hop from site to site on a regular lattice, obeying simple scattering rules. Such method is for example very useful for the modeling of liquids, where the conservation rules represent the basic conservation of momentum in the Navier Stokes equations. But such method represent interaction of simple particles and is not accurate for the modeling of connected particles [1]. This method can alternatively be applied together with other simulation methods (Molecular Dynamics for example) for the modeling of polymers in presence of solvents, where the solvent is represented by the cellular gas automata [28]. In the present project a polymer melt is represented and, for this reason, this method is not a reasonable alternative. The use of Molecular Dynamics method (MD) avoids some of this problems; more over an additional feature is the possibility to obtain complete information of the velocities and forces of the particles in the system, very important for the analysis of the present system.

Molecular Dynamics acts in the continuum, in contrast to lattice methods. It is computationally demanding but permits to modelate the dynamics of each particle because it is based on the iterative integration of the Newton equations (see for example [13] and [20] for an extensive explanation of the MD method), defined as

$$m\frac{d\overrightarrow{r}_i}{dt} = \overrightarrow{F}_i = \sum_{j_{j\neq i}=1}^{N} \overrightarrow{f}_{ij} + \left(\overrightarrow{f}_i\right)_{ext}, \tag{2.1}$$

where $\overrightarrow{f}_{ij}$ are forces derived from pair potentials. In this way the information about the forces, velocities and positions for each particle is obtained. In this project a routine which is based on a predictor-corrector algorithm of fifth order is used[14].

In the simulation protocol for the present project it is necessary, first to make NVT simulations, in order to generate initial configurations, and thereafter to make NVE simulations in order to simulate a microcanonical system, where the liquid acts as a thermostat of the tracking particle. The first step can be easily implemented using the so called Predictor-Corrector algorithm (PCA), where an stochastic thermostat is implemented in order to get a constant temperature for the system, whereas for the second step the implementation of a velocity Verlet algorithm is necessary in order to conserve time symmetry: the first step in the protocol, with the stochastic thermostat, represents the integration of a Langevin equation

$$m\frac{dv_i}{dt} = \gamma v_i + f \tag{2.2}$$

with f is the stochastic force, whereas the second step in the protocol represent the

[1] In last years some attempt was made in order to model polymers using gas automata; see for example [29]

integration of the Newton equations. This means, from the first to the second step the thermostat is switched off.

One possible solution is to apply the same algorithm for the computation of both kind of equations, say the PCA. But the main problem of PCA for NVE simulations is that it can produce a drift in the energy for long times, because the computed trajectories do not conserve the volume in the phase space; more over MD is based on the integration of the Newton's equations, which are reversible, and for PCA the time symmetry of the fundamental equations is broken. [2] On the other side, the Velocity Verlet (VV) algorithm produces trajectories that are related to constant volume elements in the phase space. An agreement must be found between both methods.

In the following section a discussion about, how the predictor-corrector algorithm of second order is equivalent to the Velocity-Verlet algorithm, is made.

2.2.2 Predictor corrector of second order as velocity Verlet

In molecular dynamics the predictor-corrector and velocity Verlet are two common integration schemes for numerical solution of differential equations, in particular for the equations of motion [20]. The main idea of the PCA is to make an extrapolation of a polynomial fit: in a first step a position and velocity are predicted by extrapolation of a polynomial fit to the derivative from the previous points, which is called the predictor step, and thereafter this result is used for the interpolation of the derivative (corrector step). The use of the corrector part is necessary given that numerical instabilities can appear from the predictor step.

The algorithm selected in the integration routine is the predictor-corrector algorithm defined up to fifth order[14]. But energy drifts can appear with such algorithm for NVE simulations [20], [13], [23]; when the predictor-corrector is tuned into a second order algorithm then it is equivalent to the Velocity Verlet: this is the point where the agreement is found.

In this subsection a proof of the equivalence of the Predictor Corrector with the Velocity Verlet algorithm is done. The Velocity Verlet algorithm (VV) can be expressed as

$$\overrightarrow{p}_i(t + \frac{1}{2}\Delta t) = \overrightarrow{p}_i(t) + \frac{1}{2}\Delta t \overrightarrow{f}_i(t), \tag{2.3}$$

$$\overrightarrow{r}_i(t + \Delta t) = \overrightarrow{r}_i(t) + \Delta t \overrightarrow{p}_i(t)(t + \Delta t/2)/m_i. \tag{2.4}$$

In the first step the momentum is computed and thereafter the position is estimated. After this last step a force computation (using the new coordinates) is carried out. The main features of this algorithm are: it is exactly reversible, it is symplectic (i.e. volume in the phase space is conserved) and it requires only one extensive force evaluation per step.

[2] Only in the limit of infinitesimal time step this algorithm becomes time reversible [19].

It is necessary to proof that the PCA is equivalent, with some approximation, to the VV algorithm. The first one depends on the constants α_1 and α_2, which are coefficients of the Taylor expansion, in order to compute the corrected velocity using the predicted one. In many works there are extensive references about the value of the optimal constants in order to make the algorithm to converges. In the present case it is shown that, for $\alpha_1 = 1$ and $\alpha_2 = 1$, the PCA converge into an VV algorithm, where the corrected velocity after the integration step is the function of the velocity of the previous integration step, which is at the same time equivalent to the predicted velocity.

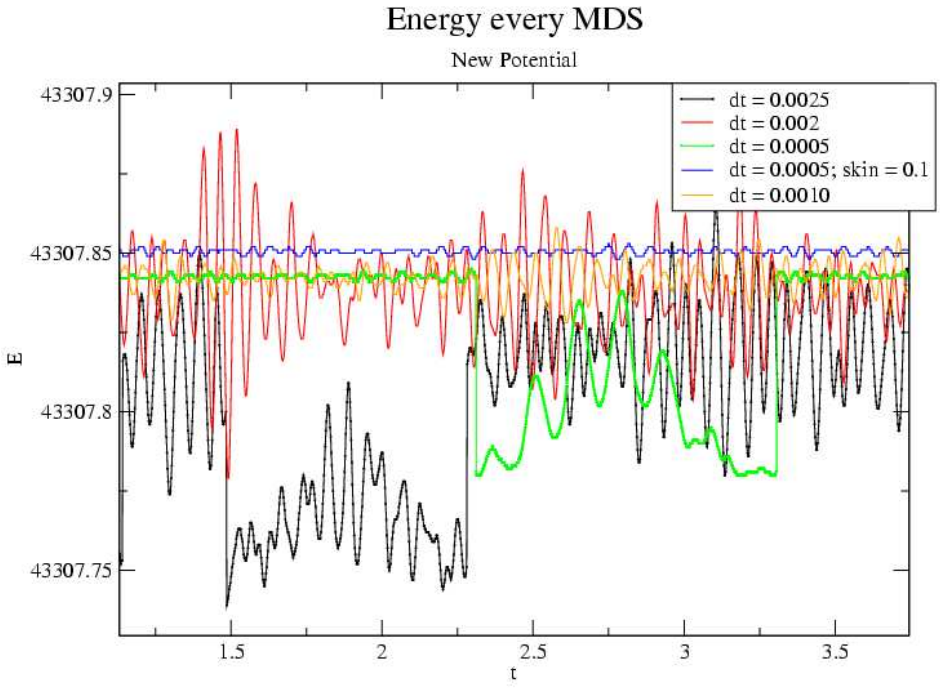

Figure 2.1: Energy and selection of the integration step. From this results it is obvious that $dt = 0.02$ is a stable integration step.

The predicted velocity in the predictor-corrector algorithm is given by

$$v^p(t + \Delta t) = v^p(t) + a(t)\Delta t. \tag{2.5}$$

Inserting the predicted part into the corrector part the following expression is obtained

$$
\begin{aligned}
v^c(t+\Delta t)\Delta t &= v^p(t+\Delta t)\Delta t + \alpha_1 \frac{\Delta \ddot{r}}{2}\Delta t^2 \\
&= v^p(t)\Delta t + a^p(t)\Delta t^2 + \alpha_1 \frac{a\prime^p(t+\Delta t) - a^p(t+\Delta t)}{2}\Delta t^2 \\
&= v^p(t)\Delta t + a^p(t)\Delta t^2 + \alpha_1 \frac{a\prime^p(t+\Delta t) - a^p(t)}{2}\Delta t^2, \qquad (2.6)
\end{aligned}
$$

where $a(t+\Delta t) = a(t)$. If $\alpha_1 = 1$ then

$$
v^c(t+\Delta t)\Delta t = v^p(t)\Delta t + \frac{1}{2}a^p(t)\Delta t^2 + \frac{1}{2}a\prime^p(t+\Delta t)\Delta t^2, \qquad (2.7)
$$

the last step in this demonstration consist to proof that the second coefficient must be equal to one; the corrected acceleration is given by

$$
\begin{aligned}
\frac{1}{2}a^c(t+\Delta t) &= a^p(t) + \alpha_2 \frac{a\prime^p(t+\Delta t) - a^p(t)}{2} \\
&= \frac{1}{2}a^p(t) + \alpha_2 \frac{1}{2}a\prime^p(t+\Delta t), \qquad (2.8)
\end{aligned}
$$

this implies, when $\alpha_2 = 1$ the algorithm coincides with the velocity- Verlet algorithm; in such case

$$
v^c(t+\Delta t)\Delta t = v^p(t)\Delta t + \frac{1}{2}a^c(t+\Delta t)\Delta t^2, \qquad (2.9)
$$

where for $\Delta t = 0$; $v^p(t) = v^c(t)$.

Although all the trajectories generated with this scheme are only approximate they do conserve a pseudo Hamiltonian, the so called "shadow Hamiltonian" [23], which differs from the true Hamiltonian by a true amount which vanishes when $\Delta t \to 0$ (integration step); so, no drift in the energy will occur (the system remains in a closed hypersurface in the phase space). In fig. 2.1 the total energy of the system is plotted using different integrations steps. From this plot it is evident that integration steps of 0.02 conserve the energy. This integration step is used for all the simulations in the present project.

2.3 The model

2.3.1 Potentials

The present model can be defined as the interplay of different Van der Waals potentials that describe the interaction between both the surface and the particles in the fluid and the interaction between the particles in the fluid. In fig. 2.1 a sketch with the main interactions and elements of the model is made. The Atomistic detail

is not of interest in the present work because it does not bring information about the essential physics, which is of interest to extract, involved in this problem and implies unnecessary use of computational power. The system that we simulate is moreover small enough and for this reason it does not experience effects related with the gravitational field.[3]. In the following section a description of the potentials, that will be used in our system, is made.

2.3.2 Selection of the potentials in the melt

The polymer chains are described by the bead-spring model, derived from the original model suggested by Kremer and Grest [17]. In this case the attractive part of the LJ potential can be included; without this the model would not have a liquid phase [18].

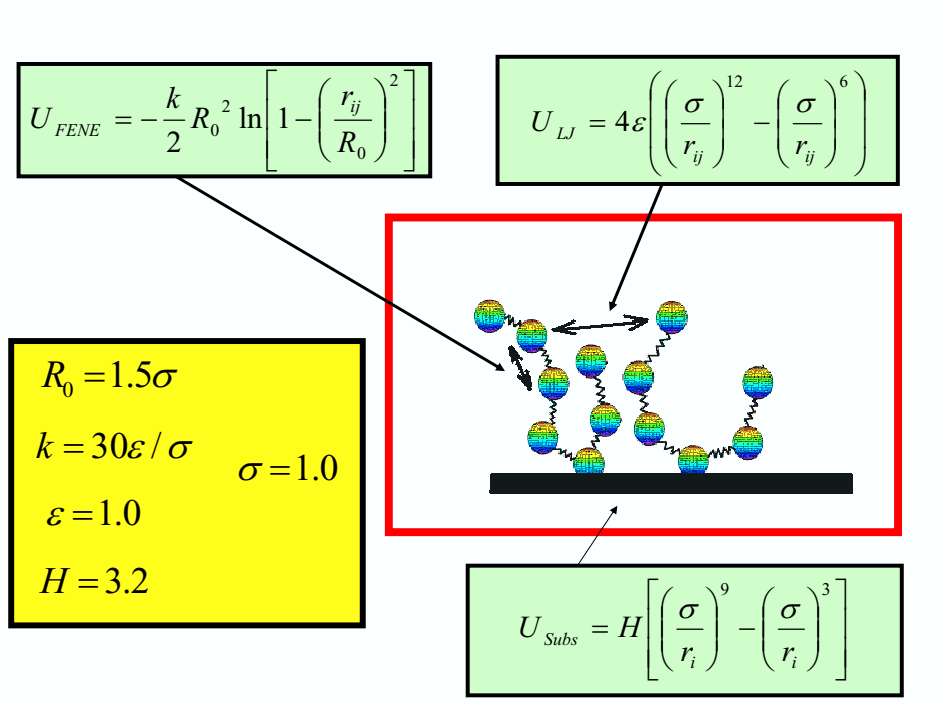

Figure 2.2: Sketch of the Bead spring model for the simulation of polymer melts adsorbed on substrates: each bead represents a monomer whose interaction with other monomers is given by a LJ potential; bond connectivity is modeled by a FENE potential. The interaction between the particles and the substrate is given by an integrated LJ potential.

[3]In a rigorous way the present computer experiments are related to experiments performed on orbit without influence of the gravitational field.

Each chain consists either of 10 or 50 monomers with mass $m = 1$ (in LJ units). A truncated LJ potential acts between the monomers and is given by

$$\Phi_{LJ}(r_i, r_j) = \begin{cases} 4\varepsilon \left(\left(\frac{\sigma}{r_{ij}}\right)^{12} - \left(\frac{\sigma}{r_{ij}}\right)^{6} \right) + \epsilon & \text{if } r_{ij} < 2(2)^{1/6}. \\ 0 & \text{otherwise} \end{cases} \tag{2.10}$$

where $\overrightarrow{r}_{ij} = (\overrightarrow{r}_i - \overrightarrow{r}_j)$, $\overrightarrow{r}_i$ and $\overrightarrow{r}_j$ being the position of two particles, σ is the collision parameter, or length scale parameter of the system, and ε is the strength of the interaction. Such potentials model interactions that are both soft and smooth.

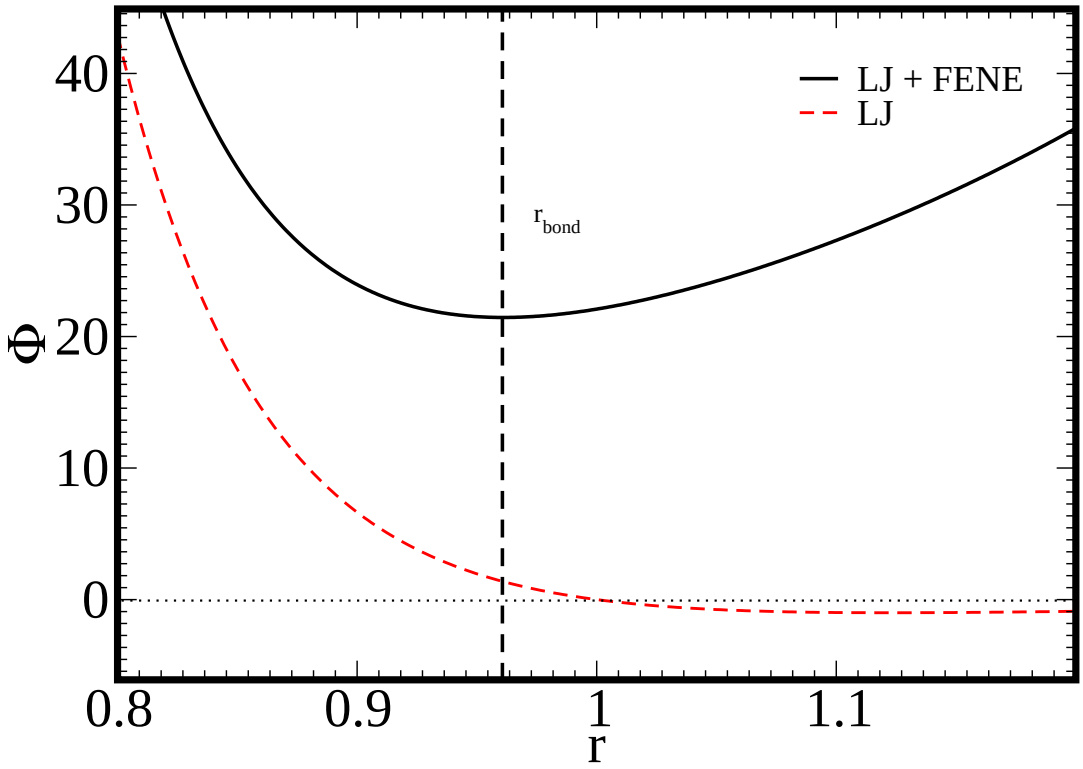

Figure 2.3: FENE and LJ potentials as a function of the distance. The LJ potential describes the interaction between monomers and the FENE potential describes the bond connectivity. The superposition of the LJ and FENE potentials defines the bond-length of the polymers, $r_{bond} = 0.9606$ (all the units are given as LJ ones). The minimum of the LJ potential is $r_{min} = 2^{1/6}$.

In addition to the previous potential a finitely extendable non linear elastic (FENE) backbone potential was applied along the chain (See fig. 2.3); this potential is given by

$$\Phi_{FENE}(r_{ij}) = -\frac{k}{2} R_0^2 \ln \left[1 - \left(\frac{r_{ij}}{R_0} \right)^2 \right], \tag{2.11}$$

in the simulations performed in this work $R_0 = 1.5\sigma$ and $k = \frac{30\varepsilon}{\sigma^2}$; the superposition of these potentials avoid high frequency modes and chain crossing. In fig. 2.3 the FENE potential is shown together with the LJ potential.

The FENE potential introduces an interaction length which is smaller than the length of the Lennard-Jones potential; in consequence, with this potential, together with the LJ potential, two incompatible length scales in the system are introduced.[4].

In this simulation more over a modified Lorentz-Berthelot mixing rule [14] was used, which defines the cross interaction between different kind of particles in the liquid, helping to make a differentiation between different particles. The cross interaction range and interaction strength are given by the following formula

$$\sigma^{ij} = \frac{\sigma^{ii} + \sigma^{ii}}{2}, \tag{2.12}$$

$$\varepsilon^{ij} = \sqrt{\varepsilon^{ii}\varepsilon^{jj}}. \tag{2.13}$$

In the simulations performed along this project there are three types of particles: fluid particles (which are represented as monomers), nanoparticle and the wall. For all the three particles the interaction range is one. For the probe particle the interaction strenght was $\varepsilon^{22} = 9$, i.e. for nanoparticle - nanoparticle interaction, and $\varepsilon^{ii}|_{i\neq 2} = 1$ for the rest of the particles.

2.3.3 Selection of the potential of the walls

The model used in the present simulations considers a flat and non structured walls. A wall can be modeled as closed packed lattices, with a LJ-atom sitting in each lattice point; the substrate as well as the superior wall can be modeled in an identical way [14]. In the present case each wall consists of a single lattice with a single LJ atom in its center; the simulation is performed in a periodic box, implying that this single lattice is repeated periodically.

The potential of the LJ atom is a Lennard Jones potential integrated on an infinite surface, the so called $9-3$ potential, which is given by the following expression

$$\phi_W(z_i) = H\left(\left(\frac{\sigma}{z_i}\right)^9 - \left(\frac{\sigma}{z_i}\right)^6\right), \tag{2.14}$$

where z_i is the height of a particle about the substrate.

The reference system in the present simulations is fixed at the substrate, which represent the laboratory system. The parameter ε_H plays the role of a Hamaker constant, which is the strength of the interaction of two particles separated by a vacuum.

[4]That avoids long range order at low temperatures [18]

The simulation of a nanoparticle-liquid film requires a substrate that strongly attracts the fluid in order to simulate a liquid that is able to wet the wall and form a homogeneous and stable film [16]. The selected constant was $H = 3.2$, i.e it represents a wall that strongly attracts the liquid (this constant is related to materials that are composed for example of gold [75]).

Is the presence of the upper wall necessary?. The main motivation of the present problem is to compute the interactions between an adsorbed film on a substrate -with a vapor interface- and a probe particle. In the step for the generation of initial configurations for the liquid film, the upper wall is necessary in order to compress the liquid up to the desired film thickness; but in the production step the upper wall could interact with the tracking particle and the liquid-vapor interface. For this reason in the production step the upper wall is either placed far away from the substrate or is completely switched off. An sketch of the model and the interactions between the particles is shown in fig. 2.2

The modeling of a particle in a film composed of a complex fluid must be defined, such that some uniform vertical distribution of the tracking particle is obtained. For this reason the definition of a particular potential describing the particle is necessary; this potential, together with a description of the different ansatz used for this model, will be discussed in the following section.

2.3.4 Interaction potential of the tracking particle

The interaction between the nanoparticle and the fluid particles is also modeled via a Lennard Jones potential[5]; in the integration routine it is allowed to make the simulation of melts with more than only one type of monomers. Using this fact, the proposed ansatz for the present simulation is that the nanoparticle is a single monomer of second class; that means, the probe particle is also a Lennard-Jones sphere, where the collision parameter represents the size of the particle. This kind of potentials leaves open the problem of the modeling of structured particles, for example clusters of particles[6].

In the first performed tests the particle flew away from the surface of the melt. In fig. 2.4 the vertical position of the nanoparticle is for two different temperatures, $T = 0.8$ and $T = 1.4$ shown; while for $T = 0.8$ the particle showed a stable position, for $T = 1.4$ the distance to the substrate grows. Similar results are obtained for different collision parameters. In particular from the plot of the force on the particle (fig. 2.5) it is posible to observe that the forces of the melt are coupled to the particle only at the beginning of the simulation; after $t = 4500$ the particle is only coupled

[5]There are many possible representations for the particle potential; for example for the simulation of AFM tips see [9]

[6]This kind of problems studied by A. Chatterji for structured particles that performs rotating Brownian motion [10]. As outlook an improvement of the present problem is possible by making a definition of structured particles defined as clusters of nanoparticles.

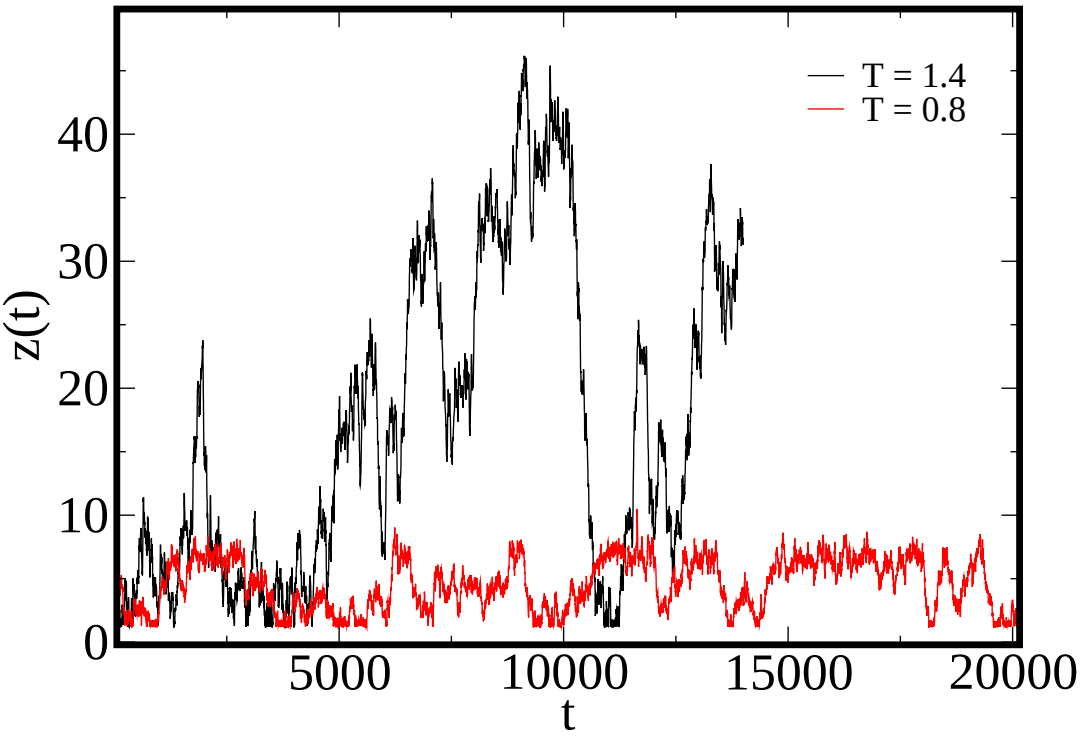

Figure 2.4: Vertical position of the particle for two constant temperatures, with $\sigma = 1.4$. For $T = 0.8$ the particle has a stable vertical position while for $T = 1.4$ the dynamics of the particle is only coupled to the thermostat, implying that the particle tends to move away from the surface of the melt.

to the thermostat. For few later times the particle is coupled again to the melt; the particle is coupled only to the thermostat. As consequence the particle has no stable trajectory near the melt; this result is not satisfactory because the temperatures where this simulation was performed are below the temperature where the liquid evaporates.

Additional NVE simulations for particles with $\sigma = 1.4$ were performed; in this case it is evident that the particles in the melt have no coupling to the probe particle; eventually, when the forces with the collisions of the neighbor particles exceed the coupling force between probe and liquid, it gets a free particle trajectory; therefore for $T = 1.4$ the particle has a pure ballistic regime: in fig. 2.6 the vertical position as well as the mean square displacement of the particle are represented; when this function is fitted with a function of the form t^x, and $x \sim 2.0$, then such regime is called ballistic, as in the present case. Only for $T \leq 0.8$ it is observed that the particle has a relative stability of its trajectory in the time window where the test was made. There a transition from a ballistic into a diffusive regime is observed suggesting that the particle is coupled to the dynamics of the melt (fig. 2.6).

The previous results show that there is a very weak coupling between melt and tracking LJ particle. Possibly for $T \leq 1.4$ the particle has a metastable state; this

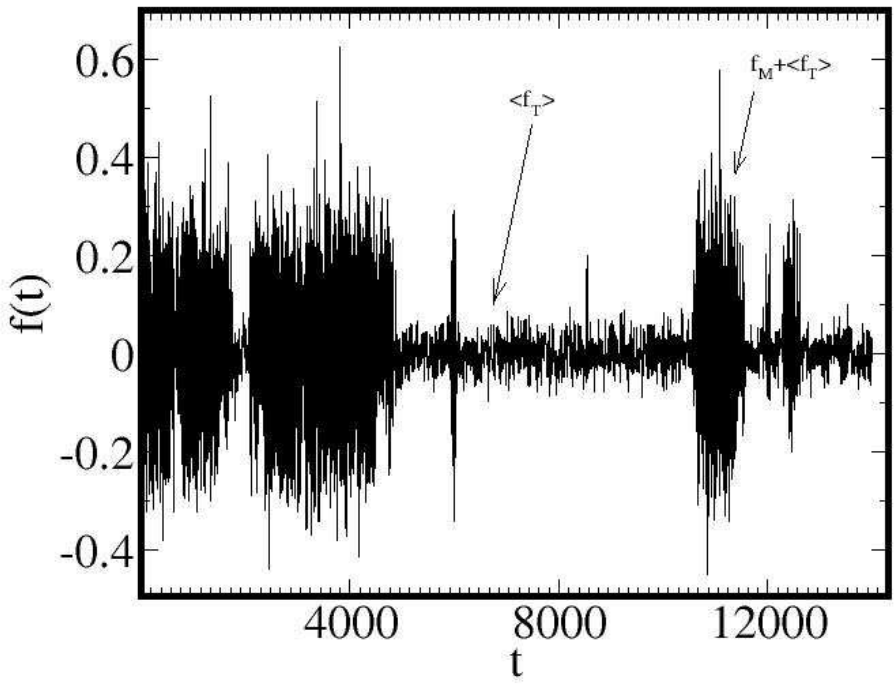

Figure 2.5: Force on the probe particle for $T = 1.4$. This plot shows that the particle has a transient coupling to the particles of the melt. After $t = 13000$ the only remaining force on the probe particle is the force of the thermostate $< f_T >$.

fact implies that the relative stability of the vertical position for $T = 0.8$ is due to the time scale where the observation is made, and possibly for later times the particle is able to get an escape velocity, even for low temperatures. That implies, it is possible to perform relative stable simulations for very small particles (near the size of a monomer) when the temperature is below to $T = 1.4$. This solution apparently represents a restriction in the value of the parameters allowed for the simulations; the main idea is to represent particles with sizes near or bigger than the typical size of the chains in the melt. For this reason new tests are necessary to proof stability of the vertical position of bigger particles for $T \leq 0.8$. For $\sigma = 3.0$ and $T = 0.8$ in a NVE simulation a similar situation in the trajectory of the particle is observed: after some simulation time t_d (a time where a decoupling of the particle to the dynamics of the melt is found) the force is equal to zero implying that the melt is no more the thermostate for the particle (fig. 2.7). Only for short times the particle has a transitory coupling to the fluid; after that, the particle follows a free particle trajectory with a constant escape velocity.

With a simple LJ potential, with large σ, the potential is repulsive for distances in the rage of the size of the nanoparticle. The coupling of the probe with the

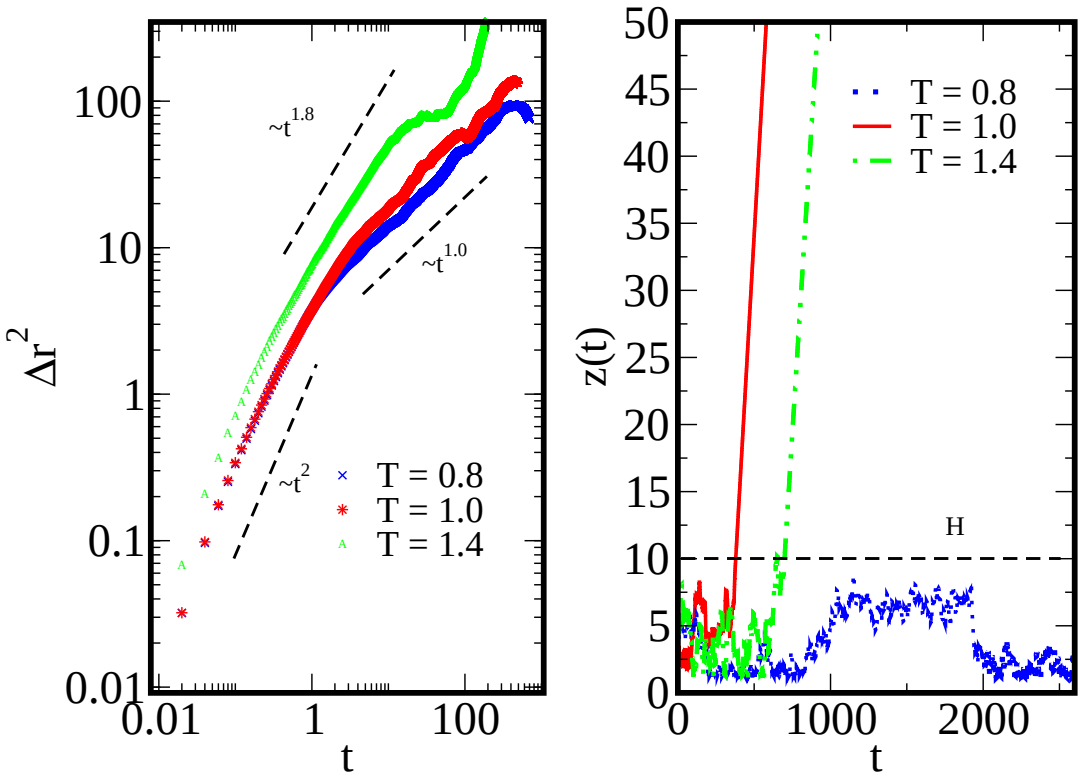

Figure 2.6: MSD and the vertical position of the particle as a function of the time for three different temperatures: $T = 0.8$, $T = 1.0$ and $T = 1.4$. The particle is represented as a LJ potential with radius $\sigma = 1.4$.The thermostat was switched off. In this simulations for $T = 1.0$ and $T = 1.4$ and after some simulation time the particle becomes a scape velocity and follow a free particle trajectory,whereas for $T = 0.8$ the particle has an apparent stable vertical position.

neighboring particles is therefore weak; if the particle obtains enough kinetic energy then for a given time the particle is able to get an escape velocity and follow a trajectory of a free particle. One possible solution is to make use of an integrated potential that could make that the particle attracts the surrounding particles in the fluid. But the use of a detailed potential is time consuming and very hard to implement [12].

The easiest option was to introduce a modification of the LJ potential, making it more attractive near the interface particle-liquid. The interaction potential of the tracking particle has the following form

$$\phi_{Coll}(r_i, r_j) = 4\varepsilon_{pm}\left(\left(\frac{\sigma_{coll}}{r_{ij} - R_o}\right)^{12} - \left(\frac{\sigma_{coll}}{r_{ij} - R_0}\right)^{6}\right) + \epsilon, \tag{2.15}$$

where R_0 is a shift on the distance and σ_{coll} is the particular length scale of the nanoparticle (see fig. 2.8). Its effective radius can be expressed as

$$R_{eff} = R_0 + \sigma_{coll}. \tag{2.16}$$

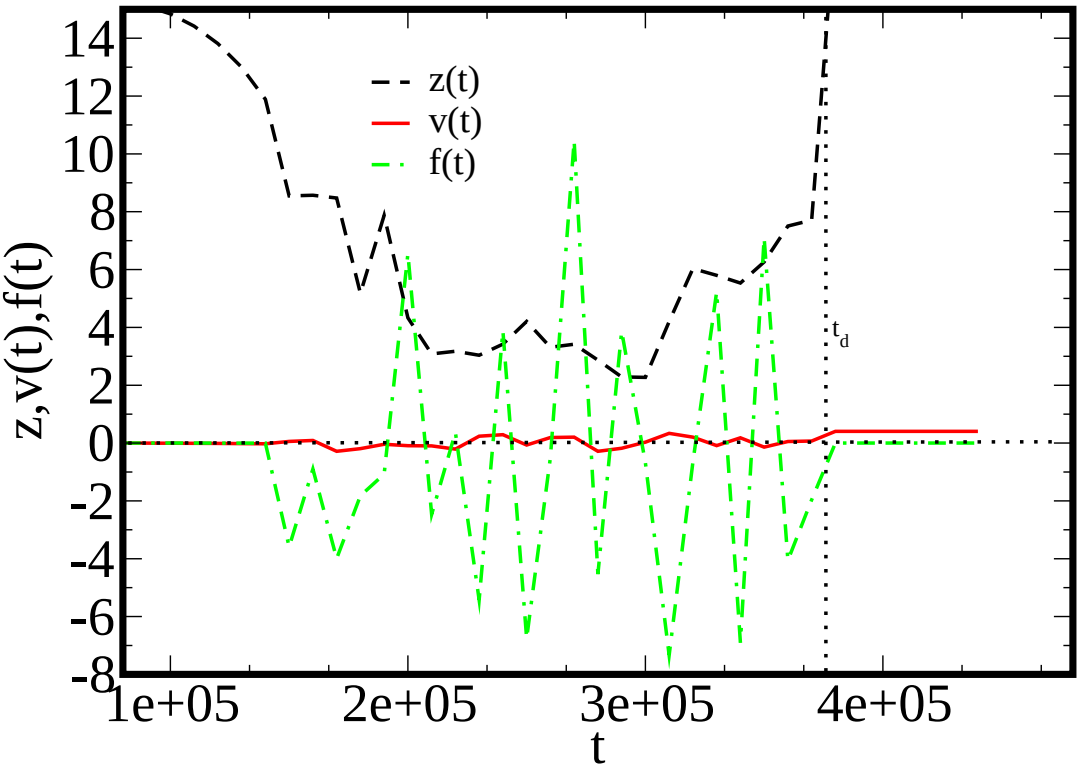

Figure 2.7: Results of NVE simulations for a tracking particle with a collision parameter $\sigma = 3.0$. Even for $T < 1.0$ the particle has no stable vertical position in the melt; after some time t_d the forces on the particle tend to be zero (suggesting that the particle is no more thermalized by the polymeric melt) the velocity is constant and the tracking particle follows a free particle trajectory.

In figure 2.8 the modified LJ potential is presented compared to a simple LJ potential. In the same plot a comparison between two modified LJ potentials with different parameters is done: one with $R_0 < \sigma$ and the other one with $R_0 \sim \sigma$. In the first one the parameters permits to improve attachment of the particles on the interface of the tracking particle by reducing the mobility of the liquid particles at the interface probe-liquid. This point will be explained later in the section about statics and in appendix A.

2.4 Simulation protocol

In the present work particles with effective radius $R_{eff} = 3.0, 4.0, 5.0$ were simulated; the interaction range was $\sigma_{coll} = 1.0$. the mass of the particle is $m = 25$ and the strength of the interaction between tracking particle and liquid particles is $\varepsilon = 3.0$. In a couple of simulations we tested only the effect of the size of the particle on its own dynamics.

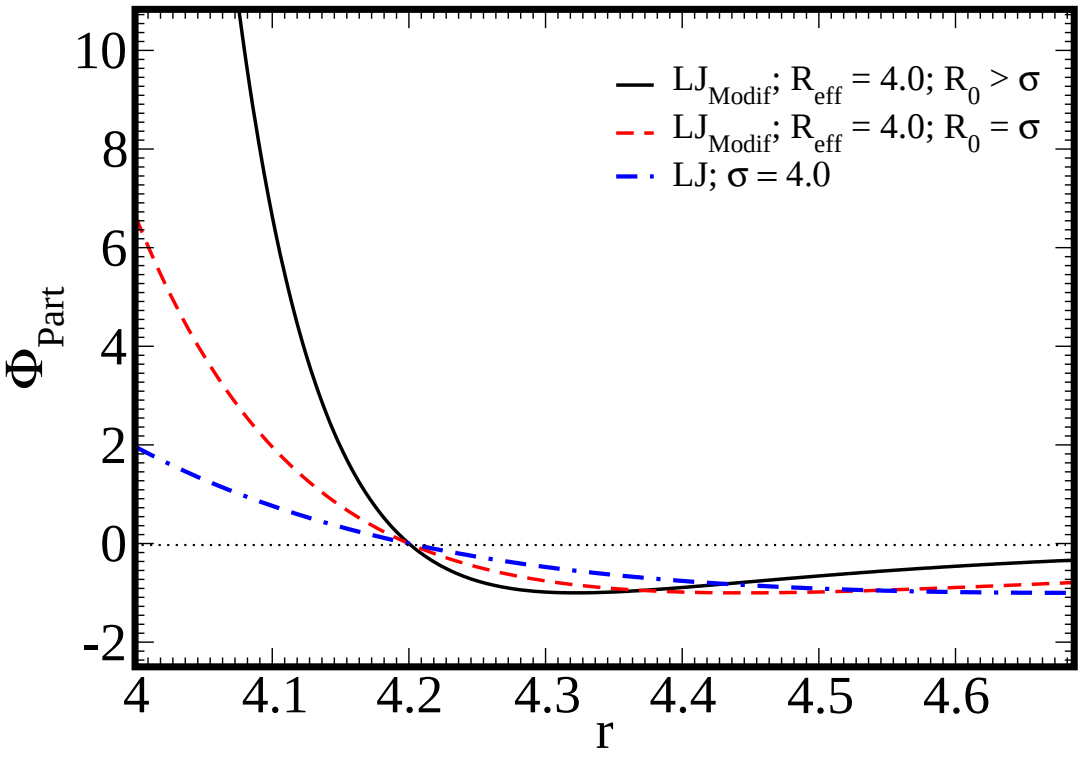

Figure 2.8: Comparison between a LJ potential with $\sigma = 4.0$ and two different potentials for the tracking particle, with radius $R = 4.0$ but different collision parameters. The minimum for the potential $R_0 > \sigma$ is near the effective radius than for $R_0 = \sigma$ and the LJ potential. That implies that the adsorption force at the interface of the nanoparticle is in the first case bigger than in the two second cases.

This variation does not leave the density of the tracking particle unchanged. In another couple of simulations a variation of the mass of the particle in relation with its radius was done in order to conserve the density of the probe.

Once the parameters are fixed, the simulation of the system melt-particle is started. The steps in the simulation protocol are: generation of first configurations, equilibration of the initial configuration for the melt and production, where the tracking particle is introduced in the configuration of the melt. In the following sections these steps will be explained.

2.4.1 Construction of the simulation

Generation of an initial configuration The creation of the first configuration is done using a random method, which consists in a simple random walk, a configurational bias Monte Carlo method called 'Recoil-Growth Algorithm' that assigns initial random positions to the chains in a periodic box [17], [14]. With such a

method it is possible to produce, in an efficient way, dense initial configurations, where the structure of the chains is near the equilibrium structure of the melt, but with many polymers overlapping. Due to the presence of flat substrate and upper wall there are two-dimensional periodic boundary conditions and a closed boundary in the third dimension. The RGA implemented in this program cannot create initial configurations of hetero polymers; so an initial configuration with homopolymers was created and then by hand the probe particle was introduced in the initial configuration.

The production of an initial configuration is made for a melt confined between two walls separated by a particular distance $d_W > H_\Gamma$ (H_Γ is the film thickness), i.e. for densities below the desired density; here a NVT method is used in order to fix the temperature of the system [16]. The walls are required for the generation of the first configuration because at high densities the RGA produces overlapping and eventually destruction of connectivity of the chains; so, after the generation of a very first configuration, it is important to compress the liquid in order to increase its density

The compression process is done moving the upper wall with a constant velocity toward the substrate [15]. The compression process is stopped when the liquid reaches the desired density. With a short simulation the configuration was equilibrated with a constant separation between both walls; in this step the fluid relaxes again and dissipates the force introduced with the upper wall. Initial dense melts were produced with $\rho \sim 0.8$ at temperatures of the order of $T = 0.8$. This value is particularly convenient [16] because it permits to obtain configurations with $\rho \sim 1.0$ at temperatures near the glass transition temperature and $\rho < 0.8$ for temperatures up to $T \sim 1.4$. With such starting configurations it is possible to make an exploration of different states of the liquid.

At this point there is an initial configuration of a thin polymeric film, composed of homopolymers. It is necessary to introduce the tracking particle and start the production of data. This step is explained in the following subsection.

Equilibration Now the upper wall is switched off and the probe particle is introduced per hand. A possible alternative is to introduce the nanoparticle in the first configuration and then make the compression of the melt together with the particle, but it is desirable that the particle "feels" the interaction of the melt without compression. Furthermore when the particle suddenly is placed on the surface of the melt it is possible that connections between monomers are destroyed, destroying the iteration process; this fact is more dramatic when additionally the system melt particle is compressed. For this reason it is preferred to run a new NVT simulation for melt-particle with the particle fixed at some distance from the melt (but not so far that the particle cannot interact with the particles of the melt). In this time the melt relaxes. Because the particle is also attached to the thermostat, it cannot fly away from the surface of the melt. This fact together with the force produced by

the fluid particles are responsible that the particle "falls" onto the fluid; in this simulation there is no gravitational interaction. In the fig. 2.9 the initial configuration for a nanoparticle above the polymer melt, with the particle placed above the melt, is shown.

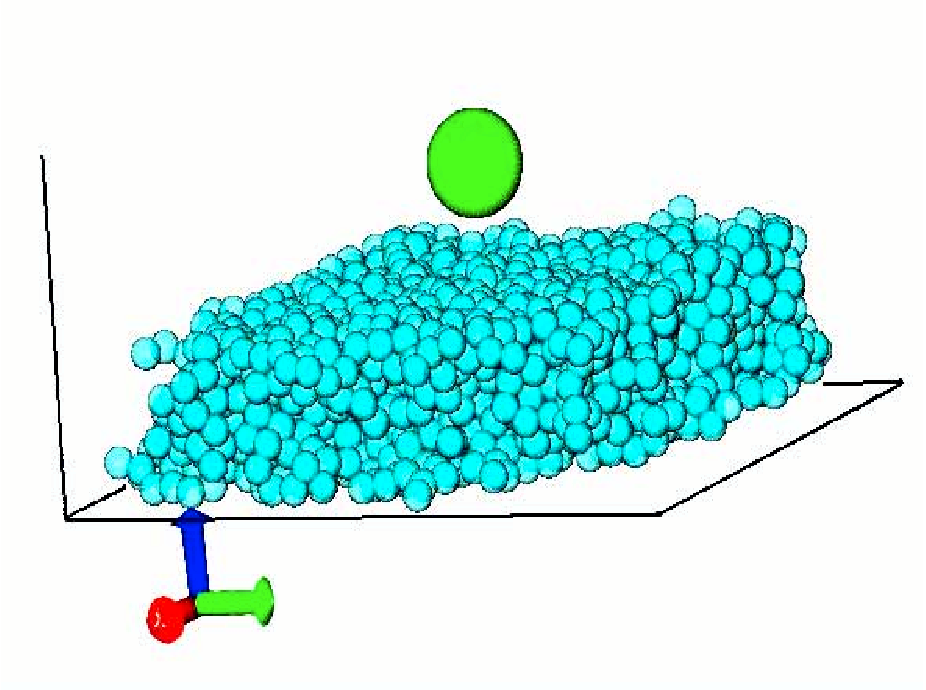

Figure 2.9: After equilibration a single particle is placed above the melt. In the present simulations there is no gravitational force; so, the single particle approaches to the melt by means of the interaction with the external thermostate and the coupling with the polymeric melt. After an equilibration time a first configuration for NVE simulations is obtained.

Using the Rouse modes and the Rouse time it is relevant to check the time required for the relaxation of the dynamics of the melt (see appendix D). From the theory it is well known that the relaxation time is given by $\tau \sim N^2$; using this information the NVT simulation is stopped.

Normally this is possible after 800000 Molecular dynamics Steps (MDS). Then the thermostat is switched off. At this moment, there is an initial master configuration at a fixed temperature of the adsorbed melt with the tracking particle. From the theory and the information obtained from other simulations of dense polymeric melts [14], [25] there is knowledge of the glass transition temperature of the system; below this temperature the system is non ergodic [17]. Therefore simulations were performed for temperatures above T_g, in particular the sample of temperatures $T = 0.46, 0.5, 0.7, 0.8, 1.0, 1.1, 1.4$ was considered (using a very intuitive language, these simulations are performed in a temperature sandwich, i.e., for temperatures above

the glass transition temperature but below the dewetting temperature of the liquid film).

For melts with small polymeric chains, short equilibration steps are enough to reach equilibration of the melt. But this method is not enough for long chains. For example in the article of Kremer and Grest [17], the initial configurations are produced after 5000000 integration steps. This time is longer than the typical time used in the present simulations. One possibility to improve the statistics of the system is doing parallel simulations and then make an average of the results obtained with each parallel run [27]. In the present work a single simulation is made, storing configurations each 10^6 MDS. Then additional parallel simulations are started with maximal simulation times 2×10^6 to 3×10^6 MDS, using as starting configuration each stored configuration in the previous step. Using the positions, velocities and forces an average of each of the observables for each of the parallel run is made. This method is applied for temperatures $T = 0.85, 0.9, 0.95, 1.2, 1.3$, i.e. temperatures where the equilibration is relatively fast. This method is time consuming, taking present that melts with 14×10^3 monomers are simulated.

The simulated system equilibrates very slowly. For this reason it is crucial to make long runs at every temperature, and in particular at low temperatures, since dynamical processes slow down upon cooling. This is a very serious problem in molecular dynamics simulations because the simulation time, as a function of the temperature, becomes larger than the largest simulation time that can be implemented within a PhD project. It is necessary to establish a compromise between the system size, the run times and the complexity of the model.

2.5 Summary

In this section the main elements required for the simulation of a dense melt with a single nanoparticle were introduced, including the simulation protocol, the potentials that describe the interactions between monomers and melt-substrate; in particular, the problems that simple LJ potentials presents for the modeling of non structured probe particles was discussed. An improvement of the stability of the vertical position of the tracking particle is obtained by defining a potential able to reduce the mobility of the liquid particles near the interface particle-liquid; it was shown that a simple modification of the LJ potential is enough in order to increase the attraction of the liquid particles to the interface of the particle.

The main problem is the time required for the production of reasonably good results; instead of longer simulation times (which are expensive in time as well as in energy), short parallel simulations was performed and averaged.

As outlook the modeling of the nanoparticle can be done using one of the two walls. This idea is interesting if the aim is to model the interaction of a dense melt with the Tip plus cantilever of an AFM microscope: in that case one proceeds to write the potential of the upper wall as the integrated Van der Waals potential for the

corresponding tip geometry [9]. Given that with the present simulation method it is possible to press the melt with the upped wall at constant velocity, then, by defining asymmetric walls, representing the upper wall as the tip of the AFM, it could be possible to simulate different force microscopic techniques (For such simulation the definition of tip geometries is necessary; see for example see [9]).

3 Interfacial effects on the dynamics of the nanoparticle.

3.1 Abstract

In this part an analysis of the distribution of the vertical position of the particle in the film is made, regarding the temperature as well as the thickness of the film. It is found that near T_g the particle is at the interface of the film; this result implies that the vertical position of the particle is sensitive to the glass transition temperature at the liquid vapor interface. One finds an hysteresis in the embedding process as a function of the temperature in the simulated time scales. This embedding process depends on the definition of the interaction between the nanoparticle and the polymer. An analysis of the solutions of the hydrostatics, in order to understand the effect that different potentials introduce in the liquid film, is made.

3.2 Introduction

The behavior of polymers in a film is different to the behavior in bulk due to the presence of external forces and of the interface; in this sense the knowledge of the surface glass transition is of fundamental interest [70]. In order to obtain information only from the film surface many experimental methods where developed, in particular the observation of the embedding of clusters of noble metals as a function of the temperature.

The observation of this effect is not easy given the difficulty to obtain good resolution of the particles with respect to the interface of the film [70] [74]. For this reason an extensive experimental effort has been undertaken with the aim to understand the behavior of the embedding process, in particular near the glass transition temperature; additional work was done in order to understand the forces on nanoparticles near polymer brushes [73]. Such methods where complemented with extensive theoretical investigation which relates the interfacial free energies with the penetration of the particle (or clusters of particles) into the film [67].

In the present section the embedding process of the nanoparticle is analyzed using fundamental definitions of wetting theory and results obtained from computer simulations, where (as was discussed elsewhere) the probe is modeled in an idealized

way as a non structured one. A relevant question is the analysis of the onset T_e of the embedding process and the effect of the thickness of the film on this embedding. From the experimental point of view, the embedding of small particles can be regarded as a measure of the glass transition temperature of the polymer in a very narrow surface region.

In the literature there are many examples of the analysis of wetting transitions on planar surfaces [62] as well as curved surfaces [60] [68]; in the last case the effects of the curvature are summed in an effective bulk term, suppressing critical as well as complete wetting. In the present computation the particle is always able to attach liquid particles to its surface[1]. In this particular case monomers at the interface of the particle do not simply collide but are also coupled to the tracking particle. In this chapter a short description of the theory on the embedding process is made. The following section is devoted to the characterization of the fluid film.

Then a qualitative analysis of the hydrostatics of LJ particles, and in particular for modified LJ particles, in fluid films is developed in order to understand the wetting behavior on such objects. The analysis of the interfacial effects of the particle and the dependence of the embedding on the temperature of the melt is done. The analysis of the dynamics of the particle is not the focus of this section (The dependence of the dynamics of the particle on different potentials is discussed in the appendix A).

3.2.1 Short theoretical background: embedding of nanoclusters and interfacial free energy

The embedding of particles in polymeric films is an effect that depends on the interfacial energies liquid-vapor, liquid-particle and particle-vapor in the absence of gravitational effects. The driving force of the embedding process is given by the contribution of the nanoparticle to the Gibbs free energy, which is lowered upon the embedding. The contribution of a single particle is given by [67]

$$F = \pi\gamma_p Z_0^2 - 2\pi R\left(\gamma_m - \gamma_{mp}\right) Z_0 + 2\pi R^2\left(\gamma_{mp} + \gamma_m - \frac{1}{2}\gamma_p\right), \tag{3.1}$$

where γ_m is the interfacial tension of the particle, γ_p is the interfacial tension of the polymer and γ_{mp} is the interfacial tension between polymer and particle. Z_0 is the penetration depth with respect to the surface of the film and R is the radius of the particle. From this expression complete embedding is expected when

$$\gamma_m - \gamma_p > \gamma_{mp}; \tag{3.2}$$

[1]This effect is related to the attractive potential of the nanoparticle

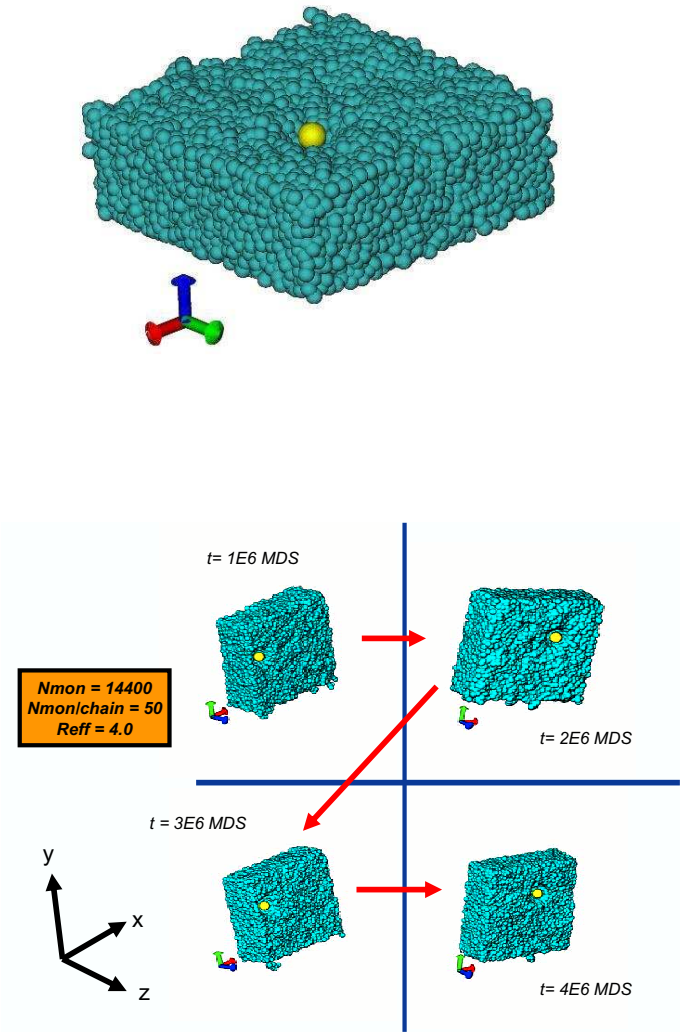

Figure 3.1: Snapshot of the position of the particle for $T = 0.46$, i.e. near the glass transition temperature. In the panel below the position of the particle is shown for different times. The persistence of the tracking particle at the interface of the film is due to the slow dynamics of the liquid at this temperature.

such expression is satisfied for metals in polymer melts. In the present case a similar theory must be valid for LJ particles; for this reason simulations with similar parameters as gold particles were performed. There the interaction between tracking particle and polymers is about three times larger than between adjacent monomers.

This implies that the mobility of the polymer chains near the nanoparticle is reduced. In fig. 3.1 a snapshot of the position of the particle at different times is shown; this plot shows the persistence of the vertical position of the particle at the interface; at the same time the interface forms a depletion region near the particle. This result will be discussed later.

3.3 Film characterization

The analysis of the dynamics of a single nanoparticle in a polymeric film requires a good characterization of this last one: the simulation of the present system needs a stable film on a substrate and therefore it is vital to select the correct parameters in the melt in order to avoid its dewetting[2] [3]. An important point in the present work is the calculation of the film profile; this information gives information about the mean film thickness, that can be related to the temperature of the melt.

In the present model the polymeric film is adsorbed on a non structured substrate with an attractive long range interaction and the simulations are performed for temperatures below the wetting temperature of the polymeric film [4]. The wetting behavior of the film can be tuned by variation of the Hammaker constant of the interaction potential of the substrate[5]; given that it is necessary to gain adhesion of the molecules with the substrate, the Hammaker constant was tuned to $\varepsilon_H = 3.2$. The number of particles and the size of the box was chosen in order to have a uniform spreading of the liquid; there is moreover no interest to make a variation of the contact angle liquid-substrate and hence the computations were made for temperatures $k_B T/\varepsilon_H < T_W$, where T_W is the wetting transition temperature; the corresponding density of the melt is in the present case $0.8 \leq \rho \leq 1$. With all the previous defined parameters a very stable film is obtained (there is no evaporation of polymer chains from the surface of the film; a more extensive report about the physics of the wetting behavior of polymer melts on substrates can be found in [16]).

The definition of the reference system for the measurement of the penetration process of the particle can not be fixed with respect to the substrate because the film has a variable thickness. Thus the information about the position of the particles relative to the interface of the melt is basic in order to make an analysis of the

[2] A wetting transition is the change of the thickness of a liquid film as a function of the temperature. An equivalent definition is, it is the change of the contact angle between the substrate and the surface of a droplet with the temperature. For example, mercury is a substance that under normal consitions does not wett any surface (for example saphire), i.e. it forms droplets; only by increasing the temperature (up to 1468 degrees) mercury tends to form a uniform film on a saphire substrate

[3] see for example [65] for a particular dewetting process

[4] Otherwise effects related to the dewetting of the film could be coupled to the dynamics of the particle; this case is out of focus of this work.

[5] Which is defined as the Gibbs energy of attraction per unit cross sectional area

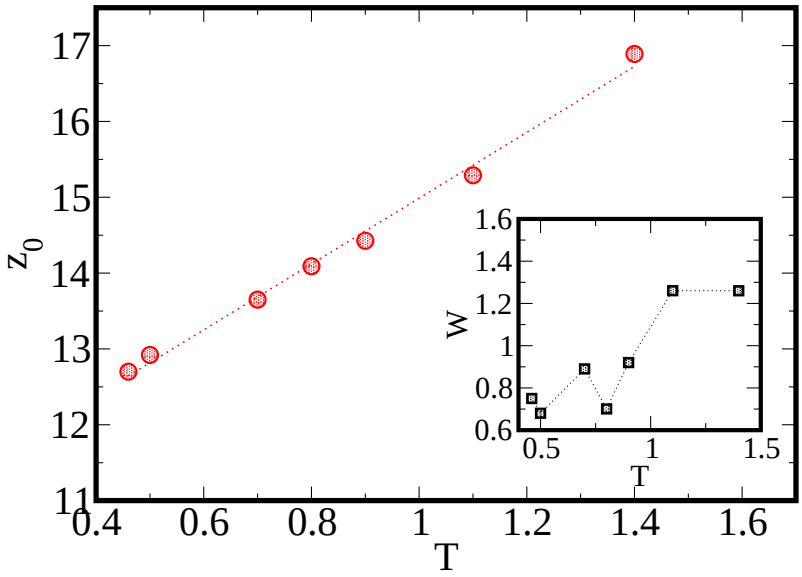

Figure 3.2: Film thickness and interfacial width as a function temperature. The thickness grows linear with temperature. In the simulated temperature range the film is below the dewetting temperature.

embedding of the probe. At a first glance (as a qualitative analysis) the penetration of the tracking particle can be analyzed by relating the density of the fluid with the density of the vertical distribution of the particle. [6] This results will be discussed later also in this section (see fig. 3.10)

At the interface the liquid density steeply decreases to the vapor density; for $z \to \infty$ the vapor density approaches zero. The interface was fitted using a tangent hyperbolic function

$$\rho(z) = \rho\frac{1}{2}\left[\tanh\left(\frac{z_0 - z}{w}\right) + 1\right], \tag{3.5}$$

where z_0 is the mean film thickness and w is the width of the interface.

[6] The distribution $H(z)$ of the vertical position of the liquid particles, as a function of the vertical coordinate, is normilized by means of the following expression

$$N = \int_0^h H(z)dz, \tag{3.3}$$

where h is the film thickness. So, given that the liquid particles have mass equal to one, the density distribution of the liquid is given by

$$\rho(z) = \frac{H(z)}{L^2} \tag{3.4}$$

in this formula L is the size of the periodic box.

Table 3.1: Thickness and density of the liquid film

T	w	z_0	ρ
0.46	0.75	12.7	1.0
0.50	0.68	12.92	1.0
0.70	0.89	13.65	0.92
0.80	0.70	14.09	0.91
0.90	0.92	14.42	0.89
1.10	1.26	15.29	0.80
1.40	1.26	16.89	0.72

In table 3.1 the result for the film-thickness and width of the interface are shown and plotted in 3.2, for a polymer film composed of 14400 particles; the lateral size of the box in this simulation was 34.6σ. The thickness of the interface grows with temperature[7]. The thickness of the film was controlled in the computations with the number of particles and the size of the box.

3.4 Hydrostatics of the gas phase

A qualitative idea about interfacial effects is obtained by solving the equations of hydrostatics for the fluid film in the system substrate-nanoparticle. For this model the contributions related to the complex liquid are zero (i.e., in hydrostatics a complex liquid is the same as a simple one). Such theory seems to be too simple but presents a powerful tool to understand the equilibrium of the liquid film [32].

The interface of the liquid film is related to the equipotential lines produced by the potential of the substrate and the potential of the particle. The total potential is defined as symmetric with respect to a coordinate q^2 and is given as a function of the two coordinates q_1, q_3

$$\phi = \Phi_T \left(q_1, q_3 \right). \tag{3.6}$$

From the hydrostatical equations the equilibrium condition between the pressure and the external potential is given by

$$\rho \delta^{ij} \partial i \Phi_T = -\partial_i t^{ij}, \tag{3.7}$$

where $t^{ij} = \delta^{ij} P$, P is the pressure in the liquid. The right hand is related to the thermodynamics of the system through the Gibbs free energy, which is given by

$$\partial_i P \left(q_1, q_3 \right) = \rho \partial_i \mu; \tag{3.8}$$

[7]This result is in accordance with Mull et al. [16]

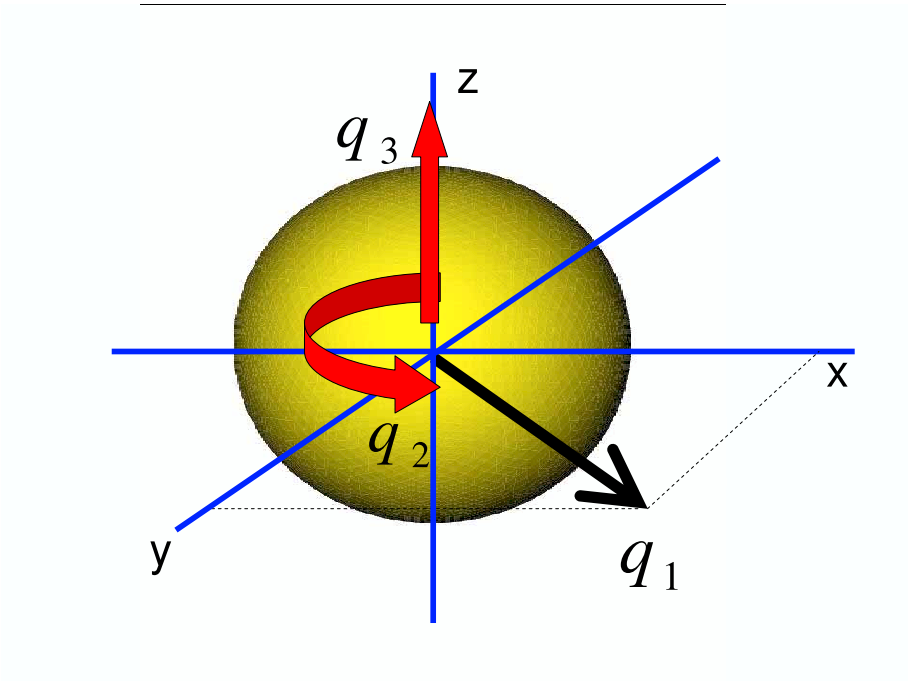

Figure 3.3: Representation of the coordinate system used in the calculation of the solutions of the hydrostatics of a liquid.

in this equation μ is the chemical potential and P is the pressure of the liquid [71].

The Gibbs equation is also valid for the gas phase, thus it is allowed to write an hydrostatical relation between the external potential and the chemical potential

$$\partial_i \Phi_T \left(q_1, q_3\right) = -\partial_i \mu. \tag{3.9}$$

With this equation it is possible to determine the film thickness as a functional of the chemical potential of the gas.

3.4.1 Film thickness away from the particle for $q^1 \to \infty$.

Far from the particle ($q^1 \to \infty$) the total potential approaches to the following potential

$$\lim_{q^1 \to \infty} \Phi_T \to \Phi_S, \tag{3.10}$$

in this equation [8]

[8] For this mathematical description the contravariant notation is used; that means the coordinate system is described for each axis as q^1, q^2 and q^3.

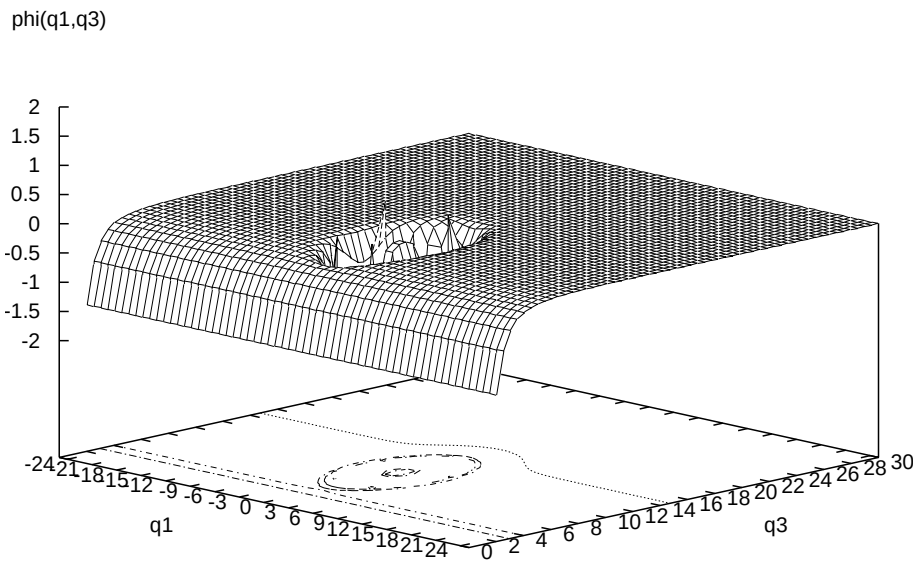

Figure 3.4: Three dimensional representation of the solution of the hydrostatics. The film thickness is represented by the contour lines, which are the equipotential lines of the potential particle substrate satisfying eq. 3.9.

$$\Phi_S(q_3) = 4\varepsilon_H \left[\left(\frac{\sigma}{(q^3)} \right)^9 - \left(\frac{\sigma}{(q^3)} \right)^3 \right]. \tag{3.11}$$

Applying this potential to the hydrostatic equation and integrating from the surface of the film $q^3 = H_\Gamma$ to infinity ($q^3 \to \infty$) one gets the following equation

$$\Phi_S(H_\Gamma) + \Delta\mu = 0, \tag{3.12}$$

with

$$\Delta\mu = \mu_\infty - \mu_{coex}, \tag{3.13}$$

where μ_{coex} is the chemical potential at the liquid-vapor interface. In such case we can asume that $\mu_\infty \to 0$, which implies that $\Delta\mu \to \mu_{coex}$. This equation can be solved for H_Γ the film thickness as unknown. At this point it is helpful to define the following variable

$$\kappa_f = \frac{\mu_{coex}}{4\epsilon_H}, \tag{3.14}$$

which replaced in eq. (3.4.1) yields to the following equation for the film thickness:

$$Y^3 - Y - \kappa_f = 0. \tag{3.15}$$

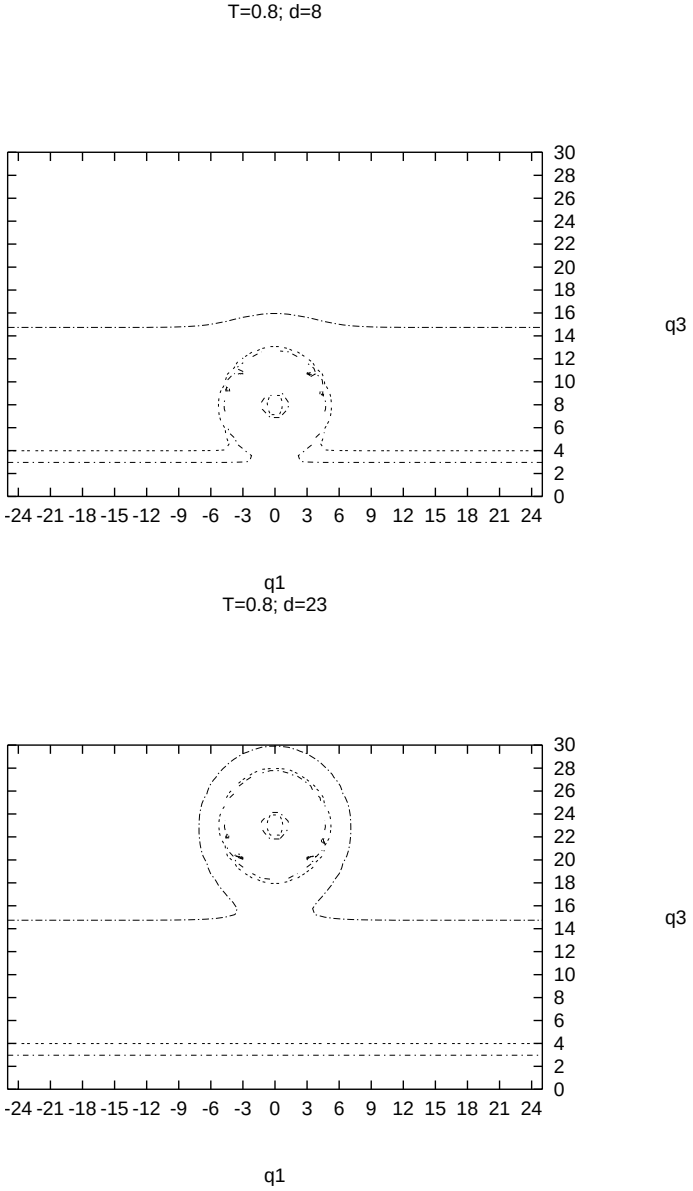

Figure 3.5: Profile of the interfacial line in hydrostatics for the particle, interacting with a modified LJ potential with the liquid, at different positions: $d = 8$ and $d = 18$. All the dimensions are in LJ units. The effective radius of the nanoparticle is $R_{eff} = 4.0\sigma$, with a hard core radius of $R_0 = 3.0\sigma$. It is possible to observe that the particle placed in bulk admits the formation of flat film interface. When the relative distance to the substrate is higher, the surface of the liquid is curved and eventually condenses on the surface of the particle.

where the following transformation was done

$$Y = \left(\frac{1}{H_\Gamma}\right)^3. \tag{3.16}$$

Furthermore it is assumed that the interaction range is $\sigma = 1.0$. This is a cubic equation that can be analyzed bymeans of the computation of the discriminant. The solutions of this kind of equation can be real or complex, but for the present problem this solution which represents a physical quantity (the film thickness) must be necessary real.

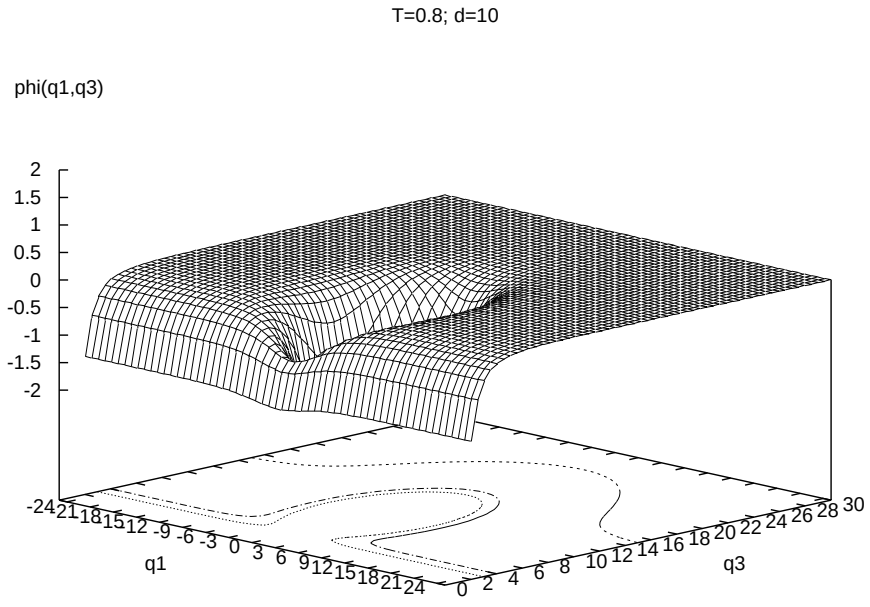

Figure 3.6: Interface in the presence of a LJ particle with radius $\sigma = 4.0$. The temperature in this system is the same as the temperature in fig. 3.5. In comparison with modified LJ potentials, this kind of potentials have a very long range interaction; hence the interface (plotted in the contour base) is curved, even when the particle is placed near the substrate.

The discriminant is given by

$$\mathrm{D} = \left(\frac{-\kappa_f}{2}\right)^2 + \left(\frac{-1}{3}\right)^3 . \tag{3.17}$$

If $\mathrm{D} > 0$ then there are one real and two conjugate imaginary solutions. If $\mathrm{D} \leq 0$ there are three real solutions.

From eq. (3.4.1), and the information of the film thickness obtained from simulation results, the chemical potential is $-0.0065 \leq \mu_{coex} \leq -0.002$, for temperatures between $0.46 \leq T \leq 1.4$ and therefore $\mathrm{D} < 0$.

The solutions of the equation (3.4.1) can be found using the so called *casus irreducibilis* [61]

$$Y_1 = 2\frac{1}{\sqrt[2]{27}}cos(\phi/3), \tag{3.18}$$

$$Y_2 = -2\frac{1}{\sqrt[2]{27}}cos(\phi/3 - 2\pi/3), \tag{3.19}$$

$$Y_3 = -2\frac{1}{\sqrt[2]{27}}cos(\phi/3 + 2\pi/3), \tag{3.20}$$

where ϕ is given by

$$\phi = arccos\left(\sqrt[2]{27}\frac{\mu_{coex}}{8\epsilon_H}\right), \tag{3.21}$$

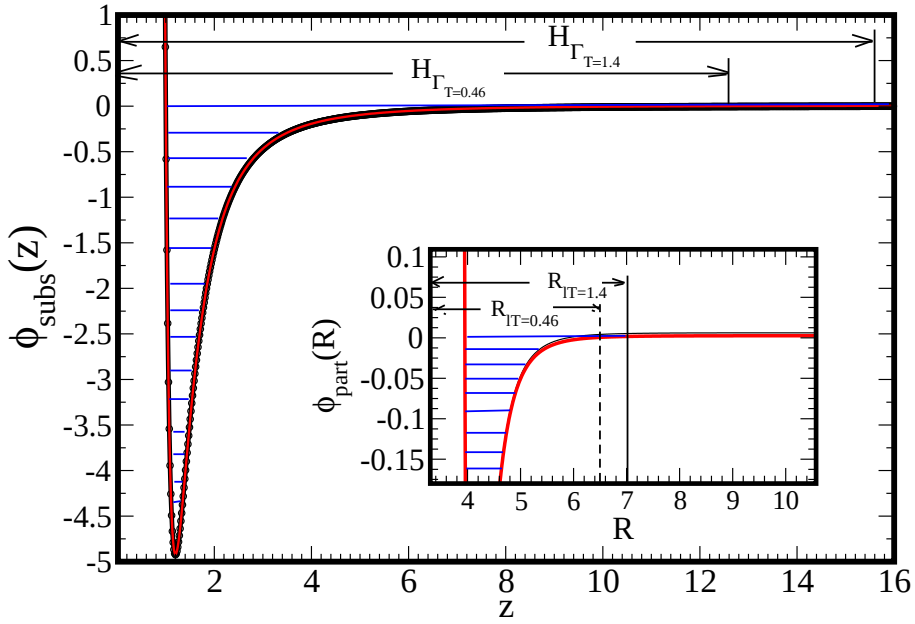

Figure 3.7: Plot of the equation (3.4.1) for $0.46 \leq T \leq 1.4$. The first zero of the function at $z \sim 0.5$, the transition from the repulsive to the atractive part of the potential; the second zero is at $z = H$, related to the film thickness. The third zero of this function is negative and has no physical meaning. Therefore the liquid film is adsorbed on the substrate in the region defined between the first and second zero. In this region each horizontal in the curve represents different chemical potentials at different temperatures. In the small panel the same situation is plotted for the potential of the nanoparticle

Using the parameters for the liquid film, one of these solutions is $H_{1\Gamma} \sim z_0$, the height of the film; the other two solutions are $H_{2\Gamma} \sim 0.49$ and $H_{3\Gamma} \sim -0.46$ for almost all the coexistence chemical potentials suggested in this section. Negative solutions for the film thickness have no physical meaning. Therefore the present solutions appears consistent with both results obtained using computer simulations and the hydrostatics, because all the solutions for the film thickness, using the

respective coexistence chemical potential, are inside the space defined by the liquid film (see fig 3.7).

The same analysis can be applied near the isolated nanoparticle. In the next subsection this analysis is done.

3.4.2 Film thickness close to the particle

Close to the particle the following potential is present

$$\Phi_T(q_1, q_3) = \Phi_S(q_3) + \Phi_{particle}(q_1, q_3); \tag{3.22}$$

in this case $\Phi_{particle}(q_1, q_3)$ is given either by the LJ or the modified LJ potential. The integration of the hydrostatic equation for the chemical potential in the gas phase, from $q^3 = H_\Gamma$ to infinity, gives

$$\Phi_T(q_1, q_3) - \mu_{coex} = 0. \tag{3.23}$$

This equation is of order 11, that means, there is no analytical solution for H, the thickness of the film.

In this equations the equipotential lines, where the potential plus the coexistence chemical potential is equal to zero, represents the interface of the liquid film; therefore the plot of such lines is the direct representation of the film thickness. This graphical solution is obtained and represented in figs. 3.4, 3.5, fig. 3.6 and fig.3.7.

The method used for the calculation of the film thickness on the substrate can be used for the calculation of the film thickness on the nanoparticle away from the substrate. In such case the equation for the liquid film on the particle is

$$\phi_{particle}(R) = \frac{\mu_{coex}}{4\epsilon_{mp}}, \tag{3.24}$$

where the potential for the particle is defined in spherical coordinates; in this case the potential of the particle is the modified LJ potential (defined in chapter 2). Making the definition of variables $\alpha_{part} = R_l - R_0$ and $\beta = \alpha^{-6}$, where R_l is the position of the liquid film on the nanoparticle, then from eq. (3.24) the following equation is obtained:

$$\beta^2 - \beta - \frac{\mu_{coex}}{4\epsilon_{mp}} = 0; \tag{3.25}$$

this is again a polynomial equation of order two that can be easily solved. The solutions of this equation are

$$\alpha_{1part} = \left(\frac{2}{\left(1 - \sqrt[2]{1 + \frac{\mu_{coex}}{\epsilon_m p}}\right)} \right)^{1/6}, \tag{3.26}$$

$$\alpha_{2part} = \left(\frac{2}{\left(1 + \sqrt[2]{1 + \frac{\mu_{coex}}{4\epsilon_m p}}\right)} \right)^{1/6} . \tag{3.27}$$

The case that is represented by the previous equations imply that the substrate is at the hardcore of the nanoparticle, i.e. for $\alpha = 0$. The equations (3.4.2) and (3.4.2) has one real and one imaginary solution if $\mu_{coex} > 0$. Making the same consideration done for a flat substrate, the chemical potential vary from $\mu_{coex} = -0.0062$ at $T = 0.46$ to $\mu_{coex} = -0.0026$ at $T = 1.4$ implying that eq. (3.25) has two real solutions: for $T = 0.46$, $\alpha_1 \sim 1.0$ (i.e $R_l \sim 4.0$) and $\alpha_2 = 3.52$ (i.e $R_l = 6.52$) and for $T = 1.4$, $\alpha_1 = 1.0$ (i.e $R_l \sim 4.0$) and $\alpha_2 = 4.08$ (i.e. $R_l = 7.08$).

In fig. 3.7 the equipotential lines for the particle, without substrate, are shown; in such case the system is at $T = 0.46$ and $T = 0.8$. The liquid film on the particle has a thickness $H(r) > 2\sigma$; and it is evident that the variation with the temperature is very smooth. Given that the size of the monomers in the polymeric film is 2σ then it is possible to conclude that the nanoparticle has always a layer of monomers (i.e. there is no wetting transition on the particle in the temperature regime considered in the present simulations)

The value of the chemical potential at coexistence controls the thickness of the film and therefore the wetting or dewetting of the fluid. In figure 3.5 different film thickness as a result of the superposition of the substrate potential with a modified LJ potential are represented. The solution for the equipotential lines for a particle interacting with the fluid through a LJ and a modified LJ potential is shown in figs. 3.5, 3.6. From this plot it is important to notice that the interaction range for the LJ particle is much bigger than for the modified LJ particle; therefore, when both kind of particles are placed in bulk, the modified LJ particle allows the formation of a flat interface, whereas the LJ particle produces a curved interface, even when the particle is near the substrate.

3.4.3 Determination of the pressure for the gas phase

The solution of the equations of the hydrostatics gives information about the pressure in the gas and in the liquid face. The density of the liquid remains constant and the conservation of the momentum, represented by the Navier Stokes equations, is given by

$$\begin{aligned} \partial_1 T^{11}_{Gas} &= -\rho_{Gas} \partial_1 \delta^{11} \Phi_T(q_1, q_3), \\ \partial_3 T^{33}_{Gas} &= -\rho_{Gas} \partial_3 \delta^{33} \Phi_T(q_1, q_3), \end{aligned} \tag{3.28}$$

where T_ij is the stress tensor; in particular $T_{11} = P(q_1, q_3)$ and $T_{33} = P(q_1, q_3)$. That means, the eq. (3.28) are two uncoupled equations on each coordinate for $P(q_1, q_2)$.

Away from the particle both equations are reduced into only one differential equation over the coordinate q_3. In the following equations the solution near the particle will be considered; if the vapor phase is considered as an ideal gas then

$$\rho_{Gas} = \frac{P_{Gas} m}{KT}. \tag{3.29}$$

then replacing (3.4.3) into (3.28) the following equations are obtained

$$\partial_1 P_{Gas} = -\frac{P_{Gas} m}{KT} \partial_1 \Phi_T(q^1, q^3), \tag{3.30}$$

$$\partial_3 P_{Gas} = -\frac{P_{Gas} m}{KT} \partial_3 \Phi_T(q^1, q^3). \tag{3.31}$$

The integration of both equations is done for the whole gas space, i.e. from liquid surface at $q_3 = H$, where H is the film thickness, to infinity, and $q_1 = 0$ to infinity. The result is

$$P(q_1, H) = P(q_1, \infty) e^{\frac{m}{KT}\Phi_T(q^1, H)}, \tag{3.32}$$

$$P(0, q_3) = P(\infty, q_3) e^{\frac{m}{KT}\Phi_T(0, q^3)}, \tag{3.33}$$

where $P(q_1, H)$ is the pressure of the gas over the liquid (the barometric pressure formula), H is the thickness of the liquid film, which is defined at the coexistence line between the liquid and the vapor phase, $P(q_1, \infty)$ is the gas pressure far away from the liquid surface and $P(\infty, q_1)$ is the pressure far away on the radial coordinate. Due that the interface is an equipotential line

$$P_{H_{Gas}} = P_{H_{liquid}}. \tag{3.34}$$

That means, the barometric formula for the gas at the interface is the same as the liquid pressure at the same point.

3.4.4 Hydrostatics for the fluid Film

In the barometric formula there is information on the dependence of the pressure on the vertical coordinate, $P_{film} = P(q_3)$. So, in the liquid phase the equation for the pressure is

$$\partial_3 t_{fl}^{33} = -\rho_{liq} \partial_1 \delta^{33} \Phi_T. \tag{3.35}$$

In case that the fluid is incompressible

$$\rho_{fl} = cte; \tag{3.36}$$

replacing this last expression in the first one it is obtained

$$\partial_3 P = -\rho_{fl}\partial_3 \Phi_T(q_3). \tag{3.37}$$

This equation is integrated in the interior of the film, that means between any q^3 and H, the liquid surface, which depends on the chemical potential through κ_f. This solution thus contains information in all the fluid space; the solution for the pressure can be written as

$$P(H(\kappa_f)) = P_{fl}(H(\kappa_f)) + \rho_{fl}\left(\Phi_T(H(\kappa_f), q^1) - \Phi_T(q_3, q^1)\right), \tag{3.38}$$

where

$$P_{fl}(H(\kappa_f)) = P_{Gas}(H(\kappa_f)), \tag{3.39}$$

this last equation represents the boundary conditions liquid-gas for the hydrostatic equations. Away from the particle the total potential tends to be the potential of the substrate. Using the contact conditions the solution for the pressure in the liquid is

$$P = P_\infty e^{\frac{m}{KT}\Phi_s(H(\kappa_f),q^1)} + \rho_{fl}\left[\Phi_s(H(\kappa_f), q^1) - \Phi_s(q_3, q^1)\right]. \tag{3.40}$$

Near the particle the solution for the pressure in the film is

$$P = P_\infty e^{\frac{m}{KT}\Phi_T(H(\kappa_f),q^1)} + \rho_{fl}\left[\Phi_T(H(\kappa_f), q^1) - \Phi_T(q_3, q^1)\right], \tag{3.41}$$

with this last equation the complete expression for the barometric formula in vapor and liquid, away and close to the particle, was obtained.

3.5 Interaction between the nanoparticle and the polymer film

Simulations at low temperatures The film thickness is computed using the formulas derived from the solutions for the hydrostatics of the fluid film. The equipotential line to $\Phi_T = \mu_{coex} - \mu_\infty$ defines the position of the interfacial line. As was assumed, $\mu_\infty \to 0$; this particular point has as consequence that the film thickness depends on μ_{coex} (in this sense it quite evident that the film thickness can be controlled using the coexistence chemical potential). The main interest is to make a contrast between the simulations and this theory.

In contrast to the solutions in hydrostatics, where is assumed that the film is in a liquid state, most of the simulations for polymeric films was performed for temperatures near the glass transition temperature T_g. This is very important to make an interpretation the results of the simulations done for low temperatures.

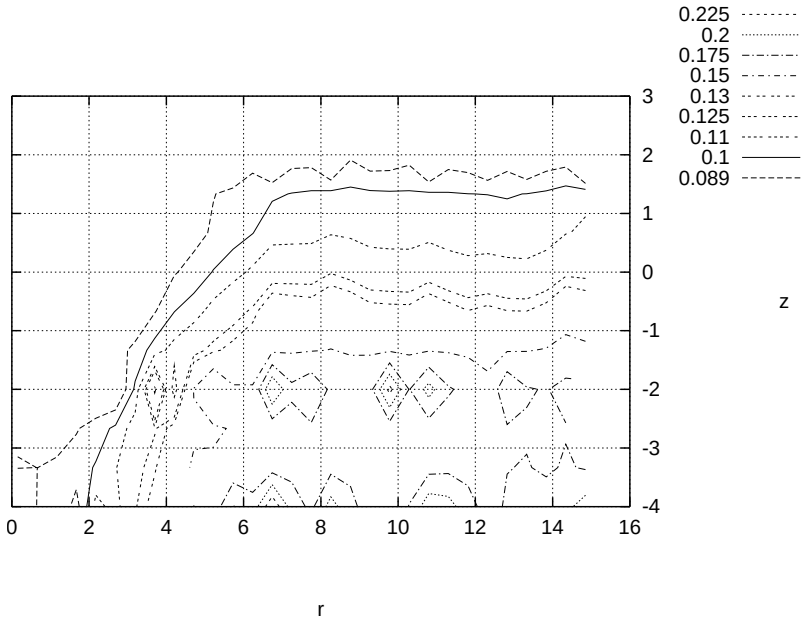

Figure 3.8: Density profile of the particles in the film close to the tracking particle at $T = 0.46$. In this plot the particle is placed at the center of the coordinate system. Here it is obvious to distinguish a depletion of the density profile near the interface particle-liquid, as the hard core of the tracking particle does not admit a layer of particles on its surface (see 3.7).

Nevertheless, the tracking particle always admits a film of particles (on the hard core), as was shown in fig 3.7, the formation of this film depends first on the position of the probe particle relative to the interface of the polymeric film and second on the dynamics of the polymers close to the particle[9]. The present simulations uses initial configurations where the nanoparticle is placed above the polymeric film; so for initial times the particle has no neighboring monomers and only after some simulation steps the particle is able to interact with the particles at the interface of the melt.

If the temperature of the system is $T > T_g$, then the interface of the melt is in a liquid phase, making possible the formation of the liquid film on the particle; therefore the particle eventually embeds into the melt and searches a position where the distance between the monomers in the polymeric film and the tracking particle d_m be $d_m \geq R$, R the layer on the particle defined from eq. (3.24). On the other hand if the polymeric film is near the glass phase, is possible also that the interface is in a glass state?

In fig. 3.8 the density profile of the monomers near the tracking particle is plotted, for $T \sim T_g$. From this plot there are two important aspects: the persistence of the position of the particle near the interface of the film (see fig. 3.1) and the formation

[9]In an intuitive way it is possible to say that the formation of a film on the particle depends on how fast the particles can move on the surface of the nanoparticle in order to form it

of a 'cup' near the particle (see fig. 3.8). The small embedding of the particle into the melt at low temperatures is an indication of the same embedding mechanism explained in the previous paragraphs. But in such case the persistence of the vertical position of the nanoparticle at the interface is an indication of the very slow dynamics of the polymeric chains at the liquid-vapor interface of the film (typically for liquids near the glass transition temperature). Therefore at $T \sim T_g$ the tracking particle has only a light embedding into the film.

The time required for the formation of the layer of particles on the tracking particle depends on the mobility of the monomers into the polymeric melt. The density profile near the particle as well as the observation of the position of the particle with respect to the interface permits to conclude that for $T \to T_g$ the polymers at the interface of the film are also near the glass phase (This fact can be related to the compliance force on the particle [74]). This result is very important because it shows very clearly that a glass transition not only happens in bulk; the 'cup' close to the particle in fig. 3.1 at $T \sim T_g$ is the result of the low mobility of the monomers at $T > T_g$ (see fig. 3.9 and appendix A).

There is one additional aspect related to the definition of the interaction potential between the tracking particle and the monomers in the film. As was discussed in chapter two about the technical details, it is necessary to choose a modified LJ potential in order to gain stability of the particle respect to the liquid-vapor interface: simulations with LJ particles were done but the probe particle never reached stability on the interface. With the computation of the film thickness using hydrostatics it is possible to observe at the interface of the film a small 'hill' just above the LJ particle, with $\sigma = 4$ and $d = 8$. Even for the particle placed at $d = 2$ the interface is curved. This result can be easily verified using again the corresponding formula of eq. (3.9) for LJ potentials; in such case the substrate is again at the surface of the nanoparticle i.e. at $R = \sigma$. For $T = 0.46$, $\alpha_1 = 1.0$ and $\alpha_2 = 3.52$ (i.e for $\sigma = 4.0$, $R_l = 7.52$) and for $T = 1.4$, $\alpha_1 = 1.0$ and $\alpha_2 = 4.08$ (i.e. $R_l = 8.08$). This result suggest that LJ particles, or particles with modified LJ potential with $\sigma > R_0$, have a very long interaction range. It is very easy to conclude that the particle can have a layer of monomers or liquid particles if the film thickness is $H >> R$. Because the stability of the tracking particle on the film depends on the layer of monomers on the particle, then the films considered in the present simulations was too thin, many of them with $H \leq R_l$, that it was impossible to guarantee the stability of the probe particle on the film.

With the modified potential for the particle, the distribution of the vertical position of the particle is more stable than for a simple LJ potential because with the first one the particle admits a stable thin liquid layer near its interface: the monomers are able to trespass the interface defined at R_{eff}, which defines the interaction range of the nanoparticle, and interact with the hard core of the particle, with $R_0 > \sigma$, where $\sigma = 1$ is the typical size of the monomers in the melt. From this last points there are additional reasons that explain why the particle simulated with a hard core potential is more stable than the simple LJ potential: First $R_{eff} < R_l$, i.e. the effective radius of the particle is smaller than the size of the liquid film that

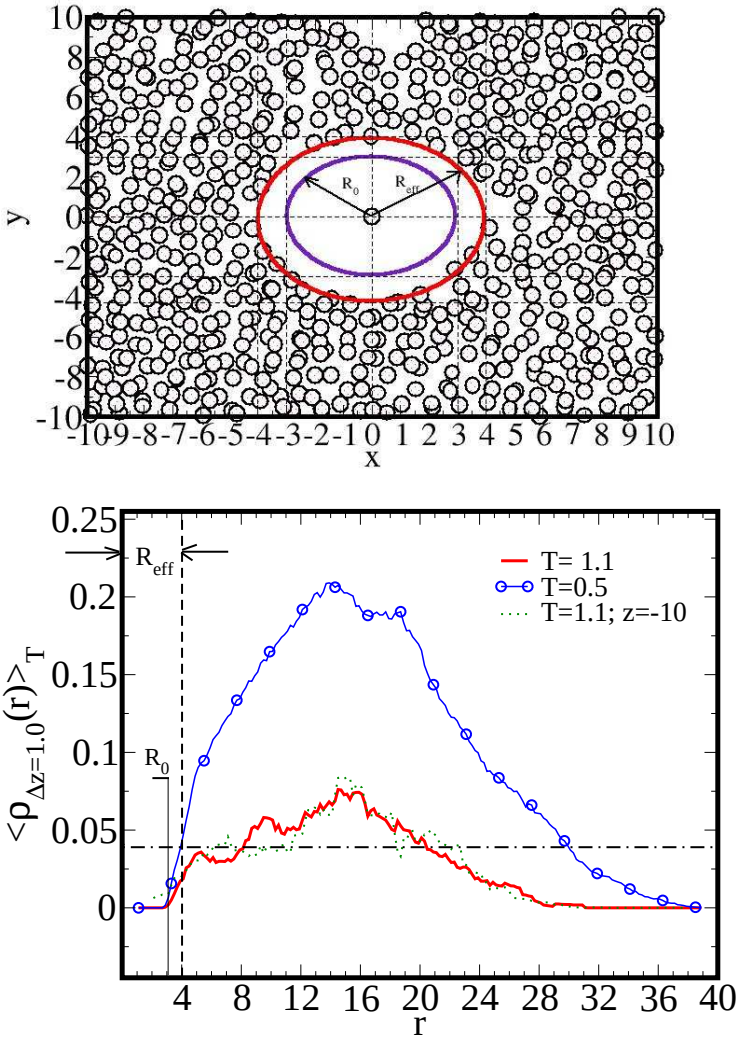

Figure 3.9: As was predicted by many authors (See for example Press et al. [67]), the embedding of nanoparticles in liquid films produces a layer of liquid particles on the particle. In the first plot a snapshot of the particles distributed around the tracking particle at $T = 1.1$ is shown; the plot below shows the density of the liquid near the nanoparticle for two different temperatures in an horizontal cut of thickness $d_{cut} \sim 1.0$. When the particle is inside the film the existence of a growth of density near the surface of the particle is obvious.

the nanoparticle, without substrate, can admit; second $|U_{eff}(r \sim R_{eff})| > |U_{LJ}|$, i.e. the potential close to the region defined by the effective radius is much deeper than the simple LJ potential (this implies, the layer formed in the region near R_{eff} is composed of particles that have much lower mobility than the rest of the polymeric film). Therefore, a simple LJ particle admits a film over its surface but the monomers in this region have still high mobility; for this reason any LJ particle with

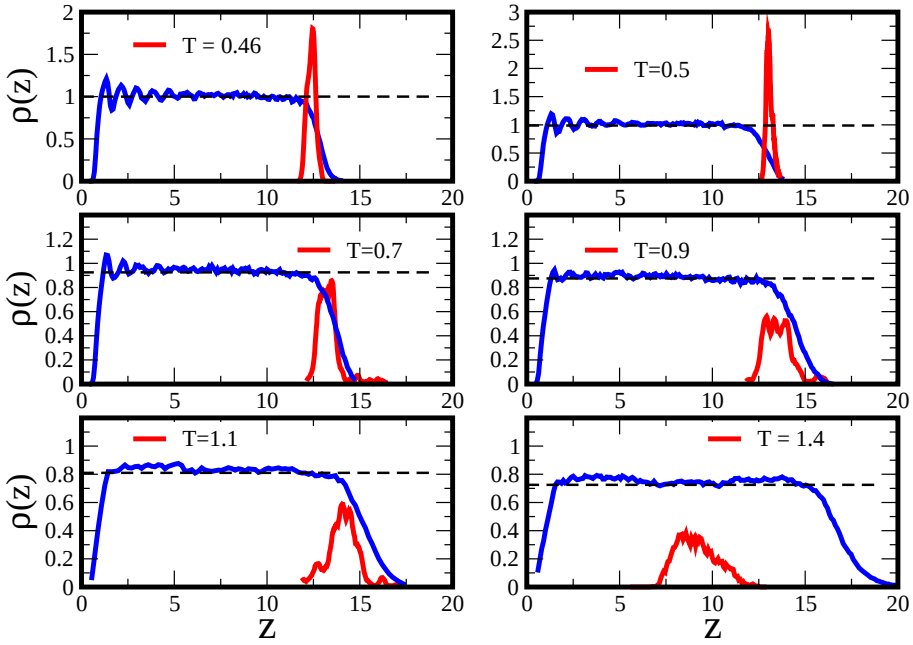

Figure 3.10: Distribution of the vertical position of the particle as a function of the temperature. The liquid has 14400 particles and $N = 10$. The horizontal lines represent the mean density of the film (see 3.2). The principal function represents the density profile of the melt as a function of z, whereas the 'peak' functions represent the distribution of the particle along the same coordinate. It is obvious to observe that this last distribution function is not Gaussian and that its breadth depends on the temperature.

any size is reflected by the polymeric film[10]

Position of the tracking particle and interfacial phenomena In the initial configuration the tracking particle is placed above the polymeric film; when the thermostat is switched off the colloid couples only to the particles in the melt. The modified LJ potential secures that the mobility of the liquid particles near the probe particle is low: without such potential the particle gets enough kinetic energy and can escape from the surface of the melt.

The position of the particle was measured with respect to the film thickness; this result, together with the variance ($\sigma^2 = \langle (z - z_0)^2 \rangle - \langle z - z_0 \rangle^2$), is presented in the table 3.2.

This result shows that the particles sink at high temperatures and indicates very nice a transition from a glass into a fluid behavior at the interface of the film. In

[10]The definition of the nanoparticle with a modified LJ interaction potential can be interpreted as a particle with hard core and a soft surface that is able to attach fluid particles. In an intuitive way is like a tenis ball with many cotton on its surface

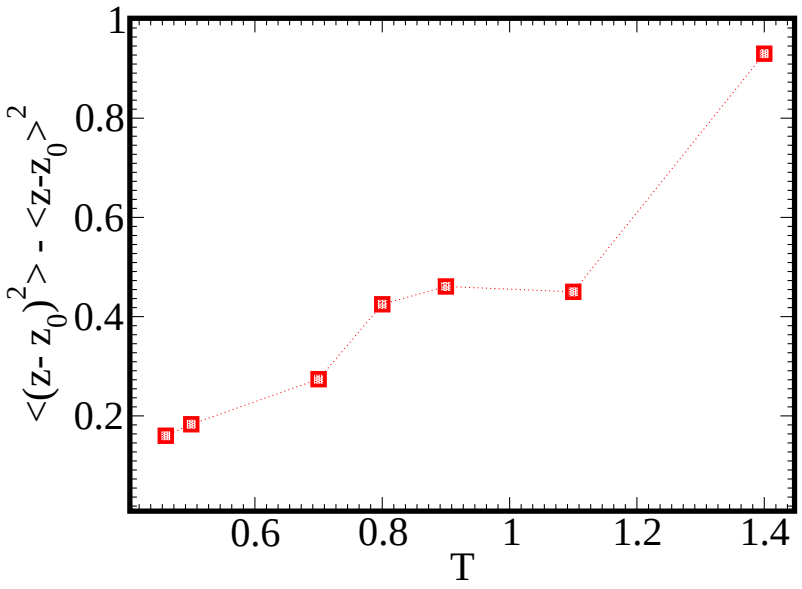

Figure 3.11: Variance of the position of the particle relative to the position of the interface as a function of the temperature. Observe the separation between nanoparticle and the position of the interface by increasing the temperature from T_g. Therefore the vertical position of the particle monitors the glass transition temperature at the interface of the melt and subsequent embedding as a function of T. This situation is confirmed experimentally [67].

Table 3.2: Position of the particle respect to the liquid-vapor interface

T	$\langle z - z_0 \rangle$	σ^2
0.46	0.49	0.15
0.5	0.87	0.18
0.7	1.31	0.27
0.8	1.79	0.42
0.9	1.61	0.46
1.1	3.06	0.45
1.4	7.61	0.93

fig. 3.10 the distribution of the particle along the z axis is shown in different plots as a function of the temperature. This plot gives more over information about the change of the density of the melt with the temperature and the dependence of the width of the distribution of the particle on the temperature. In fig.3.11 the variance of the position of the particle relative to the position of the interface is shown; from this plot the dependence of the embedding process on the temperature is very clear; this result coincides with experimental observations [67].

The method used in this simulations, as well as the analogous experimental method [67], serves to measure locally, i.e. near the nanoparticle, the glass transition

of the polymer liquid at the interface. Although the embedding of the nanoparticle proofs the existence of a glass transition at the interface (as was explained some paragraphs before), it is not totally clear if the interface is in fact in a glassy state. In the discussion above about the potential of the particle it was shown that in the simulations the nanoparticle forms a 'cup' near the nanoparticle; moreover the results for the mean position of the tracking particle with respect to the interface show that the particle is just below the interface of the film (see fig. 3.11). If the interface, close to the nanoparticle, is in a glassy state then the particle is not able to penetrate into the film. The results obtained with this simulations seems to confirm the results obtained by Teichoeb et al. [75]: for $T \to T_g$ the monomers near the interface and close to the nanoparticle are in a liquid phase.

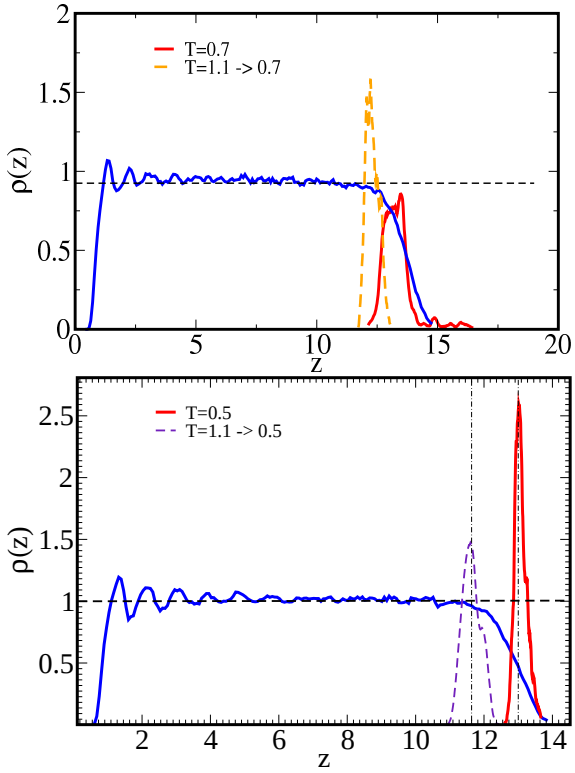

Figure 3.12: Histograms of the vertical position of the particle in a system with 14400 particles, starting from an initial configuration with a temperature $T = 1.1$ and cooling down to temperatures $T = 0.7$ and $T = 0.5$. The particle has an effective radius of $R_{eff} = 4.0$.

The previous affirmation depends on the definition of the interaction potential between the nanoparticle and the melt. As was shown in chapter two, and discussed along this chapter, the definition of a modified LJ potential ensures more stability on the vertical position of the tracking particle, implying a large attraction between the particle and the neighboring monomers. This fact has as consequence that near the tracking particle the liquid particles have low mobility; as consequence an adsorption layer appears on the surface of the particle, when the particle is in bulk. In fig. 3.9

one can observe the distribution of monomers in a lateral cut on the equatorial line of the nanoparticle, of thickness 1.0σ; in this particular case $R_0 = 3.0$ and $\sigma = 1.0$. In the same figure the density distribution of the monomers in the cut as a function of the radial coordinate r is shown for two different temperatures; here there is a dramatic growing of the density at $r = R_{eff}$, even when the particle is placed in bulk at $T \sim T_g$.

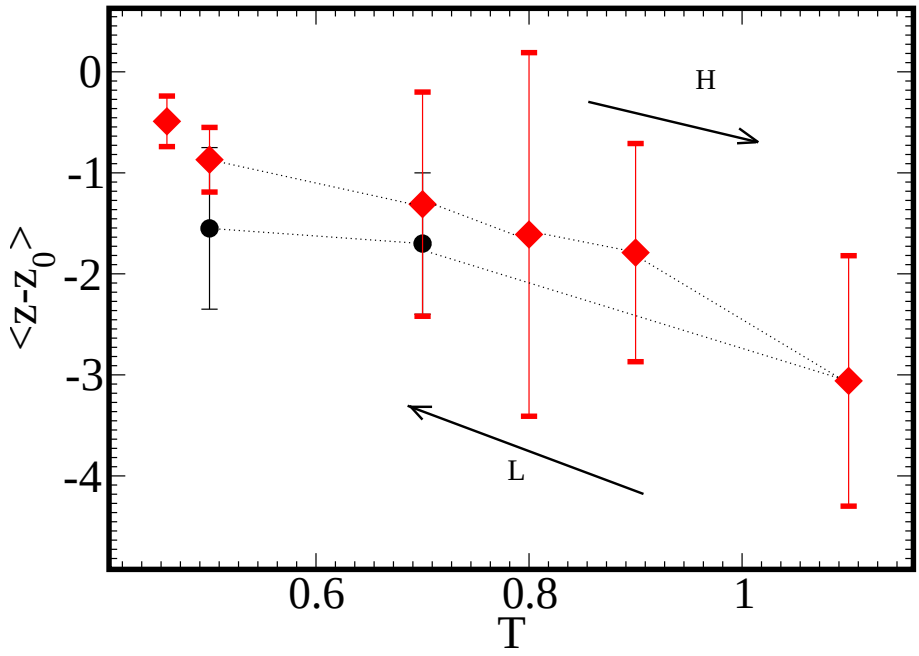

Figure 3.13: Simulation of a system with 14400 particles, starting from an initial configuration with a temperature $T = 1.1$ and cooling down to temperatures $T = 0.7$ and $T = 0.5$. The position of the particle with respect to the interface can be controlled by changing the temperature of the melt. The position of the particle with respect to the interface of the film is plotted, showing an hysteresis of the embedding of the particle by cooling.

When placing the particle above the polymer film at high temperatures it is obvious that, after long simulation times, the vertical distribution of the particle is under the position of the interface of the melt. Could the barticle go back to the interface indicating that the position followed is an equilibrium position? If the conclusions obtained in this section are right, then the particle never reaches again the interface and stays inside the film.

In order to test whether are we able to equilibrate the system, new simulations were performed with initial configurations where the particle is placed inside the film (This initial configurations are obtained from final configurations obtained from simulations at $T = 1.1$). The results are shown in fig. 3.12 and fig. 3.13: by 'heating' the system the tracking particle is able to embed into the melt and by cooling down to $T \sim T_g$ the particle approaches again to the interface, but the final vertical distribution is below the starting vertical distribution. The final temperature was $T = 0.5$; even for $T \sim T_g$ it is expected to observe the same result.

Why does the particle move from the bulk to the interface by cooling? In this case, the particle can not admit a thick layer of particles on its surface when $T \to T_g$, as was shown in the solutions for the hydrostatics on the nanoparticle (see fig. 3.7); hence when the particle is inside the film, and the system is cooled, the particle search a region with much lower density, in this case a region near the interface. But for temperatures $T \sim T_g$ the mobility of the particles at the interface is very low, preventing the particle from reaching the interface.[11]

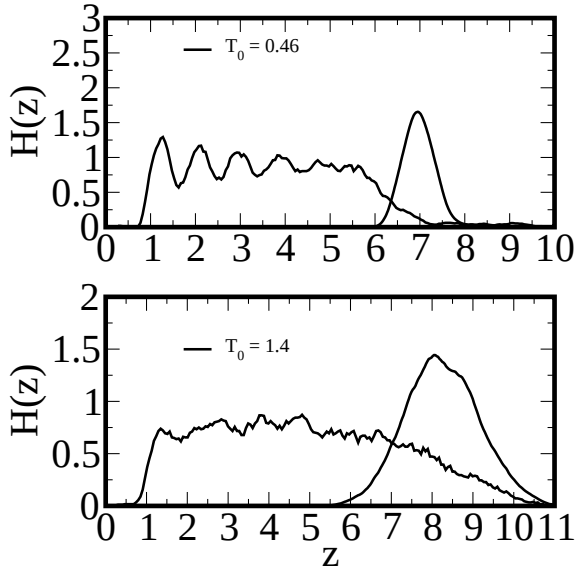

Figure 3.14: Distribution of the vertical position of the particle as a function of the temperature. The liquid has 2250 particles and $N = 10$. In this case the film is very thin and the particle can not sink; even for $T >> T_g$ it is possible to observe persistence of the position of the particle on the surface of the film.

In simulations done for very thin films the particle does not penetrate the polymer melt; even for $T >> T_g$ the distribution of the vertical position of the particle is centered near the interface of the film. In this case the very high density at the interface substrate-liquid has influence on the dynamics of the interface of the film and for this reason the particle is distributed only near the interface. In fig. 3.14 the vertical distribution of a nanoparticle in a very thin polymer film ($H \sim 3 * R_{eff}$) is shown for two temperatures. For $T \sim T_g$ the particle is distributed at the interface, as is expected, but for $T = 1.4$ the particle is also distributed at the interface of the film, in contrast to the results for thicker films (see fig. 3.14).

[11] This is therefore an interplay between the prewetting dynamics on the tracking particle and the interfacial dynamics of the film

3.5.1 Conclusions

In this section the statics of the system film nanoparticle was discussed. The vertical position of the nano particle depends on the temperature: the simulations shows that the probe has a persistence of the position near the interface when $T \sim T_g$ and is able to sink into the polymer film by increasing the temperature of the melt. This effect shows a glass transition temperature at the interface of the film by measuring the vertical distribution of tracking particles.

The density profiles in horizontal cuts of the polymer film near the particle were computed and shows the appearance of a layer of monomers on the hard core of the tracking particle, at $r = R_{eff}$. For very thin films the particle allways remains close the interface. The light embedding of the tracking particle into the film suggest that at the interface the density is smaller than inside the film.

The results of the present simulations shows hysteresis in the embedding process, implying that the presence of the nanoparticle at the interface at $T \sim T_g$ depends on whether the particle is situated in the initial configuration. If in the initial configuration the particle is above the film then the nanoparticle can be used as a sensor for the glass transition at the interface of the polymeric film; this concept is the computational analogous of the experimental method used by Teichoeb et al. [75].

The present simulations were done for non structured particles, either with LJ or modified LJ ones. In contrast with LJ particles, modified LJ ones have a hard core that allows the formation of a layer of particles close to the region defined by the effective radius R_{eff}. This potential therefore represents a particle with an adsorption surface that is able to attach monomers. This model is completely different to the simple LJ nanoparticle, which represents a smooth particle that simply collides with the liquid particles in its neighborhood.

This approximation gives reasonable good results but does not simulate real experiments, where clusters of nanoparticles of noble metals (for example gold) with diameters of 10Å are employed. As outlook it is interesting to replace the simple non structured particles by clusters of nanoparticles. An additional interesting point is the initial configuration at low temperatures: all the results obtained from the simulations at T_g were computed for particles placed above the interface of the film, but the embedding process shows that it is also possible to start simulations with initial configurations where the particle is placed inside the film. The advantage or disadvantage of each initial configuration depends on the phenomena to be analyzed. The first kind of configuration permits to make the analysis of interfacial phenomena, but is very hard to equilibrate; the second one is in contrast much easier to equilibrate. This particular point is thus a personal selection and depends on the particular problem to be investigated.

4 Dynamics of the nanoparticle in the polymer film

4.1 Abstract

The investigation about the motion of a particle in a polymeric film arises the question, whether a tracking particle can be used as a sensor of the dynamics of the complex fluid at the interface as well as in bulk.

In the present results the dynamics of the particle for different time regimes is analyzed and sensitivity of the dynamics of the nanoprobe to the glass transition temperature of the melt is found. It is shown that the diffusion coefficients of single monomers in the polymeric film is related with the self diffusion coefficient of the tracking particle. The information obtained from the displacement of the particle is used for the computation of the complex shear modulus of the liquid near the particle. The effect of the liquid-vapor interface on the dynamic of single particles is also analyzed in this section.

4.2 Introduction

4.2.1 Regarding the literature

Dynamics of the probe particles

The dynamics of particles in suspension in complex liquids is a phenomenon that has been intensively studied in the last years in order to understand viscoelastic properties of fluids [35] as well as the change of the dynamics of the fluid due to the presence of the particle [67][41]. In the first approach the nanoparticles are used as probe particles, where the response of the particle to the thermal fluctuations depends on the "mechanical susceptibility" of the fluid. This effect is studied using confocal microscopy. In this case the movement of the Brownian particle is described by a Langevin equation, but the fluctuation-dissipation theorem has a slight modification given that the medium stores energy: the correlation function between forces is no more given by a delta function but by a memory function [56], [55].

Alternative systems for complex probing particles are also studied in order to probe Glass transition behavior. The dynamics of a single rod in a glassy medium

was analyzed by Moreno and Kob with the aim to understand the diffusion of non spherical particles [47], where the particle shows similar features as the Brownian motion of single polymers.

Abdulwahab et al. used a similar approach as in the present work, making an attempt to understand transport properties of polymer-stabilized particles in environment and other applications [48]. In their simulations, they model hydrodynamic interactions that are taken into account to describe the diffusion properties of a stabilized particle; such approach is an alternative to the approach used in the present work.

Temporal and spatial scales in the system

The difference between the dynamics of the polymers and the dynamics of the liquids depends on the fluctuation frequency of the molecules and the wave length of the perturbation in relation to the separation between the molecules. In this sense, for low frequencies and long wave lengths the same molecules behaves like a mean field that conserves dynamical variables like momentum or energy; this is the starting point for the definition of hydrodynamics. But if the wavelengths are comparable with the intra molecular separation then this hydrodynamic picture is no more valid [30] [31] [32].

The Brownian motion is defined just on this scale, where the size of the nanoparticles particles can detect the motion of the surrounding liquid particles.[1]. There are two methods in order to obtain information of this system: Introducing external perturbations with some frequency it is possible to observe that for long wave-lengths and small frequencies the liquid behaves as a continuum, making possible the application of the equations of hydrodynamics; this case will be exposed later in the section dedicated to the linear hydrodynamics of moving particles on simple and complex liquids. If the perturbation frequencies are small, then the liquid behaves as a discrete medium [30]. The last situation is passive: the scale of the probe particle is on the order of the typical wave-length of the fluctuations of the particles of the liquid; in such a way the hydrodynamic effects are negligible for short and intermediate time scales [2].

4.2.2 Probe particles and microrheology

In the last years conventional experimental methods, employed for rheology based on the introduction and subsequent relaxation of perturbations in the viscoelastic

[1] In this case a rock in a liquid does not undergo Brownian motion, not only because it is very massive, with a subsequent big inertia, but also because a rock is too big in order to detect the motion of single particles in the liquid. But when the particle is not very large (but large enough respect to the classic theory for Brownian motion) then it is quite obvious that the velocity of the particle fluctuates around a mean velocity implying Brownian motion by hydrodynamic interactions [42].

[2] In some cases the velocity correlation function shows a power law decay for long times, where the exponent is given as $\frac{3}{2}$. For this long time tails it is necessary the use of hydrodynamics.

material, have evolved into the novel method called micro rheology, by means of the optical tracking of nanoparticles in viscoelastic materials [35] [50] [53].[3] In many experimental situations it is of special interest to analyze in a non invasive form the relaxation processes and dynamics of biological as well as non biological materials, for example of cellular membranes [38], making this technique a fundamental improvement for cellular and molecular biophysics. This technique is ideal for measurements at high frequency in contrast to traditional techniques in rheology. Some of the methods based on this idea are the tracking of probe particles with dynamic light scattering (DLS), fluorescence correlation spectroscopy (FCS) and single membrane channel conductance methods. The quantitative analysis of the data is based on the analysis of the displacements of the probe particles, where the Mean Square Displacement (MSD) is related to the linear relaxation kinetics obtained after a perturbation (so called Onsager Hypothesis). The first experimental approaches were based on the study of the spontaneous thermal fluctuations of gel materials using DLS; with this same technique the thermal fluctuations of particles in actin are studied. Using superior spatial and temporal resolution with photo diode detection (SPT) the investigation of viscoelastic materials at sub cellular and macromolecular level is done. Recent advances of SPT allow to apply this technique to study of macromolecules and cytoskeleton networks. With this technique it is also possible to understand molecular and cellular forces, being a complement to the standard method of the atomic force microscopy (AFM). Another application is the study of the dynamics of DNA and its conformational dynamics without perturbations, as well as the dynamics of such macromolecules in aqueous solutions. In this sense, the use of micro rheology is a basic milestone in the modern biophysics [52], because it brings the study of the complex mechanical response of bio materials from *in vitro* to *in vivo* experiments.

In these experiments, the local viscosity is represented by small scale structure and is estimated via the measurement of the displacement of small particles, whereas bulk viscosity could show bulk moduli. The connection between the Brownian motion of the particle and the bulk viscosity can be approached as an elasticity that is the same for a purely viscous fluid, under the assumption of non slip-Stokes-Einstein relationship can be generalized to all the frequencies. In this way a mean field assumption relates macroscopic stress relaxations with microscopic stress relaxations, i.e. there is no differentiation between local and global viscosity [50].

Another approach takes the elastic component of the suspending medium more directly into account. Non slip boundary conditions facilitates the movement of a sphere immersed in a viscous compressible liquid; if this sphere is subjected to a particular frequency the increase of the net velocity of the fluid around the sphere (compliance) is proportional to the inverse of the shear modulus. But for small frequencies this coupling does not exist, and the osmotic compressibility of the medium may also influence the Brownian motion of the tracking particle. Therefore

[3]The knowledge of the local viscosity can have additional applications in the comprehension of the conformation of proteins [66]

both the suspending and transverse moduli may influence the motion of a Brownian probe below some critical frequency[43] [44].

4.2.3 Structure of the present chapter

In the first section a short introduction about the theory of the dynamics of the nanoparticle as well as of the melt is made, where the analysis of different time regimes offers particular information on the behavior of the liquid molecules. In an special section the fundamentals of micro-rheology are explained.

In the part devoted to the exposition of results are described for short and intermediary time regimes the dynamics of the particle. A main point in this section is to analyze if it is possible to use the nanoparticle as a probe for the dynamics in the melt; for this reason the relation between the dynamics of the particle and the polymer dynamics is analyzed. Finite size effects as well as effects induced by the interface are also discussed. Finally some results of the computation of transport coefficients are shown. A particular point is the implementation of the computation of the viscoelasticity of the film using the velocity correlation function (VCF) of the particle.

4.3 Theoretical background

4.3.1 Short and intermediary time regimes

Equations of motion

The basic assumption in MD simulations is that there is a system with many particles that can be solved integrating the Newton equations of motion; in this way the equations of motion defines a density of points in the phase space which is constant. In particular there is interest in one relevant point, say a_1, the trajectory of the particle of interest, and a_2 the rest of particles. The Liuville equation in this case is [42]

$$\frac{\partial}{\partial t}\begin{pmatrix} a_1 \\ a_2 \end{pmatrix} = \begin{pmatrix} L_{11} & L_{12} \\ L_{21} & L_{22} \end{pmatrix}\begin{pmatrix} a_1 \\ a_2 \end{pmatrix} \tag{4.1}$$

where L_{ij} are the elements of the Liuville operator. The solution of the equation for a_2 is

$$a_2 = e^{L_{22}t}a_2(0) + \int_0^t e^{L_{22}(t-s)}L_{21}a_1(s)ds; \tag{4.2}$$

making a substitution of this equation into the differential equation for a_1 the fol-

lowing differential equation is obtained

$$\frac{\partial a_1}{\partial t} = L_{11}a_1 + L_{12}\left(e^{L_{22}t}a_2(0) + \int_0^t e^{L_{22}(t-s)}L_{21}a_1(s)ds\right). \tag{4.3}$$

In this equation the information of the initial conditions for $a_2(0)$ is irrelevant and replaced by a mean fluctuating element, which is the noise of the system. So the previous equation is equivalent to the generalized equation for the dynamical variable a_1 expressed as [30]

$$\frac{\partial a_1}{\partial t} = i\Omega_0 a_1 + R(t) - \int_0^t K(s-t)a_1(s)ds, \tag{4.4}$$

where Ω_0 accounts for the existence of propagation process associated with the time evolution of the time variable, $R(t)$ represents the random fluctuations in the system and the function $K(s-t)$ represent the memory or retardation effect of the liquid.

Two functions are necessary for the analysis of the dynamics of the particle: the Mean Square Displacement of the particle, MSD, and the Velocity Correlation Function, VCF. The MSD defined as

$$\Delta r^2 = \sum_{i=1}^{3}\left\langle \left(q^i(t) - q^i(0)\right)^2 \right\rangle, \tag{4.5}$$

where $q^i(t)$ is the coordinate of the particle, and the VCF defined as

$$\Psi(t) = \frac{\langle \dot{q}^i(t).\dot{q}^i(0)\rangle}{\langle \dot{q}^i(0)\dot{q}^i(0)\rangle}; \tag{4.6}$$

in this formula the VCF is represented in its normalized form.

From this equation is possible to make a derivation of the differential equation that describes the VCF, which is given by [30]

$$\frac{d\Psi(t)}{dt} = -\int_0^t K(t-t\prime)\Psi(t\prime)dt\prime. \tag{4.7}$$

The information obtained from this equation contains essential features of the relaxation dynamics of the system. For very short times the behavior of the memory function is similar to the Force Correlation Function, FCF. For long times the memory function equation tends asymptotically to the simple Langevin equation; in an asymptotic limit the memory effect vanishes and gives

$$\frac{d\Psi(t)}{dt} = -\gamma\Psi(t), \tag{4.8}$$

that means, for infinite times the correlation function decays exponentially; this asymptotic limit is the Markovian limit of the general non Markovian generalized Langevin equation. In fig. 4.1 is possible to observe the contrast between a pure Markovian example and some results taken from computer simulations.

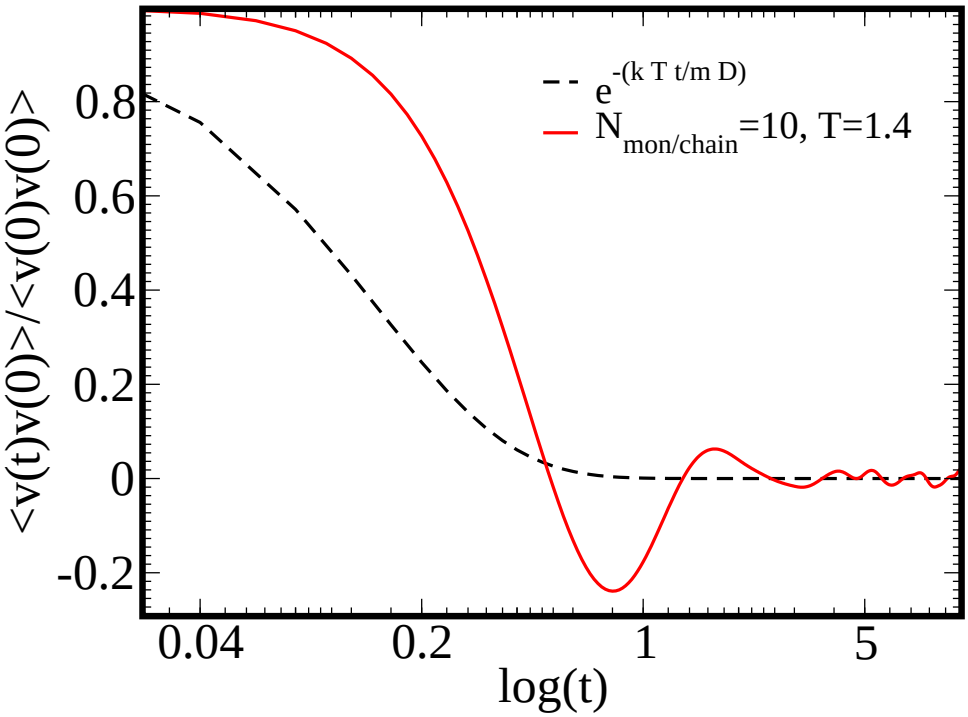

Figure 4.1: VCF of a tracking particle in a complex fluid ($N_{mon/chain} = 10$) in contrast with the prediction of the conventional theory for Brownian motion at $T = 1.4$. The conventional theory does not take into account the appearance of memory effects in the VCF.

Some aspects of the kinetic theory

The movement of the particle in a liquid is due to the collision of fluid particles with the probe particle. For simple liquids one considers two principal time windows: the ballistic regime and the transition from a ballistic into a diffusive regime [34]. The ballistic regime is characterized by the inclusion of switch on effects, i.e. for $t >> 0$, $v(0)e^{-t\alpha}$, that means the relaxation of the initial velocity of the Brownian particle is take into account[4].

In dense or complex liquids, the intermediary time scale is given by the convolution of relaxation processes that take place in the liquid and is sensitive to variations of temperature and density. So, in this time regime the VCF reflects essential characteristics of the fluid (please refer to fig. 4.1 and fig. 4.2). For low densities $\Psi(t)$ decays exponentially, as is shown in the figure 1, whereas for complex fluids this function is like a damped oscillation (fig. 4.1 and fig. 4.2); this fact is related to many body correlation effects in the fluid.

For high densities the VCF shows an over damped behavior and after some time eventually reaches negative values. This fact is related to repetition of correlated

[4]That means, the ballistic regime is the relaxation of the initial velocity of the Brownian particle.

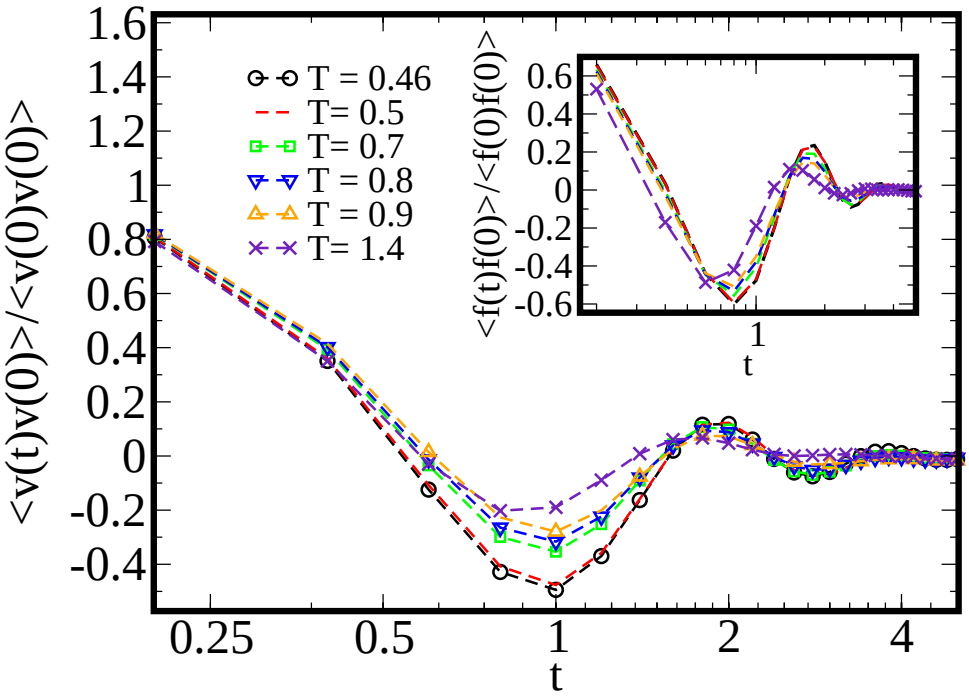

Figure 4.2: Computation of the VCF of a tracking particle embedded in a polymeric fluid with 14400 monomers, each polymeric chain consist of 10 monomers, adsorbed on a flat substrate. The simulation was performed in a two dimensional periodic box. This plot show a damped oscillation of the VCF, suggesting an oscillation inside the solvation shell; for infinite times the VCF tends to be zero. For short times a negative tail of the function appears, even for temperatures above the glass transition temperature.

collisions with neighboring particles; this last ones form the so called 'cage' around the particle [56] [63]. After some time the particle is able to escape from the cage and the correlations in the system relaxes; in such a time regime the particle is able to diffuse.

4.3.2 Long time regimes: diffusion

With the information of position and velocity it is quite evident that the possibility to deduce the transport coefficients in the liquid using the dynamical variables of the nanoparticle. The first coefficient that can be directly estimated is the diffusion constant. There are two equivalent methods for the estimation of this coefficient: the first one is based on the measurement of the Mean Square Displacement, the second on the VCF. The diffusion coefficient can be computed as

$$D = \lim_{t\to\infty} \frac{1}{2d} \frac{\langle \Delta \overrightarrow{r}^2 \rangle}{t}, \tag{4.9}$$

in this equation $\overrightarrow{r} = r_i \overrightarrow{e}^i$ and d is the dimensionality of the Brownian motion of the particle. In the present system there are periodic boundary conditions on x and y; in this plane the particle is able to diffuse. Along the axis z the particle is able to stay on the fluid surface or sink into the film; hence the movement is confined on this direction and no diffusion can occur (The fluid film is like a swimming pool where the swimmer is free to move on an horizontal plane; but the swimmer is restricted to submerge only to the bottom of the pool). In order to avoid problems related to anisotropic diffusion (which is out of the focus of this project) the MSD is measured in the (x, y) plane. In the figure 3 the effect that the anisotropy induces on the MSD is nicely shown.

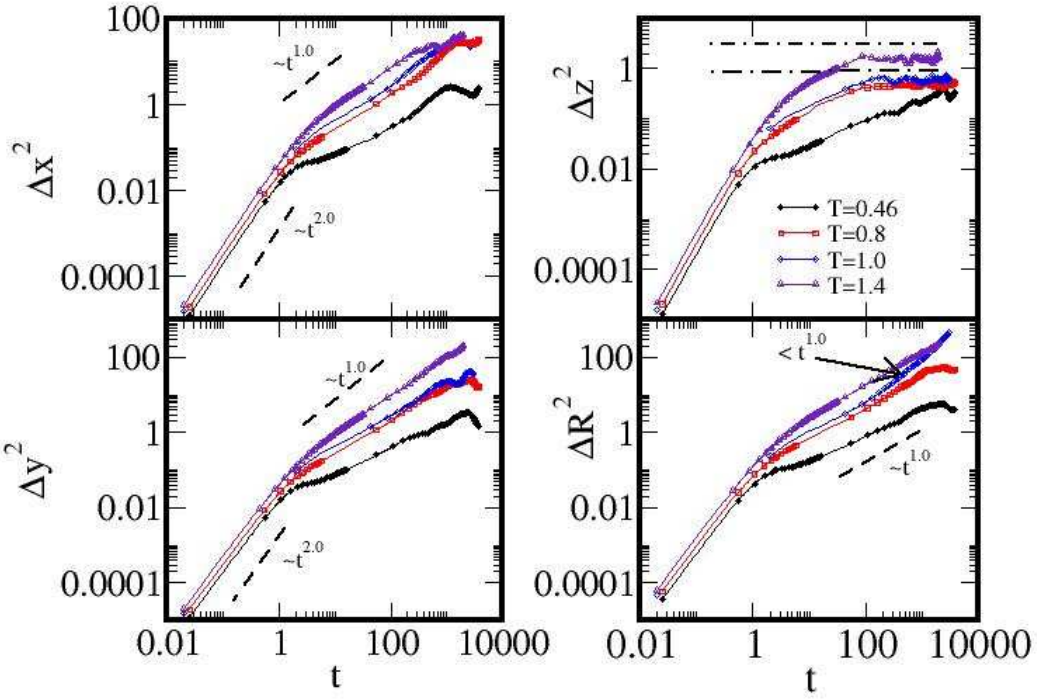

Figure 4.3: In this plot the MSD of the tracking particle in the fluid film is resolved along the x, y and z axis together with the total radial coordinate $R^2 = x^+y^2 + z^2$ ($N_p = 2250$, $N = 10$). The particle diffuses freely along the $x - y$ axis, but reaches a saturation for many of the simulated temperatures along the z axis. It is quite evident to recognize a diffusive behavior when the MSD can be fitted by a function t^{D*t}. The effect introduced by the anisotropy is evident in the non diffusive behavior of ΔR^2.

From a statistical mechanics point of view it is possible to make the computation of the diffusion coefficient using the correlation of the velocities of the particle [33]. This correlation first relaxes in very short times to zero; only for long times it is

expected that the diffusion equation is valid. The diffusion coefficient is obtained as the integral in time of the VCF, for times longer than molecular times

$$D = \frac{1}{d} v_0^2 \lim_{t\to\infty} \int_0^t \Psi(t\prime) dt\prime; \tag{4.10}$$

here d is again the dimension of the system. [5] The plot of $D_{VCF}(t)$ shows for short times a principal peak (which corresponds to the negative tail of the VCF, i.e. the effect of the cage on the particle) and a repetition of secondary peaks which again represent the oscillation of the particle inside the cage.

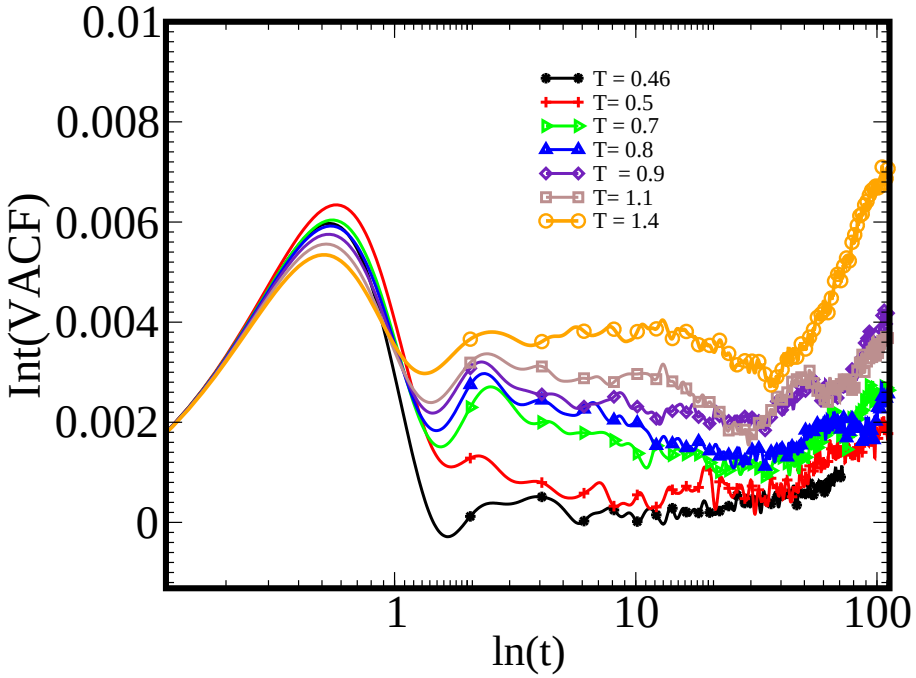

Figure 4.4: $D_{VCF}(t)$ obtained as the integral of the VCF in the time. For long times the formation of a plateau like behavior is evident; this corresponds to the region where the particle freely diffuses, i.e. where D is a constant. For short times memory effects appear to dominate the system; this fact implies an oscillatory behavior of this function.

The main interest here is the long time behavior for the measurement of the self diffusion constant. The division of the MSD by time, which converges to the same value as the integrals of the VCF, the value of the diffusion constant of the particle. In fig. 4.5 this method is presented for simulations performed for a nanoparticle in a polymeric film with $N = 10$ (in this plot only the long tail for $D_{MSD}(t)$ is plotted; the results for $N_{mon/chain} = 50$ will be presented later). For longer times D_{MSD} and D_{VCF} converge into a plateau like behavior which corresponds to the value of the self

[5] Here $T = \frac{2}{d}\frac{1}{K}\left\langle \frac{1}{2} m \sum_i v_i^2 \right\rangle$ such that $\langle v^2 \rangle = \frac{2KT}{m}$.

diffusion coefficient. For short times repeated collisions on the suspended particle take place, the so called ring collisions. These are correlated collisions which leads to non linear kinetic equations. Such correlations are more evident for a probe particle of variable size and mass in a dense fluid. If the particle is large, then correlated collisions will be considered, because $R_{coll} >> \Sigma$, where Σ is the mean path of the molecule. In such case many ring collisions take place before the molecule moves away.

After long times the diffusion coefficient for large molecules, considering slip boundary conditions, is given by

$$D = \frac{k_B T}{4\pi\eta\,(R_{coll}/2)}. \tag{4.11}$$

In the simulations the slip condition holds for all the particles in the fluid. In particular, the simulation considers a non structured probe particle and therefore this relation holds for the nanoprobe immersed in the fluid [6].

Microrheology

A polymeric liquid presents a kind of duality between a solid and a pure liquid. Solids store mechanical energy and are elastic; fluids dissipate mechanical energy and are viscous. Many materials, including polymer melts, are viscoelastic; i.e. store and dissipate energy. The elastic susceptibility is described by means of the complex shear modulus. In the following section there will be developed the theory related to the viscoelastic response of a probe in a liquid.

The complex shear modulus[7] describes the elastic susceptibility

$$G^*(\omega) = G\prime(\omega) + G"(\omega), \tag{4.12}$$

which is the stress in a material when an oscillatory force is applied. The real part is the storage modulus, which is the ratio between the elastic component of the stress tensor with the strain, and the imaginary part is the loss modulus; in this case the stress and the strain are in phase

$$G\prime = \frac{\sigma_{el}^{ij}}{\dot{\gamma}^{ij}}. \tag{4.13}$$

The imaginary part of the susceptibility is the ratio between the viscous part of the

[6] The slip boundary conditions can be modified if the displacement of the particle is measured together with adsorbed layer: in this case the particles at the interface of the particle can induce slip length or stick boundary condition. But in the present case only the tracking particle is considered.

[7] This modulus is similar to the complex dielectric constant.

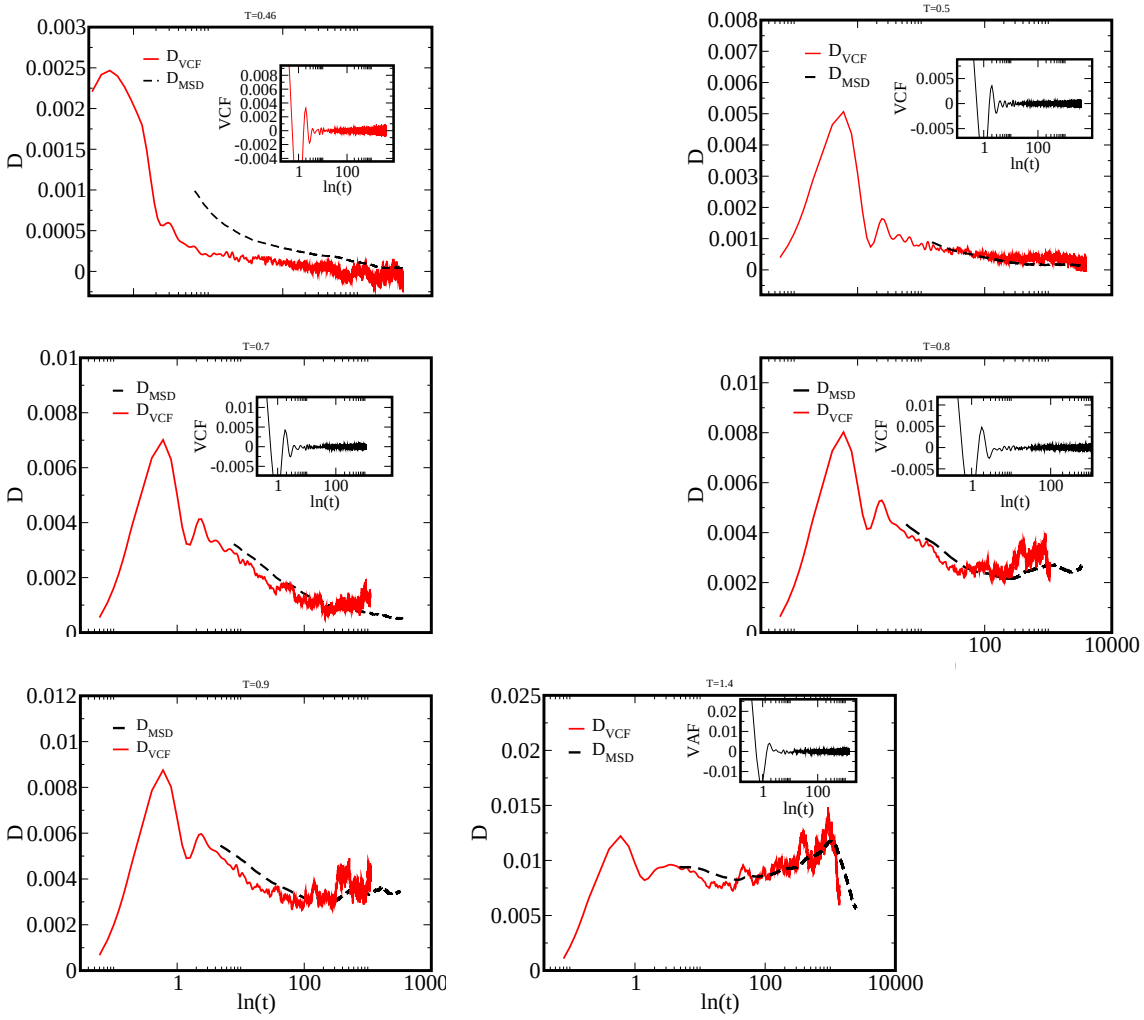

Figure 4.5: Method for the computation of the Diffusion coefficient. $D_{MSD}(t)$ corresponds to the MSD divided by the time, whereas $D_{VCF}(t)$ correspond to the integral of the VCF. In this plot only the long time behavior of D_{MSD} is represented. The convergence region, where both functions reaches a plateau, is the diffusion regime where the diffusion coefficient is a constant. In this system $N = 10$ and $N_p = 14400$.

stress and the strain and is called the loss modulus; the tress is out of phase with the strain

$$G" = \frac{\sigma^{ij}_{visc}}{\dot{\gamma}^{ij}}. \tag{4.14}$$

By causality the stress and strain are related through the Kramers-Kroning relation

$$G\prime(\omega) = frac2\pi \int_0^\infty \frac{G"(\zeta)d\zeta}{\zeta^2 - \omega^2}. \tag{4.15}$$

The contributions of the storage and the loss modulus depend on the frequency. For simple liquids frequencies are big enough to make measurements with conventional

experimental methods. But for complex fluids the relevant frequencies can be very small, because there is in those system a coupling of many different time scales. It is necessary either to improve the experiments in order to cover a big spectrum of frequencies or to propose novel experimental alternative methods. This improvement is based on the measurement of the displacement of nanoparticles, as proposed by Mason and Weitz [44] [35] [50]. In those experiments the bulk mechanical susceptibility is coupled to the response of the colloid. Is there a justification in the theory for the implementation of this method?(see for example [39] for a resume about microrheology). The viscoelasticity appears like the response of a viscoelastic medium to external perturbations; and in this case the perturbations are the thermodynamic fluctuations of the colloidal particle. Therefore the determination of the response of the viscoelastic fluid is done in the frequency regime of the thermal fluctuations. In this computation there are two main expressions that include two principal relaxation processes: first the viscoelastic stress tensor expressed as the convolution of the strain with a memory function, called the Maxwell constitutive equation

$$\sigma^{ij} = \int_0^t K_{visc}(t\prime)\dot{\gamma}^{ij}(t - t\prime)dt\prime, \tag{4.16}$$

and the equation for the velocity correlation function

$$m\frac{d\phi(t)}{dt} = -\int K_{VCF}(t\prime - t)\phi(t\prime)dt\prime, \tag{4.17}$$

where the VCF is defined as

$$\phi(t) = \langle v(t)v(0)\rangle\,. \tag{4.18}$$

The Laplace transform of the first equation gives

$$K_{visc}(s) = \frac{\sigma^{ij}(s)}{\dot{\gamma}^{ij}(s)} = \eta, \tag{4.19}$$

that means, this memory function is connected with the viscosity of the system; this function can be either a tensor of fourth grade or a constant (that means the tensor reduces to constant coefficients in the diagonal). From the theory of viscoelasticity it is known that the shear modulus is connected with the viscosity (for infinite frequency)

$$G^*(s) = s\eta(s). \tag{4.20}$$

The fundamental supposition in the present theory is that the Memory Function for the VCF is related with the Memory Function for the viscoelastic medium. In Hydrodynamics the stress tensor is defined as the sum of the pressure-stress tensor, the stress tensor connected with the bulk viscosity and the shear stress tensor

$$\sigma^{ij} = \sigma^{ij}_P + \sigma^{ij}_{bulk} + \sigma^{ij}_{shear} = g^{ij}\left(P + \eta_{bulk}\nabla^i v^i\right) + \eta_{shear}\nabla^i v^j, \tag{4.21}$$

so the viscosity stress tensor is the sum of one tensor that is a functional of the metric tensor and a second tensor

$$\sigma^{ij} = g^{ij}\sigma_{bulk} + \sigma^{ij}_{shear}, \tag{4.22}$$

where σ^{ij}_{Shear} has off diagonal elements different from zero. That is, the memory function for the viscoelasticity can be expressed as a functional of such metric

$$K_{visc}(s) = K_{visc}(s)\left[g^{ij}\sigma_{Bulk} + \sigma^{ij}_{Shear}\right]. \tag{4.23}$$

Now, if small perturbations around the bulk viscosity are introduced and a functional expansion of this memory function in therms of the general viscosity is made, then

$$K_{visc}(s)[\sigma^{ij}] \sim K_{visc}(s)\left[g^{ij}\sigma_{Bulk}\right] + \frac{\partial K_{visc}(s)}{\partial[\sigma^{ij}_{Bulk}]}\frac{\sigma^{ij}_{Shear}}{\dot{\gamma}^{ij}} + \cdots, \tag{4.24}$$

for σ^{ij}_{Shear} small [8]. If the fluctuations of this memory function around the shear tensor are small then the memory function can be expressed as

$$K_{visc}(s) \sim K_{visc}(s)\left[g^{ij}\sigma_{Bulk}\right]. \tag{4.25}$$

In the present case all the elements of the fourth rank tensor reduce to the elements of the diagonal that are different from zero, because it depends only on the metric tensor; physically, this last result implies that the memory function expresses the dissipation function in the bulk.(So strictly speaking a computation of the shear modulus accounts only for bulk contributions).

Due to the fact that in the fluctuation-dissipation theorem the fluctuation is connected to the dissipation in the bulk it is quite obvious to relate the memory function for the VCF with the memory function in the bulk

$$K_{visc} \sim K_{VCF}. \tag{4.26}$$

This affirmation must be taken with care and is no more valid when the oscillations of the memory function in the shear regime grow, for example near interfaces. The memory function at the left side is related with a global relaxation function; the right function is local; that means, this equation is a mean-field like approximation.

[8] For very complex experimental or simulation conditions the element $\frac{\partial K_{visc}(s)}{\partial[\sigma^{ij}]}$ can be approximated as the differential of the memory function respect to the stress tensor, i.e.:
$\frac{\partial K_{visc}(s)}{\partial[\sigma^{ij}]} \sim \frac{K_{visc}(s_2) - K_{visc}(s_1)}{\sigma^{ij}(s_2) - \sigma^{ij}(s_1)}$
The use of this general formula requires the knowledge of the variation of the memory function with respect to the bulk viscosity.

Applying the Laplace transform to this equation on the relation for the memory function the following expression is obtained

$$sm\phi(s) - m\phi(0) = -K(s)\phi(s), \tag{4.27}$$

implying

$$K(s) = \frac{k_B T}{\phi(s)} - sm, \tag{4.28}$$

where $\phi(0) = k_B T/m$, is the initial correlation function (k_B is the Boltzmann constant). Wherefore the complex shear modulus is given as a function of the VCF as

$$G^*(s) = \frac{s}{4\pi R}\frac{k_B T}{\phi(s)} - s^2 m, \tag{4.29}$$

where the first therm reflects the fluctuation-dissipation in the system; here R is the radius of the nanoparticle; in this relation it is taken into account that slip boundary conditions are present[9]. The second therm is related to inertia. If $s \to 0$ this therm is negligible. In this manner one obtains a frequency free viscosity connected with the diffusion of a free particle; i.e., given that

$$s^2 \Delta r^2 = 6\phi(s); \tag{4.30}$$

then

$$G^*_{Diff}(s) = \frac{1}{4\pi R}\frac{k_B T}{s\Delta r^2}, \tag{4.31}$$

taking into account the sum over all the contributions of the collisions of the fluid particles with the nanoparticle. It is then possible to express the Laplace transform as a functional of the Fourier transform cosidering that

$$G^*_{Diff}(s) = \frac{1}{2\pi}\int_{-\infty}^{\infty} d\omega \frac{G^*_{Diff}(\omega)}{s - i\omega}, \tag{4.32}$$

for $s \sim i\omega$ the integral reduces to $G^*_{Diff}(s) = G^*_{Diff}(\omega)$. Using this result the following expression for the shear modulus is obtained

$$G^*(\omega) = i\omega\frac{1}{4\pi R}\left[\frac{k_B T\left(\phi\prime(\omega) - i\phi"(\omega)\right)}{\phi\prime(\omega)^2 + \phi"(\omega)^2} + \omega^2 m\right]; \tag{4.33}$$

from this computation the storage modulus is thus

[9]This a modification with respect to Weitzs theory: there, the experiments are for structured nanoparticles with stick boundary conditions; but in the computer simulations the nanoparticle is represented as a soft LJ one that can not produce stick. So, the factor 6 in the original theory must be changed to the prefactor 4 in the computer simulations.

$$G\prime(\omega) = \frac{1}{4\pi R}\frac{\omega T \phi"(\omega)}{\phi\prime(\omega)^2 + \phi"(\omega)^2}, \tag{4.34}$$

and the loss modulus is

$$G"(\omega) = \frac{1}{4\pi R}\left[\frac{\omega k_B T \phi\prime(\omega)}{\phi\prime(\omega)^2 + \phi"(\omega)^2} + \omega^2 m\right]. \tag{4.35}$$

Both results satisfy the Kramers-Kroning relation. This result is only valid if the radius of the particle is small compared to the mean free path of the bath particles; therefore for very large particles this relation is no more valid (strong dependence on the diffusivity of the particle on the size of the particle).

4.4 Results

The dynamics of the particle is analyzed using the information of its displacement. The Hamiltonian describing the dynamics of the melt contains the potentials introduced in the section dedicated to the technical details; such Hamilton functions has no intra molecular bond angle potential and therefore there is no tendency in the chains of the melt to become stiffer at lower temperatures. Consequently, the size of the chains does not change dramatically along the whole temperature range of the present simulation. [18] [80] [45]

For the analysis of the following results Δr^2 was fitted using the formula

$$\Delta r^2 = at^x \tag{4.36}$$

The simulation of a single particle produces a very poor statistics. In the present results the statistics of the measurements done on the particle is improved by doing parallel runs for each temperature in the melt. In fig. 4.6 the vertical position of the particle for different runs is shown; in this result it is obvious that in some of these runs there are further relaxation process that allows further embedding of the nanoparticle. This effect induces a change in the slope of the MSD. This case will be shown later in the section devoted to the description of the results (see fig. 4.14).

4.4.1 Short times

Ballistic regime and analysis of $\Psi(t)$

First the nanoparticle has a ballistic behavior, where the MSD is proportional to the square of the time. The ballistic regime is related to the mean kinetic energy of the melt; so, dividing the MSD with the temperature a coincidence of the MSD appears for all the temperatures in all of the computations. In this case, the displacement of the nanoparticle is proportional to the time elevated to a constant $x < 1$. In

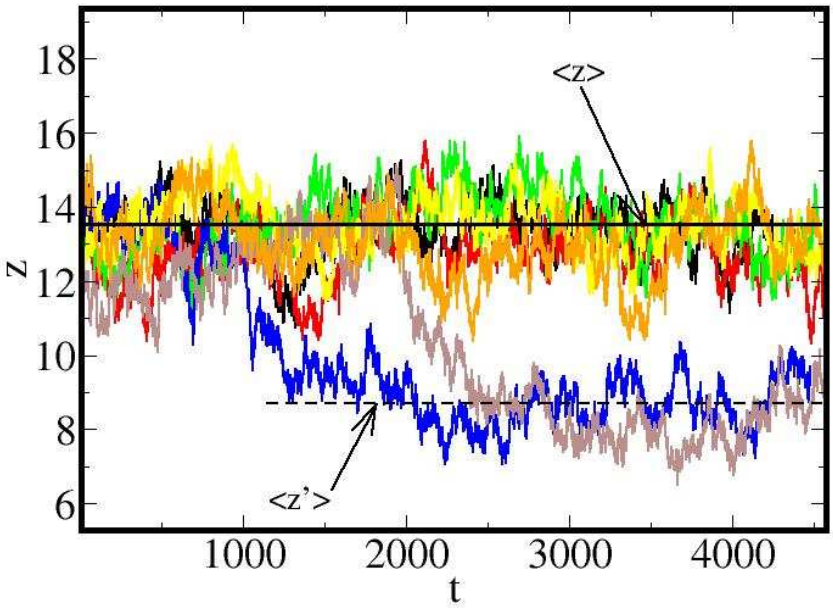

Figure 4.6: Parallel runs for each temperature were performed in order to improve the statistics of the system. In this plot there are represented the runs for $T = 1.2$, showing the vertical position (z coordinate) of the particle. For some of these runs an additional embedding of the particle in the melt after some simulation time is quite evident, suggesting that further relaxation process takes place in the melt. This additional embedding affects the computation of the MSD.

the conventional Langevin equation the memory function is taken to be a constant that describes the dissipation in the system; therefore the VCF has an exponential decay: the average of the product of two velocities is the same as the equilibrium ensemble average, as the system is ergodic (the phase average can be identified with a time average over infinite time). This theory implies that the particle lost very fast the information of the initial collisions. The simulations of the tracking particle shows in $\Psi(t)$, for particles with $R_{eff} > 1$, that this behavior does not hold. Even for $T = 1.4$, $\Psi(t)$ shows an oscillatory character similar to a Bessel function of order zero. For very short times it is quite evident that $\Psi(t)$ is the same for all the temperatures. Then for $0.25 < t < 0.5$ the characteristic dip of the function is observed, making each VCF a function of the temperature. For $t \sim 1$, $\Psi(t)$ has a negative tail; thereafter follows a peak -characteristic also for all temperatures- and then the function relaxes (refer again to fig. 4.2). For $t \to \infty$ one has $\Psi(t) \to 0$. This result shows that molecular motions in the time region $t \to \infty$ are dominated by the repulsion of neighboring molecules, leaving to conclude that the behavior of the nanoparticle in a complex fluids does not approaches the conventional Ornstein-

Uhlembek process, even for high temperatures (fig. 4.1). The derivative of the VCF is related to the memory function associated to $\Psi(t)$. The result of the simulations suggest a persistence of the memory function for $0 < t < 2$. For high temperatures this function relaxes in $1 < t < 2$, whereas for low temperatures this function relaxes for $t \sim 2$. The effect of the number of monomers in each chain is reflected in the dynamics of the particle at long times and will be analyzed in the next sections; for short and intermediary times the connectivity of the chains has no influence in the dynamics of the nanoparticle and therefore there is no particular difference in $\Psi(t)$ for two different simulations in two different melts (see fig.4.7).[10].

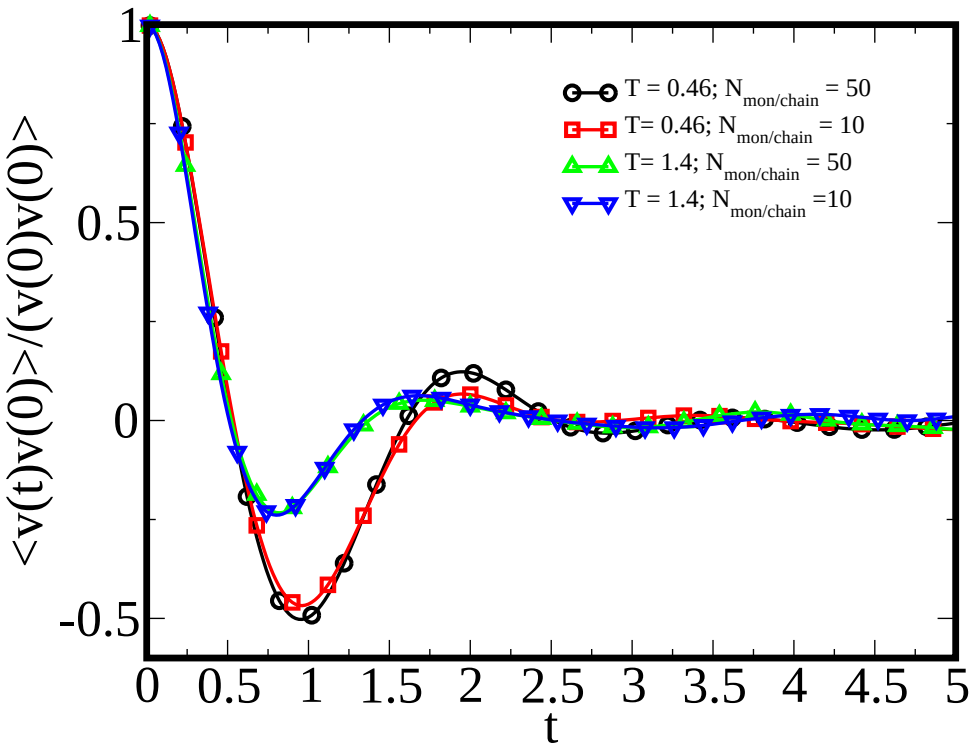

Figure 4.7: Two different VCF of the tracking particle for two different situations: one when the liquid is composed of polymer chains with $N_{mon/chain} = 10$ and the other one with $N_{mon/chain} = 50$. In short times and $T > T_g$ the VCF of the nanoparticle has no dependence on the number of monomers in the chain.

Time behavior of the caging and relaxation of the displacement of the nanoparticle

The duration of the caging for g_0 is $0.1 < t < 100$, i.e. it has a long duration. Making a comparison with the duration of the caging of the single nanoparticle it is found that the time duration of the plateau in the MSD of the tracking particle

[10]Fluctuations of the VCF after this times are thus associated to noise and not to relaxation effects.

is smaller than the time of the plateau of single monomers [80] [14]. The MCT relates the relaxation time with the glass transition temperature of the liquid [25]. In fig. 4.8 the trajectory around the particle in the $x-y$ plane is shown for two different temperatures. For temperatures close to the glass transition temperature an arresting of the trajectory appears, which is related to the cage of the particle.

From a qualitatively point of view it is evident where the caging for single monomers in the melt begins at $t_{cg\_g_0}$; for the center of mass of the chains this time is approximately 0.1, similar to the time where the caging of the nanoparticle begins, t_{cg_prt}. For simulations done with $N_T = 2250$ monomers the particle evolves sooner from a ballistic into a caging regime than for a system with $N_T = 14400$ (please see fig. 4.9 and fig. 4.12). In the present simulations the difference of the cage size was $\Delta\sigma_{cage} \sim 0.01$.

It is interesting to observe that the size of the cage for $R_{eff} = 5.0$ is similar to the size of the cage for $R_{eff} = 4.0$; this result suggest that the size of the cage does not changes by changing the size of the particle. For $T >> T_g$ the particle pretend to evolve from a ballistic into a diffusive regime for all the system that was simulated. That implies, the caging of the nanoparticle is related to the typical glass behavior of the melt.

Caging of single monomers in the polymer film: tracking particles to define the glass transition of the liquid

The dynamics of the tracking particle is compared with previous results obtained for similar systems (in particular results obtained from the simulation of dense melts between two plates, presented in fig. 4.10. The displacement of single monomers in the melt is given by

$$g_0 = \left\langle \left[q^i(t) - q^i(0)\right]^2 \right\rangle \tag{4.37}$$

where q^i is the position of a single monomer, and:

$$g_3(t) = \left\langle \left(\overrightarrow{R}_G(t) - \overrightarrow{R}_G(0)\right)^2 \right\rangle \tag{4.38}$$

where $\overrightarrow{R}_G$is the center of mass of the chain. [11]

[11] In the same model the displacement of the single monomers is also analyzed; for the inner monomers the displacement is analyzed using the following definition

$$g_1(t) = \left\langle \left(\overrightarrow{r}_{N/2}(t) - \overrightarrow{r}_{N/2}(0)\right)^2 \right\rangle \tag{4.39}$$

whereas the displacement of the end to end monomers is defined as

$$g_4(t) = \left\langle \left(\overrightarrow{r}_{end}(t) - \overrightarrow{r}_{end}(0)\right)^2 \right\rangle \tag{4.40}$$

It is possible to make equivalent definitions in the center of mass reference frame of the chain, denoted by $g_2(t)$ for the inner monomers and $g_5(t)$ for the end monomers.

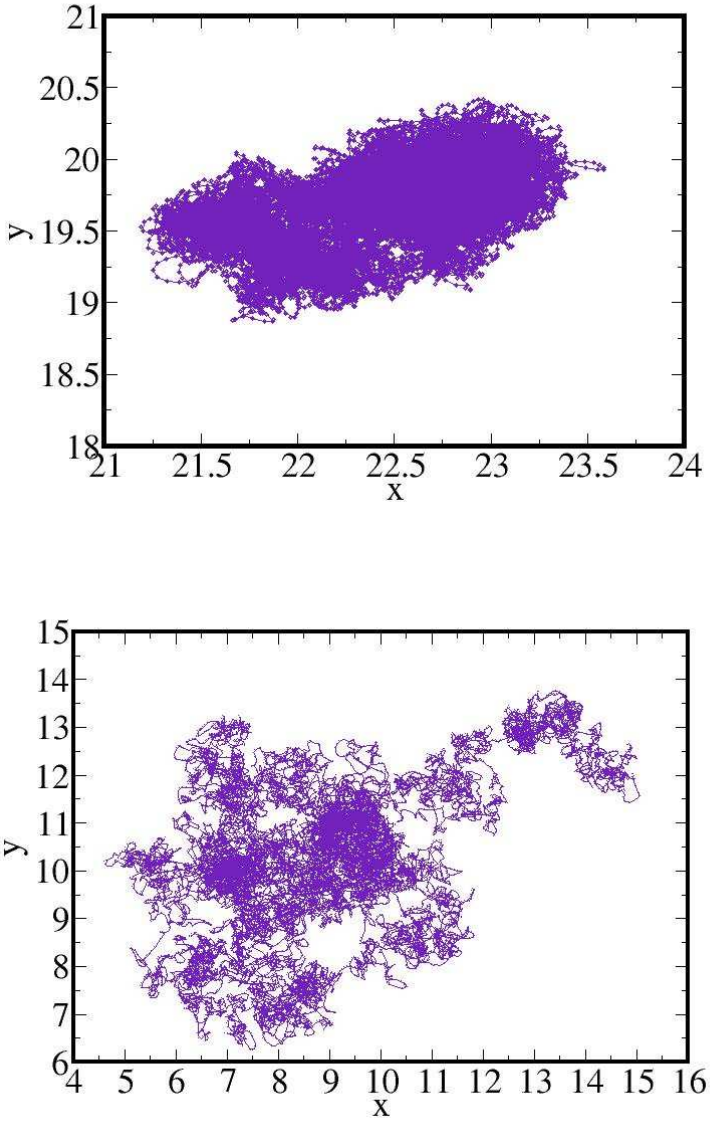

Figure 4.8: Position of the particle in the $x - y$ plane. In the first panel the temperature of the melt is $T = 0.46$; in the second one the temperature is $T = 1.4$. In both cases the displacements are shown for three million of molecular dynamics steps. At low temperatures it is easy to observe that the solvation shell prevents the free diffusion of the particle; for $T > T_g$ the particle has diffused in all the simulation box.

At relatively low temperatures the ballistic regime of g_0 evolves into a sub diffusive behavior predicted by many theories [28]. For temperatures close to the glass transition there is a coupling of many relaxation effects. Thus for short times the dynamics of single monomers evolves from a ballistic regime into a plateau like regime that precedes the sub diffusive one. This plateau is related with the cage which is

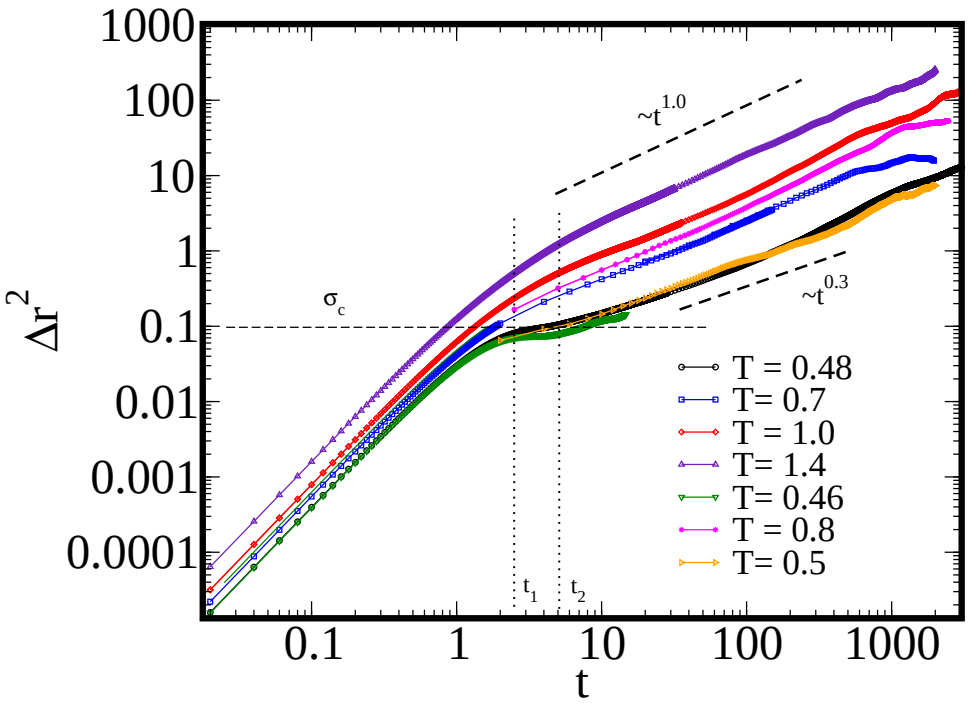

Figure 4.9: Radial MSD for a liquid composed of 2250 particles. In this plot a transition form a ballistic into a diffusive regime is observed for temperatures above the glass transition temperature; for temperatures close to the glass transition temperature a plateau in the MSD appears, which is related to the caging of the particle. The duration of the caging regime is relatively short and MSD evolves into a subdiffusive regime with a characteristic slope of 0.3.

typical for glass formers (see for example in Varnik or Aichele [80] [14]). Given the extension in time of this behavior, the diffusive behavior is only found after long times. The results of the present work show very nicely that, for temperatures close to the glass transition temperature, the dynamics of the single nanoparticle has also a transition from a ballistic into a plateau like behavior. The caging of the particle depends on the density and temperature of the liquid and can be observed for also for simple liquids. The size of the cage of the nanoparticle is bigger than the typical size of the cage for monomers encountered in previous works: the present result show that $0.03 < \sigma_{cage(part)} < 0.04$, whereas the cage for monomers is $0.3 < \sigma_{cage(g_0)} < 0.4$ (For this comparison the results computed by M. Aichele, fig. 4.10 were used); making the comparison of the size of the cage for g_3 it is quite evident that it is more related with the cage of the tracking particle. Additionally, the size of the cage of a nanoparticle in a complex fluid in bulk is slightly smaller than the size of the cage for a nanoparticle on a film [12]. Therefore for short times the dynamics of the nanoparticle is coupled to the dynamics of the center of mass of the chains. This result is interesting because using the displacement of tracers in a

[12]This affirmation is valid only when the particle in the initial configuration is above the film

dense melt it is possible to measure the critical behavior of the last one; the crossover from a ballistic regime into the cage is a function of the size of the nanoparticle. So the relaxation at later times must also be a function of the dimensions of the particle. This point is problematic if the tracking particle is used as a detector: it is quite obvious that it is possibly to use it in a qualitative way but not as an accurate quantitative method.

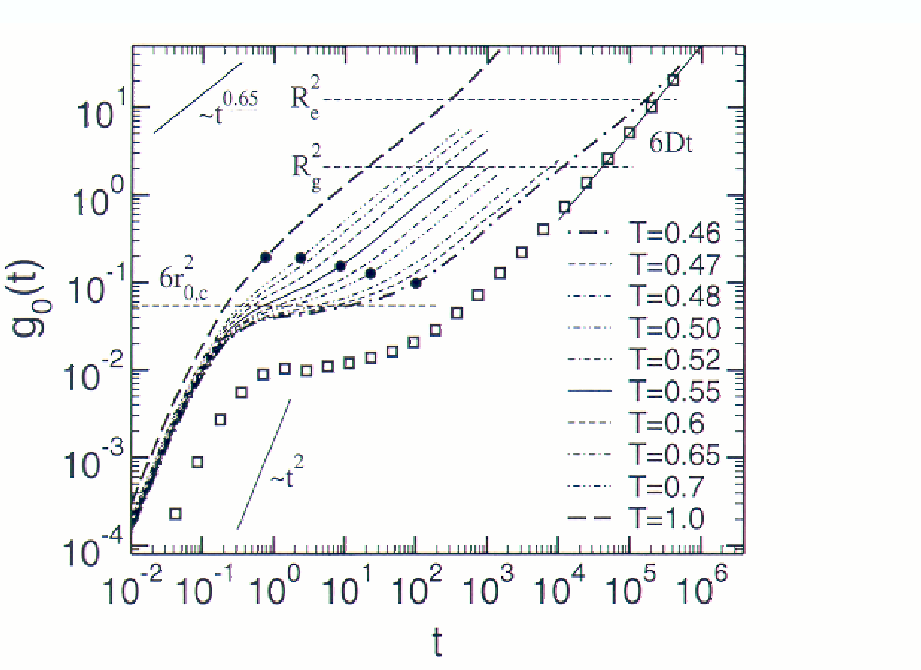

Figure 4.10: Dynamics of single monomers and CM of the chains. This results was taken from M. Aichele's PhD. Work.

It was shown that the embedding of the particle depends on the the temperature in the melt. In the fig. 4.11 an snapshot of the particle in the liquid for two different temperatures (and after two million of simulation steps) is shown; there it is evident that at temperatures close to the glass transition temperature the particle is near the liquid-vapor interface. For temperatures above the glass transition temperature the particle sinks (See chapter 3). This fact implies that the relaxation of the nanoprobe depends not only on the relaxation of the polymers in the liquid but also on the relaxation of interfacial phenomena (probably capillary waves). The relation of the slope of the MSD for a nanoparticle in a bulk must be different to the particle in the film. So the main idea is to proof the effect of the interface on the dynamics of the nanoparticle by making representative simulations in bulk (at two temperatures) for simple as well complex fluids (the film thickness is either $H_{0\Gamma} = 9$ or $H_{0\Gamma} = 15$, i.e. large enough in order to take into account the influence of the substrate on the

particle). In the bulk of the complex fluid, the occurrence of the plateau happens earlier than in the film, whereas in a bulk (of a simple liquid) the starting time of the sub diffusive regime is comparable with this time for the system particle-film (see fig. 4.15). After the caging of the particle there is in bulk a transition into a sub diffusive regime with a characteristic slope for the fit for Δr^2 of $x \sim 0.5$ in the complex liquid and $x \sim 0.9$ for the simple liquid. So, this result shows sensitivity of the dynamics of the particle to the connectivity of the monomers.

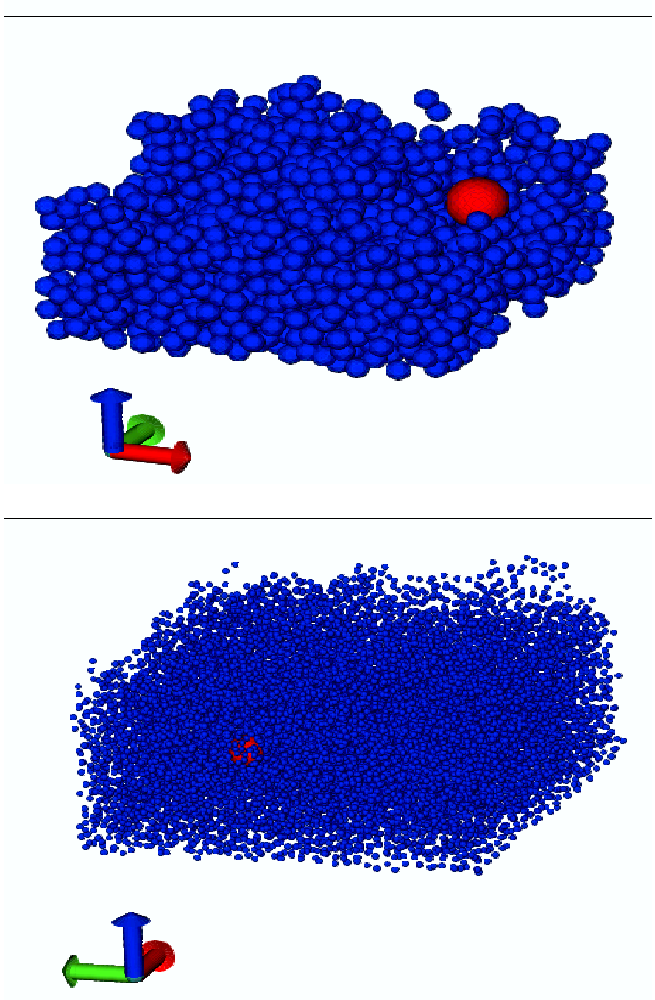

Figure 4.11: Snapshots showing the position of the probe particle for $T = 0.46$ and $T = 1.1$ after several million of simulation steps. As was discussed else where, the vertical position of the particle is sensitive to the temperature of the melt. In the first case the particle is on the surface of the liquid; in the second case the particle sinks into the liquid.

Finite size effects and dependence on the radius of the particle

The use of periodic boundary conditions may manifest in time correlation functions as a local disturbance that can propagate through the system and reappear in the same place. This effect depends on the temperature and it was shown that the relaxation times are dependent of the size of the system.

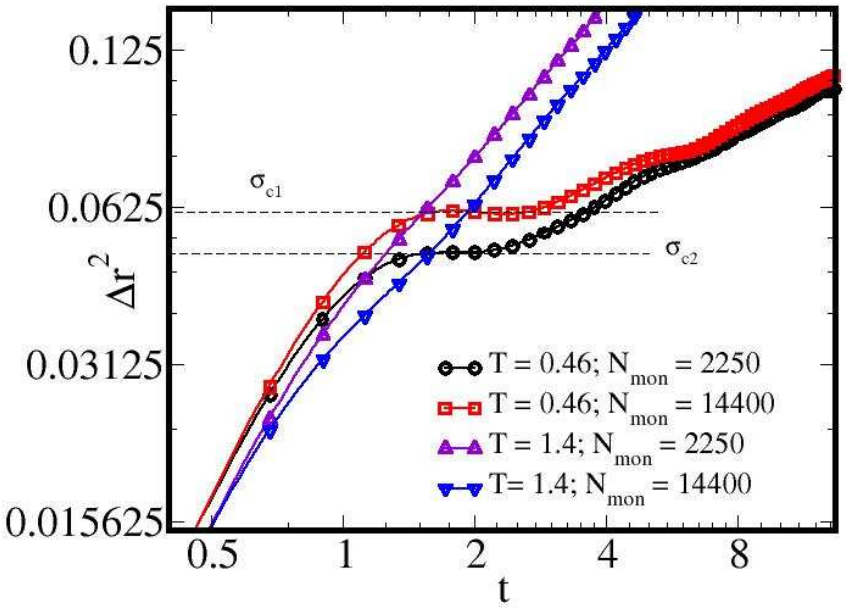

Figure 4.12: Two different simulations with different number of particles, but same size of chains. The lateral size of the box is the same for both simulations; the thickness is different but the density is the same. This result suggest a finite film thickness effect.

The dependence of the MSD of the nanoparticle on the number of particles in the box was tested. The results are presented in fig. 4.12. A test for two films with same density and size of periodic box was made: one with $N_p = 14400$ and the other with $N_p = 2250$. For very short times it was found that the MSD is the same for both systems. But for $T \to T_g$ it is observed that the plateau in both systems is different (in both cases the particle is at the interface of the film). Given that the particle is close to the interface of the film it is possible to conclude that inter facial effects have a dependence on the size of the system (i.e. finite size effects should occur for intermediary and large times). For $T = 1.4$ it is quite obvious that both curves does not coincide; but in this case it is not clear if such difference is related to finite size effects, as for $N_T = 2250$ the particle does not completely sinks into the melt. Given that finite size effects can influence the computation of diffusion constants, the estimation and analysis of diffusion of tracking particles is

done preferably for thick films with many particles(for glass formers the ideal size of the system is $N_p > 1000$ [51]) [13].

The size of the particle itself has also influence on its dynamics; the bigger the particle the bigger the probability of occurrence of correlated collisions. The results of a simulation performed with 2250 monomers (each polymer with ten monomers pro chain) and two different effective radius, $R_{eff} = 3.0$ and $R_{eff} = 4.0$, is shown fig. 4.13. The effect of the size of the particle is evident at $T = 0.46$ in the size of the cage; at $T = 1.4$ the particle with $R_{eff} = 3.0$ evolve direct from a ballistic into a diffusive regime, whereas the particle with $R_{eff} = 4.0$ shows a subdiffusive regime, giving a clue of the persistence of correlated collisions on the particle.

4.4.2 Long times: Displacement of the particle and polymer dynamics

If the particle is connected with the dynamics of the liquid then its relaxation behavior must be related with the relaxation of the melt. The relaxation behavior can be analyzed by observing the self diffusion behavior. In the present section a comparison between the displacement of the particle and the displacement of the melt is made.

The short time behavior showed a coupling to g_3 [14]; that implies that for low temperatures the displacement of the particle is insensitive to the dynamics of single monomers. For intermediary times it is here possible to observe that $x < 1$.

In comparison with other results [14] it is obvious that in the present simulations the duration of the plateau is much shorter: in this case the particle leaves earlier its own cage. [15] Therefore the relaxation process of the particle is not related to the dynamics of single monomers of the chains. But it is interesting to observe that still for $T \to T_g$ and long times the slope of the MSD is $x \sim 0.66$, even in bulk. This fact implies that relaxation processes in intermediary times of single monomers couples with the dynamics of the nanoparticles. The slopes of Δr^2 are similar to the characteristic slopes for g_0. Thus, the dynamics of a single probe particle shows in a qualitative way the coupling to the dynamics of single monomers and the chains in the melt.

In simulations for $N = 50$ the MSD has a no stable slope (see fig. 4.14): after an intermediary time regime the particle reaches a diffusive regime and then the slope

[13] Given that the tracking particle can not completly sink into the very thin film at any temperature, the dynamics of the particle is more coupled to the dynamics of the interface, in contrast to thick films

[14] Here the longitude scale of the nanoparticle is identical to g_3, because the displacement of the particle is only possible when many of the nearest monomers move out from the neighbor of the tracking particle. When there are N monomers, then its center of mass have moved $\frac{1}{N} g_0$ [59].

[15] One possible explanation of this fact is that the cage of the single nanoparticle vanish earlier because the particle is not correlated with its neighbors; in contrast each monomer is correlated at least with one neighbor particle due to its connectivity

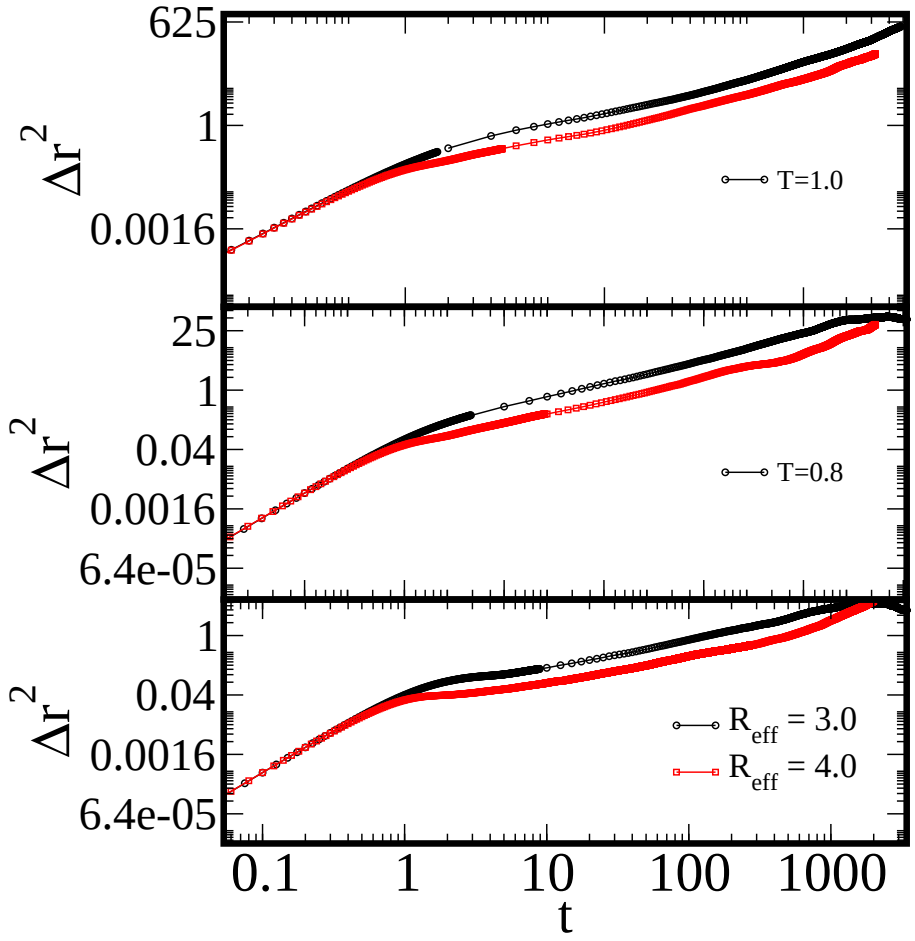

Figure 4.13: Dependence of the MSD of the particle on its radius for three different temperatures: $T = 0.46, 0.8, 1.1$. This result was obtained from a simulation with $N_p = 2250$ and $N = 10$. From this plot it is evident that the bigger the particle the bigger the persistence of correlated collisions. Self for $T = 1.0$ the MSD shows a subdiffusive regime after the ballistic regime.

decays into a value $x < 1.0$ Analyzing separate parallel runs it observed that in some of them the particle penetrates further into the melt; this fact is an indication that the vertical position that a particle reaches at a particular time is strongly varying with the possibility of metastable states and that it can be subjected to further relaxation processes.

Effect of the interface

The present problem has two possible scenarios: the probe particle is either on the film or in bulk. In fig. 4.15 the MSD of the tracking particle in bulk as well as in the film is plotted. In both cases the temperature is $T = 0.46$, implying that in the film case the particle is at the liquid-vapor interface. In bulk it is obvious that the transition from a plateau into a sub diffusive behavior with a characteristic slope of

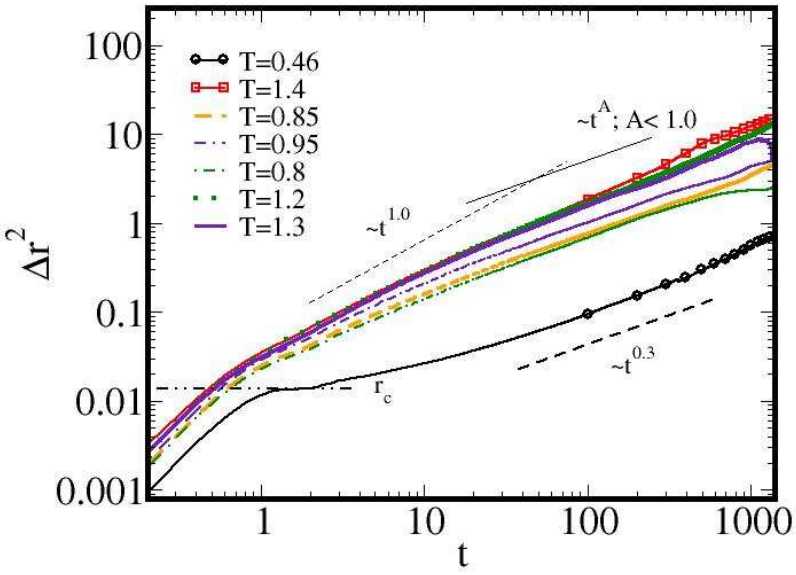

Figure 4.14: Averaged MSD for $N_p = 14400$ and $N = 50$. For long times the slope of the MSD shows a cross over; this fact is related with further relaxation effects of the probe particle in the liquid (which takes place in some parallel runs).

$x \sim 0.5$. In film there is a transition from the plateau into a sub diffusive behavior with an slope of $x \sim 0.3$.. In this last case the proximity of the nanoparticle to the interface implies that the particle is coupled to the interfacial particles, which are pertaining in collective modes, the so called capillary waves, whose relaxation time is different from those of collective modes in the bulk.

After some time the slope of the MSD tends into $x_1 \sim 0.5$ and for much bigger times eventually the particle reaches a diffusive regime. That implies, the dynamics of the particle detects not only the dynamics of the molecules but also the interfacial dynamics. The consequence of this coupling is that the particle needs very long times to reach a complete relaxation into a diffusive regime, because the capillary waves need long relaxation times, imposing a fundamental methodological problem, because it is necessary to make simulations in long times in order to improve the statistics. Even with parallel runs it is hard to obtain good statistics.

Diffusion

The determination of the diffusion coefficients, as was discussed in this section, has been made using the division of the MSD by time and the integral in the time of the VCF. In fig. 4.16 the result of the integral of the VCF for $N = 50$ is presented; in fig. 4.5 there a similar plot is shown but for $N_{mon/chain} = 10$. The caging of

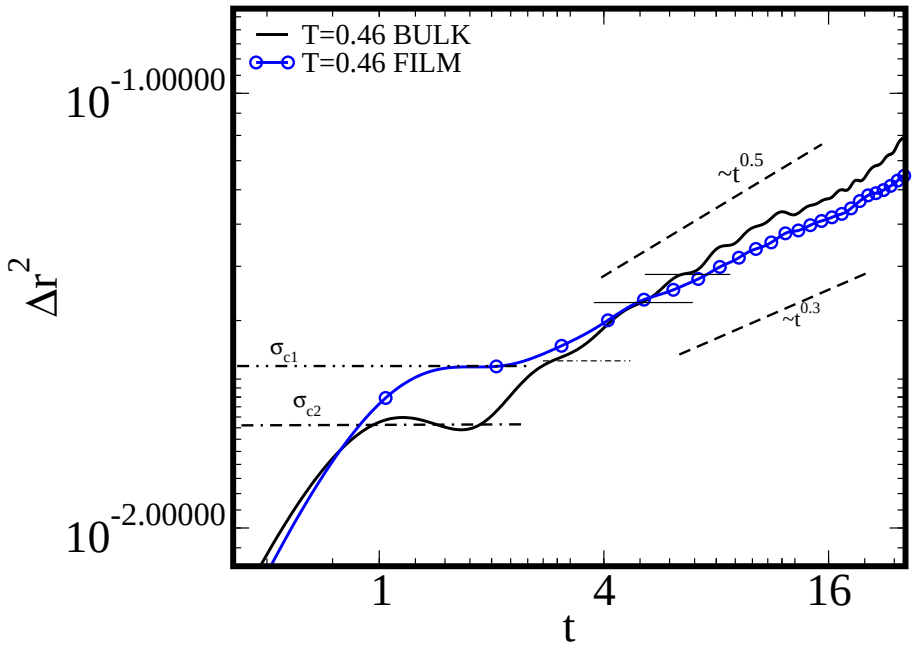

Figure 4.15: Comparison of the MSD in film and in bulk at $T = 0.46$ for a film with $N_p = 14400$, $N_{mon/chain} = 10$. For long times the slope of the MSD in the film is small than in bulk. Given that the particle is at the surface of the film this plot suggest that the particle is subjected to relaxation processes at the interface. For a simple liquid (LJ particles) the subdiffusive regime evolves into a diffusive one; in this last case the density of the liquid was small in order to observe caging of the particle. The fluctuations of the MSD are related to oscillations of the particle inside the wetting layer (please refer to the corresponding appendix).

the particle and its oscillation into the solvation shell, represented by the second peak can be clearly seen, before the particle begins to diffuse. The time where both $D_{MSD}(t)$ and $D_{VCF}(t)$ are constant is the time regime where the particle diffuses in the film (this regime is represented by a plateau like behavior of both functions $D(t)$).

Because the present system relaxes very slowly it is very difficult to obtain very accurate values for this constant. In particular the diffusion constant drops rapidly upon cooling and then comes a point in temperature where it is no longer possible to extract meaningful values from the long time behavior of the MSD. For this reason simulations for temperatures above T_g was started. In the following table the results extracted from this both plots for the diffusion constant is presented, for a melt consisting of 10 monomers per chain. A relevant characteristic of the self diffusion coefficients in polymer melts is the dependence on N, where the dynamics is described in terms of Rouse model[16]. The estimation of the self diffusion coefficient for $N = 50$ is made and then compared with previous computed diffusion coefficients. For example for $T = 1.2$, $\frac{D_{50}}{D_{10}}|_{part} = 0.2$.

[16]The central prediction of the Rouse model is that $\eta \sim N$

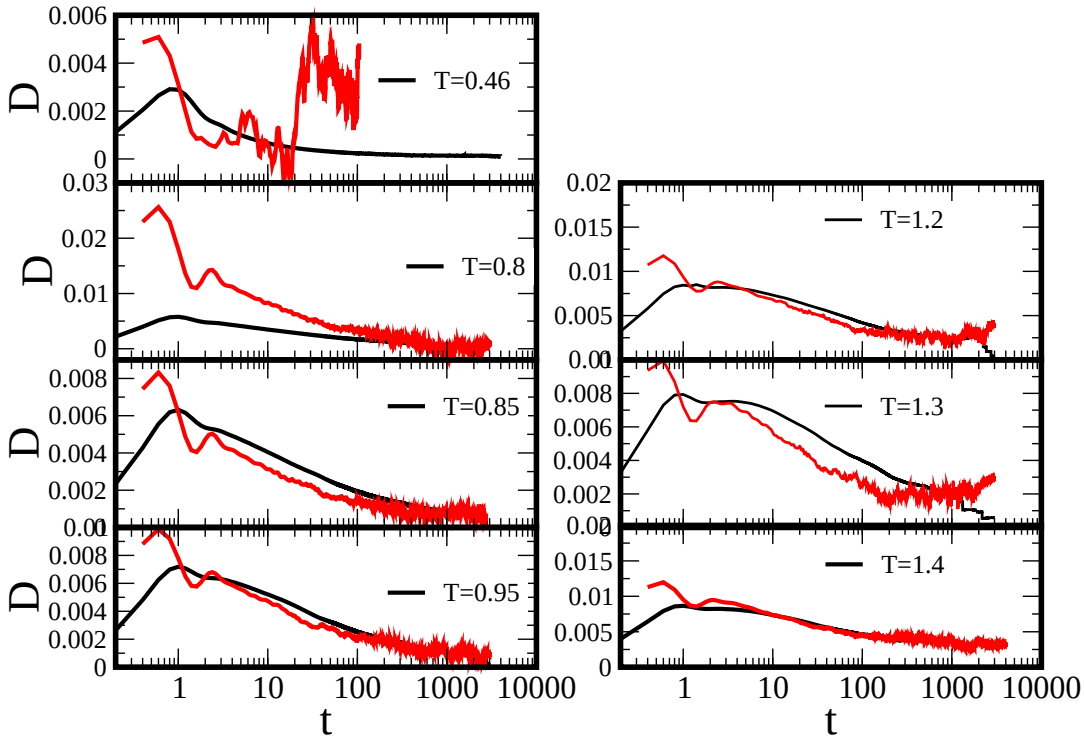

Figure 4.16: Integral of the VCF and MSD divided on the time for the determination of the Diffusion constant of the liquid film. $N_{mon/chain} = 50$ and $N_p = 14400$. The region of convergence of $D_{MSD}(t)$ and $D_{VCF}(t)$ corresponds to the diffusive regime of the tracking particle.

Table 4.1: Diffusion coefficients as a function of the temperature

T	D	ΔD
0.46	2.8*10^{-5}	3.39*10^{-5}
0.5	0.00012	1.3*10^{-4}
0.7	0.0008	0.000135
0.8	0.002	0.0002
0.9	0.00309	0.0002
1.1	0.0086	0.0005
1.4	0.004	0.00035

Contrasting with the results obtained from the Rouse theory it is well know that $\frac{D_{50}}{D_{10}} = 0.2$ [58]. Therefore, the dynamics of the single particle do reflects the Rouse dynamics of the polymer melt. In fig. 4.17 the logarithm of the self diffusion coefficients as a function of the inverse of the temperature is presented. The fit with an exponential function permits to make the conjecture about the existence of an Arrhenius Law governing the diffusion coefficients. The result of the fit permits

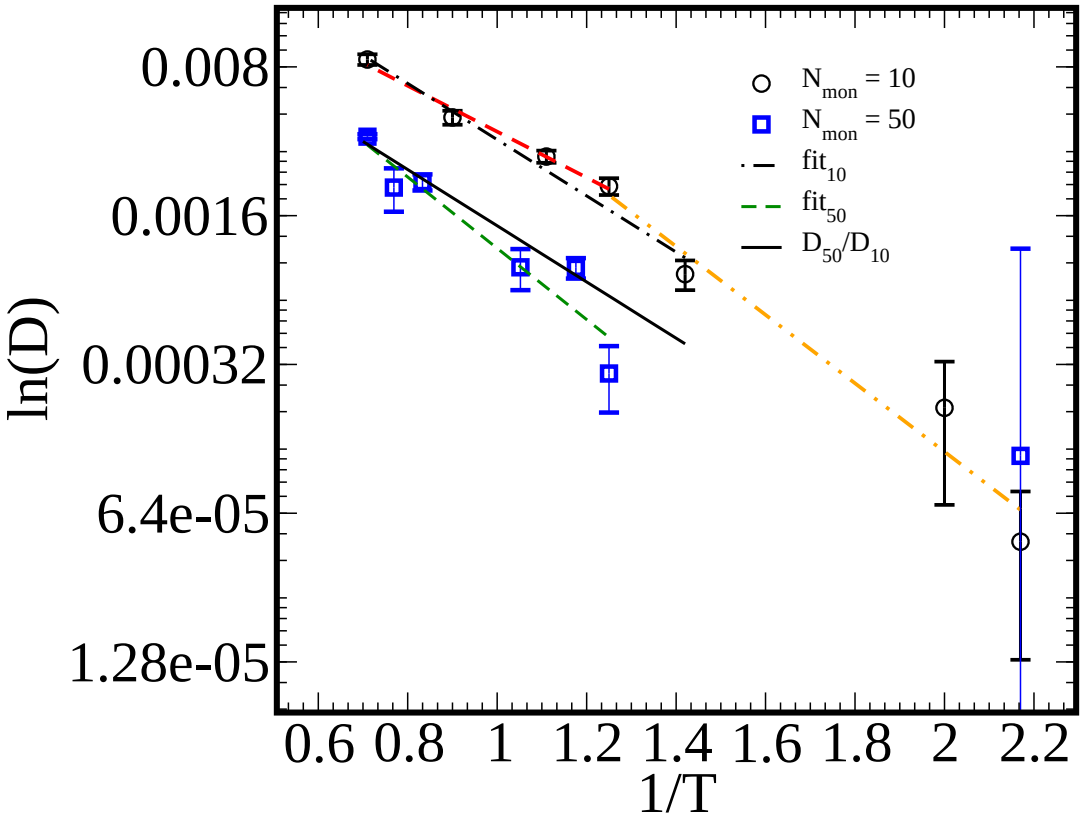

Figure 4.17: Plot of the diffusion coefficients (in logarithmic scale) as a function of the inverse temperature for $N_{mon/chain} = 10$ and $N_{mon/chain} = 50$. This result suggest that the Arrhenius law is valid for the computed self diffusion coefficients; a cross over in the fit could be related with a transition in the interface allowing the particle to 'sinks' into the melt. A second fit was made taking into account the dependence of the self diffusion coefficient on the number of monomers in each chain; such fit shows good agreement with the present results.

to conclude that such law hods relatively well for the self diffusion constant of the nanoparticle. But it is interesting to observe the existence of a cross over in the diffusion coefficients. In a previous section the vertical position of the particle was discussed and it was concluded that for $T \sim T_g$ the molecules at the interface has low mobility, but for some particular temperature the mobility of such molecules increase (the interface becomes softer) and the particle is allowed to sink. Therefore this cros over probably indicates the temperature where a transition at the interface occurs letting the particle sink inside the film.

4.4.3 Microrheology results

The time evolution of the MSD provides a measure of the frequency dependent linear viscoelastic modulus of the film. The magnitude of the complex modulus is given

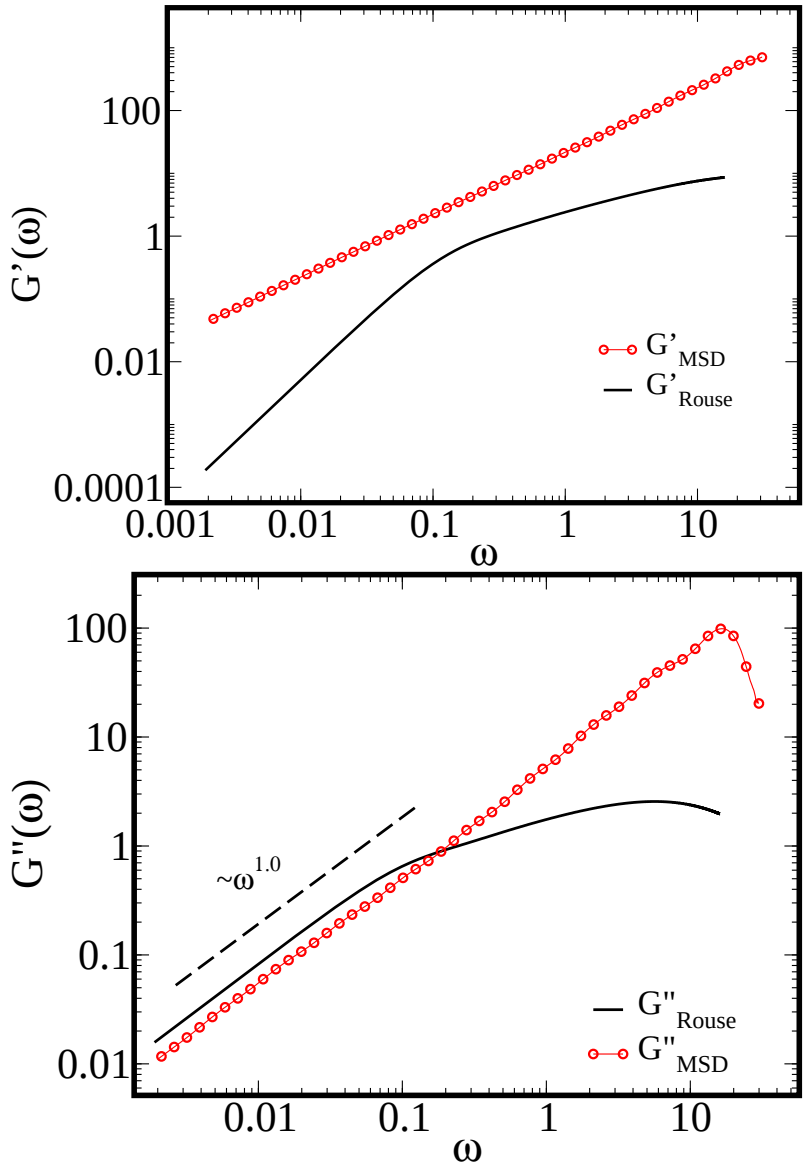

Figure 4.18: Real and imaginary part of the shear modulus for a polymer film composed of 14400 monomers, where $N_{mon/chain} = 10$. The first panel corresponds to the elastic modulus and the second panel corresponds to the viscosity modulus; in both cases the predicted Rouse modulus is plotted [58] [54].

by $G(s) = k_B T/(\pi R_{eff} s \Delta r^2(s))$, where s is the Laplace frequency.

For the computation of the storage and loss modulus it is necessary first to perform the Fourier transform of the VCF [17] or of $D(t)$, the so called power spectrum. The imaginary part of the transform of any function $\varkappa(t)$ can be estimated making the transform over the sinus function

[17] The upper boundary of the integral on time is the maximal simulation time; the integral is moreover multiplied by two given the symmetry of the transformation

$$\varkappa"(\omega) = 2\frac{1}{2\pi}\int_0^\infty \varkappa(t)\sin(\omega t)dt \tag{4.41}$$

whereas the real part can be computed over the cosines function:

$$\varkappa\prime(\omega) = 2\frac{1}{2\pi}\int_0^\infty \varkappa(t)\cos(\omega t)dt \tag{4.42}$$

when a transformation over the frequency $\omega = 2\pi\nu$ is made then it is possible to lost the symmetry with the inverse transformation [95] [58]; for this reason the transforms are multiplied by the factor $\frac{1}{2\pi}$. These results are non normalized

$$\phi(\omega) = \phi\prime(\omega) - i\phi"(\omega) \tag{4.43}$$

The transformation is made over the whole simulation time. For this reason an alternative method as the conventional Weitz et al. method was developed. The description of the alternative computation is made in appendix C; the diffusion function is used, derived from the MSD, $D_{MSD}(t)$, and the VCF, $D_{VCF}(t)$, and is Fourier transformed (in the second case this relation is a direct derivation from the VCF). So the Stokes-Einstein equation relates the viscosity, as a function of $D(t)^{-1}$, and the complex shear modulus.

In fig. 4.18 the storage and the loss modulus are shown. This result was obtained for a system with $N_p = 14400$ and $N = 10$ at $T = 0.9$ and a comparison with theoretical values is done [58] [54]. In the first case there is no convergence to the theoretical predicted value, where the curve has a characteristic slope of $\sim \omega^1$. In the second case the loss modulus has convergence to the theoretical predicted value for low frequencies; in this case for $t \to 0$, $G''/\omega \sim \eta_0$, with η_0, the viscosity close to the particle. This value has again coincidence with the viscosity computed using the results for the self diffusion coefficient of the nanoparticle.

In macroscopic rheological experiments the aplyed strain is pure stress; on the other hand in microrheology the tracking particle responds to all of the thermally excited modes of the system, including the longitudinal compression modes of the melt [53]. This point implies that the results obtained with microrheology only converge to conventional results in a restricted frequency domain, where the response of the particle is related to the stress in the fluid.

The introduction of the probe particle reduces moreover the density in the melt in the vicinity of the particle [18]. Therefore the response of the tracking particle is only sensitive to the local environment and is not capable to measure observables in bulk for all the time scales. One possible solution is to make the correlation of the fluctuations of two probes, separated by enough distance, in order to improve the results obtained using microrheology[19].

[18]The thin layer at the surface of the tracking particle

[19]For an account about the measurement of the viscosity at high frequencies see [57].

4.5 Outlook and Conclusions

A film consisting of a complex fluid presents a phenomenology covering many scales, from the dynamics of single monomers to macroscopic observables like diffusion and viscosity coefficients. Such phenomenology requires many particular experimental methods in order to extract accurate information. The point in this section is, whether a nanoparticle can be used as single experimental method in order to extract the information of such phenomenology. In answering this question three main problems were regarded: the coupling of the nanoparticle to the dynamics of single monomers, the coupling of the nanoparticle to the polymeric chains and the effect of the dynamics of the liquid-vapor interface.

The particle in the liquid is a Brownian particle that responses to the thermal fluctuations of the liquid particles. Instead of simple collisions (like simple liquids) the present case presents a more complicated phenomenology due to the connectivity of the particles, which is related to a memory function that depends on the temperature of the liquid. The analysis of the VCF of the tracking particle has shown that the particle is caged when the temperature is near the glass transition temperature T_g; given that the particle is at the interface of the film (as was shown in chapter 3) this result probes glass transition at the interface. The present result was confirmed in all the simulations performed with different number of monomers and polymers.

The analysis for short times has shown that the dynamics of the nanoparticle is not quantitatively related to the dynamics of single monomers for temperatures near the critical temperature. For long times the MSD as well as the VCF permit to extract information of macroscopic coefficients; in this case it was shown that the self diffusion coefficient of the probe is related to the diffusion coefficient of the center of mass of the polymer chains (as is predicted in the Rouse model).

In such time regimes a particular question arises: the use of the Stokes-Einstein formula (which relates the diffusion coefficient to the viscosity) as a method for the determination of the bulk viscosity of the melt. The results obtained with the present method show a good agreement of the loss modulus with the theoretical value predicted by the Rouse model, but the storage modulus shows a considerable deviation from to the predicted function. In this case it is quite evident that the results obtained with a microrheological probe are related to its local behavior and does not completely reflect the bulk shear modulus (as is predicted by Lubensky et. al. [53]). Only for low frequencies the results obtained with microrheology coincides with conventional rheology (in particular with the shear modulus predicted by the Rouse model).

Notwithstanding the simplicity of the simulation concept, the main problem in the simulation of this system is the computational time. The melt requires long simulation times to get equilibration and the statistics of a single particle is poor (the improvement of the statistics of the particle requires a lot of simulation time). So, the advantage in using a single test particle is compensated by the disadvantage in the long simulation times. The simulation of a couple of million of MDS of parallel

configurations is an alternative method for the improvement of the statistics of the single particle.

A probe particle has proofed to be a good qualitative method and, in some cases, to be a good quantitative method, not withstanding the poor statistics that can be obtained with a single particle. As outlook it is interesting to introduce two probes instead of only one, placed far away from each other, in order to make the correlation of their fluctuations, the so called two point microrheology. With such method it is theoretically possible to obtain a better measure of the bulk shear modulus. Moreover the present problem is an idealized case where the particle is non structured; so the question is, whether a structured particle has a different dynamics as a simple one.

5 Linearized hydrodynamics of a polymeric film under load of a nanoparticle

In this section the solutions of the Navier-Stokes equation, describing a thin liquid film under an external small perturbation, are calculated. The perturbation is induced with an oscillating Lennard-Jones potential on the vertical coordinate. The fundamental motivation of this work is to make a description of the interaction between the liquid and an idealized tip of an AFM [77] [1].

The equations for an incompressible fluid are solved. In this approximation it is shown that the computed solutions are trivial because the interface is at rest. This implies, that only the compressibility of the fluid allows the transmission of external perturbations into the bulk of the liquid. The solution for a compressible liquid is non trivial; the result shows non vorticity of the velocity, with a maximal hydrostatical pressure at the vapor-liquid as well as the liquid-substrate interface. Inside the liquid damped oscillation of the magnitude of the pressure are observed. Such a pressure profile has also a damped oscillation on the radial axis, with a maximum pressure under the particle and at the interface substrate-liquid.

Hydrodynamics is a description of systems whose typical scales are greater than the scale of the molecules that compose it. Experimentally this supposition implies that the fluid must be in bulk. In the present calculation a liquid film will be considered with a thickness bigger than the typical gyration radius of single polymer chains (consisting of 10 to 50 monomers pro chain). The aim of this calculations is to model a liquid under similar conditions as in the simulations that were described above. For the following calculations the film thickness is about 14.7 LJ units, with a liquid with density $\rho = 0.8$ (quantities are given in terms of LJ units).

Hydrodynamics is a description of liquids, whose relaxation time is slower than the relaxation time of the component molecules [32]. The Navier Stokes equation, together with the continuity equation, describe the equilibrium dynamics of the liquid and are given in a general form as

$$m\partial_t v^i = \nabla_j T^{ij}, \tag{5.1}$$

[1] In a previous work the computation of the interaction between a film and a curved surface was made in order to understand the interaction between a big AFM tip and a fluid film [92]

$$\partial_t \rho + \nabla_i \rho v^i = 0. \tag{5.2}$$

where v^i is the covariant component of the velocity and T^{ij} is the stress tensor. The first equation represents the momentum balance: the momentum change on left hand is given by the gradient of the stress tensor (which contains a pressure tensor) on the right side. This tensor contains information on the forces and relaxation processes in the liquid. The second equation, the so called continuity equation, shows the conservation of mass in space and time. In the present problem consideration of the equilibrium of energy is not needed since constant temperature is assumed.

The system to be modeled consists of a particle suspended over a liquid film, which is adsorbed on an impermeable substrate. The target is to obtain information about the mechanics of the fluid when a small mechanical perturbation is introduced into the system through the particle ; in this case the system remains in thermal equilibrium. The particle creates a Van der Waals like external potential for the liquid; which depends on the distance between the particle and the substrate (see 5.1) [2]

$$d_T = H_{0\Gamma} + d, \tag{5.3}$$

where H_Γ is the film thickness in thermal equilibrium and d is the distance between the interface of the particle and liquid film. The effective radius of the nanoparticle is $R_{eff} = \sigma + R_0$; this definition preserves the old definition of the radius of the particle done for the simulations. So, the mechanical perturbation is a function of the distance parameter between particle and the liquid-vapor interface of the film. The aim of this model is to emulate, for example, the harmonic movement of a cantilever in an AFM microscope; in this case the particle represents the tip of the AFM without cantilever [3].

For the present calculation the perturbation represented by small perturbations of the external potential (see fig. 5.1)

$$\phi \rightarrow \phi + \delta\phi. \tag{5.4}$$

is given by

$$\delta\phi = \left(\frac{\partial\phi}{\partial d}\right)\delta d, \tag{5.5}$$

where

$$\delta d = H_0 \sin(\omega t), \tag{5.6}$$

with ω the frequency and H_0 the amplitude of the oscillation motion of the nanoparticle along the z axis. In experimental situations the perturbation is represented

[2] See in the chapter about technical details the section about the potential of the particle

[3] In the present case a simple model for the particle, represented as a LJ one, is shown. Nevertheless there are many possible potentials that can simulate the tip of an AFM; see for example [93]

as a contact-separation of the tip from the liquid surface, the so called tapping mode.[4].

The perturbation induces in the same way small perturbations in the velocity and pressure fields around the equilibrium value for both variables

$$v^i \to v^i + \delta v^i, \tag{5.7}$$

$$P \to P + \delta P. \tag{5.8}$$

From the hydrostatics it is well known that the velocity field in equilibrium is $v^i = 0$; thus in the present case there is only a field of small velocities generated by the small perturbations of the nanoparticle. The description for this field is made via the so called linearized Navier-Stokes equations: due to small perturbations the non linear differential equations can be approximated by linear ones.

Additionally at the boundary between film and vapor there will be a fluctuating interface. Then the linearized thickness is defined as

$$H_\Gamma(r,t) = H_{0\Gamma} + \delta H(r,t), \tag{5.9}$$

[4]In the present project a Gaussian as well as an harmonic perturbation will be considered.

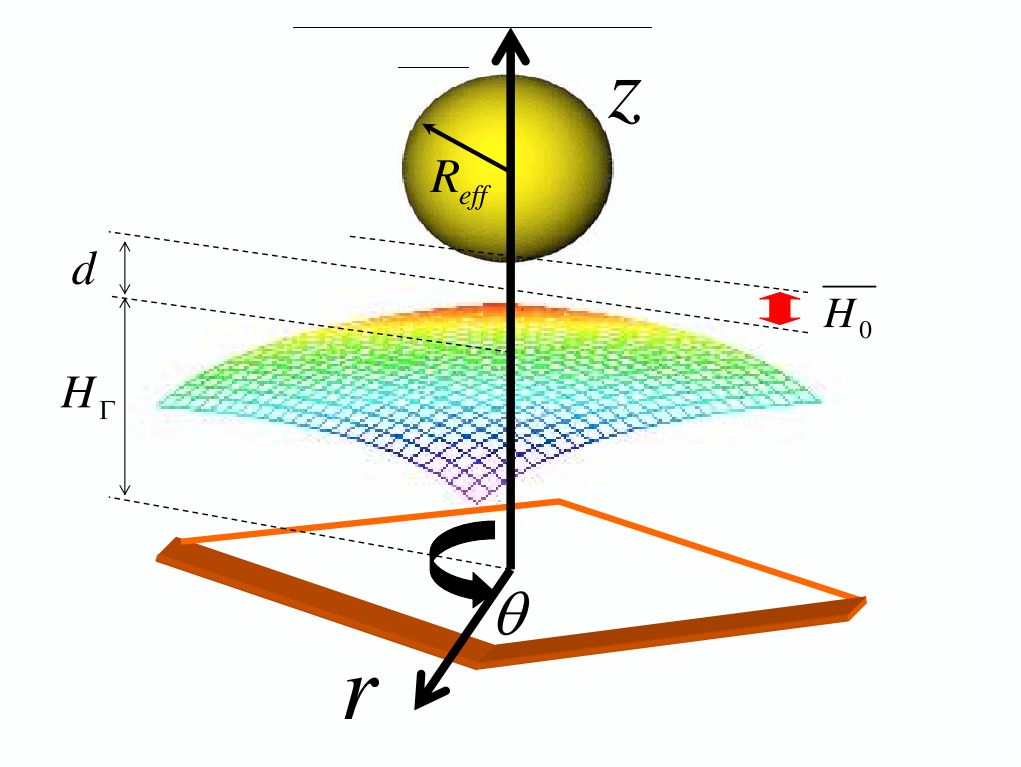

Figure 5.1: Coordinates of the system particle -liquid film. The nanoparticle has a small oscillation above the liquid-vapor interface, with thickness H_Γ

where $H_{0\Gamma}$ is the thickness of the film at equilibrium and $\delta H(r,t)$ is the time dependent perturbation.

The modeling of this fluid, using the Navier Stokes equations, generates a dependence of the solutions on the following parameters

$$v^i = v^i(t,r,z)[\{H_0\},\{\rho,\eta,\varsigma\},\{\varepsilon,\sigma,d,R_{eff}\}]. \tag{5.10}$$

In that case the fields that solve the system of equations depend on the radial and vertical coordinate (the solution of the present problem assumes a cylindrical symmetry). Regarding the different parameters: one family of parameters is the amplitude of the external perturbation; the second family of parameters corresponds to the nature of the liquid, i.e. its density, shear viscosity and bulk viscosity. If the fluid is incompressible then the velocity depends only on the shear viscosity. The third family of parameters corresponds to the external potential: the form of the particle, which is simulated through this potential, the strength of the potential and the separation between the particle and the substrate. In the calculation of the final results, $\varepsilon = 1$, $\sigma = 1$ and $R_{eff} = 4$. The density is in the present case $\rho = 0.8$, which corresponds to the density of a polymeric film with thickness $H_0 \sim 14$ and $N_p = 14400$. The value of this density was measured in the simulations for $T = 0.9$.

5.1 Hydrodynamics of compressible and incompressible fluids

In the first part of this section the right boundary conditions are derived for the interface vapor-liquid of the liquid film in the presence of the nanoparticle. For the derivation of these equations, a general mathematical form for the surface condition is used, which is valid for any extensive quantity by considering a global balance equation [76] [81]. The solutions for the linearized hydrodynamics for a compressible as well as an incompressible liquid are explored. Both simple and complex fluids are considered. All the results are computed using LJ units.

5.1.1 Boundary conditions at the interface

In the present case, a small oscillation over the fluid film is introduced in order to obtain a mechanical response; this oscillation is thermal equilibrium but it is not small enough to ignore oscillations of the interface, implying a time dependent surface curvature [5]. This scenario is more complicated than the trivial case of a flat

[5] The theory is a mean field theory and therefore there are no thermal fluctuations as, for example, capillar waves [83]

interface and it is necessary for the determination of the desired solutions, where the inclusion of curved surfaces cannot be avoided.

The balance equation at an interface for any field ψ_1 for a phase 1 in a region G_{ph1} and ψ_2 in a region containing phase 2, G_{ph2}, is given by the following expression [76] [6]

$$\overrightarrow{e\prime_z}\left(\overrightarrow{\Psi}_1 - \overrightarrow{v_\Gamma}\rho_1\psi_1\right) - \overrightarrow{e\prime_z}\left(\overrightarrow{\Psi}_2 - \overrightarrow{v_\Gamma}\rho_2\psi_2\right) - \left(\frac{d\chi}{dt} - 2S_\Gamma\left|\overrightarrow{v_\Gamma}\right|\chi\right) + \tau = 0, \quad (5.11)$$

with $\overrightarrow{v_\Gamma}$, the velocity of the interface Γ and χ the surface density defined as the distribution of the field ψ at the interface Γ. $2S_\Gamma$ is the curvature tensor for the interface, τ the surface source density and $\overrightarrow{e\prime_z}$ the unit normal vector for a point on the interface. The field $\overrightarrow{\Psi}$ describes the flux density of the field ψ in each phace; it is defined as

$$\overrightarrow{\Psi} = \overrightarrow{\Phi} + \rho\psi\overrightarrow{v}. \quad (5.12)$$

Given that the interface is a fluctuating surface, the normal vector is given by

$$\overrightarrow{e\prime_z} = N\left(-\varsigma(r,t)\overrightarrow{e_r} + \overrightarrow{e_z}\right), \quad (5.13)$$

where $\varsigma(r,t) = \frac{d\delta H(r,t)}{dr}$; here $\delta H(r,t)$ is the amplitude of fluctuation of the interface. In a similar way it is possible to rewrite the tangential vector as

$$\overrightarrow{e\prime_r} = N\left(\overrightarrow{e_r} + \varsigma(r,t)\overrightarrow{e_z}\right). \quad (5.14)$$

The second tangential vector is trivially $\overrightarrow{e\prime_\theta}$. In both equations the prefactor N is given by

$$N = \frac{1}{\sqrt[2]{\varsigma(r,t)^2 + 1}}, \quad (5.15)$$

which is the normalization function. The total film thickness is given by the superposition of the mean film thickness and the fluctuation of the interface, i.e. $H_\Gamma(r,t) = H_{0\Gamma} + \delta H(r,t)$, where $\delta H(r,t)$ is a small perturbation of the surface. Therefore, it is important to consider $\varsigma(r,t)^2$ as a very small function; this supposition allows to linearize the previous equations and implies that the normalization factor is $N = 1$. The equation eq. (5.11) is useful for the determination of the conservation of mass and momentum at the interface; both particular cases will be discussed in the calculation of the boundary conditions.

[6] This means, the interface is two dimensional

5.2 Solution of the NS equations in the liquid film

5.2.1 Incompressible fluids

The starting strategy is to use the method of separation of variables because the symmetry of the system is known. It is advantageous to formulate the solution as an expansion in periodic functions of r and z which preserves the symmetry of the system

$$v^i = \sum_{mn} f^i_{nm}(t) f_{v_r}(mr) f_{v_z}(nz), \tag{5.16}$$

where $f_{v_r}(mr)$ and $f_{v_z}(nz)$ are periodic functions. As ansatz for the velocity and pressure fields for an incompressible fluid an expansion in a Fourier-Bessel series over the r coordinate is proposed: an expansion in Fourier series in z leads to a trivial solution for the velocity fields when the initial conditions are applied (the pressure in the incompressible core is not trivial), because a solution in the form

$$f_{nm}(t) = f_0 e^{-\tau_{nm} t}, \tag{5.17}$$

is obtained. This result indicates that the transmission of external perturbations into the liquid film is only possible when the density of the fluid is not a constant, i.e. the transmission of external perturbations into the film is related to the transmission of sound waves in the liquid. In the following the compressible NS equations for a film under external load by a nanoparticle will be solved (see appendix H to see the complete solution for the incompressible case).

5.2.2 Compressible fluids

The concept of compressible fluid is related to a non constant liquid density. This particular aspect, under the light of linearized hydrodynamics, implies fluctuations of the density related to fluctuations of the pressure and velocity. This means that the Navier Stokes equations must have an additional term that contains an isothermal bulk coefficient.

The isothermal bulk modulus for a substance is defined by [94]

$$\kappa_T = -V \left(\frac{dP}{dV} \right)_T ; \tag{5.18}$$

this coefficient has units of pressure (for examples for typical polymers see Appendix I). In the previous expression, P is the pressure and V is the volume of the substance. If the mass of the substance remains constant, the linear relation between density and pressure is given by [7]

[7] $\delta\rho = \frac{d\rho}{dv}\delta V = -\frac{m}{V^2}\delta V = \frac{\rho}{\kappa_T}\delta P$

$$\delta\rho = \frac{1}{\kappa_T}\rho\delta P, \tag{5.19}$$

where ρ is the density of the liquid.

For compressible liquids, in the frame of linear hydrodynamics one has to take into account that the density will have small perturbations; such fluctuations can be expressed as

$$\rho \to \rho + \delta\rho, \tag{5.20}$$

where ρ is the density in equilibrium and $\delta\rho$ is a small perturbation of this density. Using the condition of compressibility of a liquid one obtains

$$\rho + \delta\rho = \rho\left(1 + \frac{1}{\kappa_T}\delta P\right). \tag{5.21}$$

In this equation δP is a small pressure perturbation. The density has a small perturbation around an equilibrium density, which is related to fluctuations of the pressure. Using this expression it is possible to write the correct continuity and Navier Stokes equations for the compressible liquid.

Therefore the following form for the continuity equation is obtained (in order to simplify the notation, the differential equations are writen for A instead of δA)

$$\partial_t P + C_T\left(\nabla_r v^r + \nabla_z v^z\right) = 0, \tag{5.22}$$

where $C_T = \frac{\kappa_T}{P_0}$ is a constant given in terms of the isothermal bulk modulus. The Navier-Stokes equations are

$$\partial_t v^i = -\partial_i P - \rho\partial_i\phi\prime\delta d + K_\eta\Delta v^i + K_\varsigma\delta^{ii}\partial_{\bar{i}}\left(\nabla_j v^j\right), \tag{5.23}$$

here $i = r$ and $j = z$; on the right side the stress tensor represents a compressible fluid, where K_η is the kinematic viscosity (also called dynamic viscosity [94]) and K_ς is a constant defined from the bulk-stress coefficient, the so called bulk viscosity [94][79]; for typical polymers with Newtonian behavior the coefficient of viscosity η is in the range of 10^{-3} to 10^{-1} Nsm^{-1}. In appendix I all of these constants will be explained in detail.

The solutions can again be expressed as an expansion of periodic functions, which preserves the symmetry of the system. As ansatz, the solution for velocity v^i as well as pressure P is given in terms of a Fourier-Bessel-Fourier series in r and z

$$v^r = \sum_{n,m} f_{nm}(t)\cos(nz)J_1(mr), \tag{5.24}$$

$$v^z = \sum_{n,m} g_{nm}(t)\sin(nz)J_0(mr), \tag{5.25}$$

$$P = \sum_{n,m} A_{nm}(t)\cos(nz)J_0(mr), \tag{5.26}$$

$$\widehat{\phi\prime} = \sum_{n,m} \overline{H_0} B_{nm}(t)\cos(nz)J_0(mr). \tag{5.27}$$

The last of the previous equations expresses the expansion of the perturbation introduced with the external potential in a Fourier-Bessel series, where B_{nm} are the expansion coefficients.

Using the same ansatz defined for the solutions of the velocity fields, it is advantageous to express the last differential operator of the Navier Stokes equations as

$$\overrightarrow{\nabla}.\overrightarrow{v} = \sum_{n,m} \left[m f_{nm}(t) + n\pi g_{nm}(t) \right] \cos(nz)J_0(mr). \tag{5.28}$$

The vector defined in terms of the two velocity fields and pressure is an eigenvector of the Navier Stokes equations.

The equations for the time function of the pressure $A_{nm}(t)$, $f_{nm}(t)$, the time function for the velocity field in r and $g_{nm}(t)$, time function for the velocity field in z, are obtained as

$$\begin{aligned} \frac{df_{nm}(t)}{dt} &= mA_{nm}(t) + m\varepsilon_c B_{nm}\overline{H_0}\sin(\omega_c \bar{t}) \\ &\quad -(\pi^2 n^2 + m^2)K_\eta f_{nm}(t) + \\ &\quad K_\zeta \left(-m^2 f_{nm}(t) - \pi mn g_{nm}(t) \right), \end{aligned} \tag{5.29}$$

$$\begin{aligned} \frac{dg_{nm}(t)}{dt} &= \pi n A_{nm}(t) + \pi n \varepsilon_c B_{nm}\overline{H_0}\sin(\omega_c t) - \\ &\quad (m^2 + \pi^2 n^2)K_\eta g_{nm}(t) + \\ &\quad K_\zeta \left(-\pi^2 n^2 g_{nm}(t) - \pi mn f_{nm}(t) \right), \end{aligned} \tag{5.30}$$

$$\frac{dA_{nm}(t)}{dt} + C_T \left(m f(t) + \pi n g(t) \right) = 0.$$

In order to facilitate the calculation of the solutions, the following parameters are defined

$$B_1 = \left(m^2 + (n\pi)^2 \right) K_\eta + m^2 K_\zeta, \tag{5.31}$$

$$B_2 = \left(m^2 + (n\pi)^2 \right) K_\eta + (n\pi)^2 K_\zeta. \tag{5.32}$$

Substitution into the time equations for the velocity fields yields

$$\frac{df_{mn}(t)}{d\overline{t}} = -B_1 f_{nm}(t) - \pi mnK_\zeta g_{nm}(\overline{t}) + mA_{nm}(t) + m\varepsilon_c B_{nm}\overline{H_0}\sin(\omega_c t), \tag{5.33}$$

$$\frac{dg_{mn}(\overline{t})}{d\overline{t}} = -\pi mnK_\zeta f_{nm}(\overline{t}) - B_2 g_{nm}(\overline{t}) + \pi nA_{nm}(\overline{t}) + \pi n\varepsilon_c B_{nm}\overline{H_0}\sin(\omega_c \overline{t}). \tag{5.34}$$

These equations can be written in an equivalent vectorial form as:

$$\frac{d}{dt}\begin{pmatrix} A_{nm}(t) \\ g_{nm}(t) \\ f_{nm}(t) \end{pmatrix} = \begin{pmatrix} 0 & -C_T\pi n & -C_T m \\ \pi n & -B_2 & -\pi nmK_\zeta \\ m & -\pi nmK_\zeta & -B_1 \end{pmatrix}\begin{pmatrix} A_{nm}(t) \\ g_{nm}(t) \\ f_{nm}(t) \end{pmatrix} + \begin{pmatrix} 0 \\ \pi n\varepsilon_c B_{nm}\overline{H_0}\sin(\omega_c t) \\ m\varepsilon_c B_{nm}\overline{H_0}\sin(\omega_c t) \end{pmatrix}, \tag{5.35}$$

which is a first order inhomogeneous, linear differential vector equation. There are two possible ways to solve the previous equation. The first one is to make a Fourier transform in order to obtain an algebraic equation in the frequency space, the second is to diagonalize the matrix and obtain uncoupled equations for each time coefficient. The first alternative is convenient if the target is to make an analysis on the frequency domain of the solutions; the second alternative is a solution in the conventional time domain. In the following sections both solutions will be explained.

5.2.3 Solutions in the time domain

The solution of the differential equation in the time domain can be found by uncoupling each differential equation for each coefficient; for this target a diagonalization of the matrix with constant coefficients of the differential equation is performed. The following linear transformations are proposed

$$v_{nm}(t) = (n\pi)\, f_{nm}(t) - m g_{nm}(t), \tag{5.36}$$

$$u_{nm}(t) = (n\pi)\, g_{nm}(t) + m f_{nm}(t). \tag{5.37}$$

Making the substitution of eq. (5.36) and (5.37) into eq. (5.35), and after some algebraic manipulations, the following differential equations for the fields $u_{nm}(t)$ and $v_{nm}(t)$ is obtained

$$\frac{du_{nm}(t)}{dt} = \left(m^2+(n\pi)^2\right)A_{nm}(t) - \left(m^2+(n\pi)^2\right)\left[K_\eta + K_\zeta\right]u_{nm}(t) + \left(m^2+(n\pi)^2\right)\varepsilon_c B_{nm}\overline{H_0}\sin(\omega_c t), \tag{5.38}$$

$$\frac{dv_{nm}(t)}{dt} = -\left(m^2+(n\pi)^2\right)K_\eta v_{nm}(t), \tag{5.39}$$

$$\frac{dA_{mn}(t)}{dt} = -C_T u_{nm}(t). \tag{5.40}$$

After these transformations the equation for $v_{nm}(t)$ is uncoupled from the other two fields. The solution of equation (5.39) is

$$v_{nm}(\overline{t}) = \beta_0 e^{-K_\eta\left(\pi^2n^2+m^2\right)\overline{t}} \tag{5.41}$$

where β_0 is a constant which depends on the initial conditions.

For $A_{mn}(t)$, $u_{nm}(t)$ the following equation is obtained

$$\frac{d}{d\overline{t}}\begin{pmatrix} P_0A_{mn}(t) \\ \kappa_u u_{nm}(t)\end{pmatrix} = \begin{pmatrix} 0 & -C_T \\ (m^2+\pi^2n^2) & -\left[\pi^2n^2+m^2\right](K_\eta+K_\zeta)\end{pmatrix} \times \begin{pmatrix} P_0A_{mn}(t) \\ \kappa_u u_{nm}(t)\end{pmatrix} + \begin{pmatrix} 0 \\ (\pi^2n^2+m^2)B_{nm}\varepsilon_c H_0\sin(\omega_c t)\end{pmatrix}. \tag{5.42}$$

At this point it is possible to make the following definitions:

$$\widehat{A} = \begin{pmatrix} 0 & -C_T \\ (m^2+\pi^2n^2) & -\left[\pi^2n^2+m^2\right](K_\eta+K_\zeta)\end{pmatrix} = \begin{pmatrix} 0 & p_{12} \\ p_{21} & p_{22}\end{pmatrix} \tag{5.43}$$

$$\overrightarrow{\chi}(\overline{t}) = \begin{pmatrix} A_{mn}(t) \\ u_{nm}(t)\end{pmatrix} \tag{5.44}$$

$$\overrightarrow{h}(\overline{t}) = \begin{pmatrix} 0 \\ (\pi^2n^2+m^2)B_{nm}\varepsilon_c H_0\sin(\omega_c t)\end{pmatrix}. \tag{5.45}$$

Using these definitions one gets

$$\frac{d\overrightarrow{\chi}(t)}{dt} = \widehat{A}\overrightarrow{\chi}(t) + \overrightarrow{h}(t) \tag{5.46}$$

which is of first order in t, and linear with an inhomogeneity given by the vector $\overrightarrow{h}(t)$.

This equation can be solved diagonalizing the matrix $\widehat{A}$. If $\widehat{M}$ is the modal matrix, then

$$\widehat{M}^{-1}\widehat{A}\widehat{M} = \widehat{S}, \tag{5.47}$$

where $\widehat{S}$ is the spectral matrix consisting of the eigen values of the matrix $\widehat{A}$

$$\widehat{S} = \begin{pmatrix} \lambda_1 & 0 \\ 0 & \lambda_2 \end{pmatrix}. \tag{5.48}$$

The eigen values of matrix $\widehat{A}$ are

$$\lambda_1 = \frac{p_{22} + \sqrt[2]{p_{22}^2 + 4p_{12}p_{21}}}{2}, \tag{5.49}$$

$$\lambda_2 = \frac{p_{22} - \sqrt[2]{p_{22}^2 + 4p_{12}p_{21}}}{2}. \tag{5.50}$$

The real or complex character of the solution of the NS equations depends on λ_i. From the previous equations it is quite evident that λ_i is complex if $(m^2+n\pi^2)(K_\eta + K_\zeta)^2 < C_T$. For typical polymer fluids [88] it is observed that $(1+\pi^2)(K_\eta + K_\zeta)^2 > C_T$ and for this reason the results computed in this work are real.

The matrix equation will be satisfied by the following modal matrix

$$\widehat{M} = \begin{pmatrix} -\frac{\lambda_2}{p_{21}} & -\frac{\lambda_1}{p_{21}} \\ 1 & 1 \end{pmatrix}, \tag{5.51}$$

$$\widehat{M}^{-1} = \begin{pmatrix} -\frac{p_{21}}{\lambda_2-\lambda_1} & -\frac{\lambda_1}{\lambda_2-\lambda_1} \\ \frac{p_{21}}{\lambda_2-\lambda_1} & \frac{\lambda_2}{\lambda_2-\lambda_1} \end{pmatrix}. \tag{5.52}$$

Using the previous equations, in particular eq. (5.52), an uncoupled equation for a vector $\overrightarrow{G}(t)$ is obtained

$$\overrightarrow{G}(t) = \widehat{M}^{-1}\overrightarrow{\chi}(\overline{t}), \tag{5.53}$$

$$\overrightarrow{G}(t) = \begin{pmatrix} \alpha_{nm}(t) \\ \varpi_{nm}(t) \end{pmatrix}. \tag{5.54}$$

Therefore, an equation for $\overrightarrow{G}(t)$ is obtained

$$\begin{aligned} \frac{d\overrightarrow{G}(t)}{dt} &= \widehat{S}G_l(t) + \widehat{M}^{-1}\overrightarrow{h}(t) \\ &= \begin{pmatrix} \lambda_1 & 0 \\ 0 & \lambda_2 \end{pmatrix} \begin{pmatrix} \alpha_{nm}(t) \\ \varpi_{nm}(t) \end{pmatrix} \\ &\quad + \begin{pmatrix} \left(\frac{-\lambda_1}{\lambda_2-\lambda_1}\right)(\pi^2n^2+m^2)\, B_{nm}\varepsilon_c H_0 \sin(\omega_c t) \\ \left(\frac{\lambda_2}{\lambda_2-\lambda_1}\right)(\pi^2n^2+m^2)\, B_{nm}\varepsilon_c H_0 \sin(\omega_c t) \end{pmatrix}. \end{aligned} \tag{5.55}$$

This equation is an uncoupled equation for each component of the vector $\overrightarrow{G}(t)$ and is symmetric with respect to the parameters λ_i; the solution of this equation is

$$\alpha_{nm}(t) = \left(e^{\lambda_1 t}\alpha_0 + \frac{\lambda_1 B_{nm}\varepsilon_c \overline{H_0}\,(\pi^2 n^2 + m^2)}{(\lambda_1^2 + \omega_c^2)\,(\lambda_2 - \lambda_1)} \left[\omega_c \cos(t) + \lambda_1 \sin(t)\right] \right), \tag{5.56}$$

$$\varpi_{nm}(t) = \left(e^{\lambda_2 t}\varpi_0 - \frac{\lambda_2 B_{nm}\varepsilon_c \overline{H_0}\,(\pi^2 n^2 + m^2)}{(\lambda_2^2 + \omega_c^2)\,(\lambda_2 - \lambda_1)} \left[\omega_c \cos(t) + \lambda_2 \sin(t)\right] \right). \tag{5.57}$$

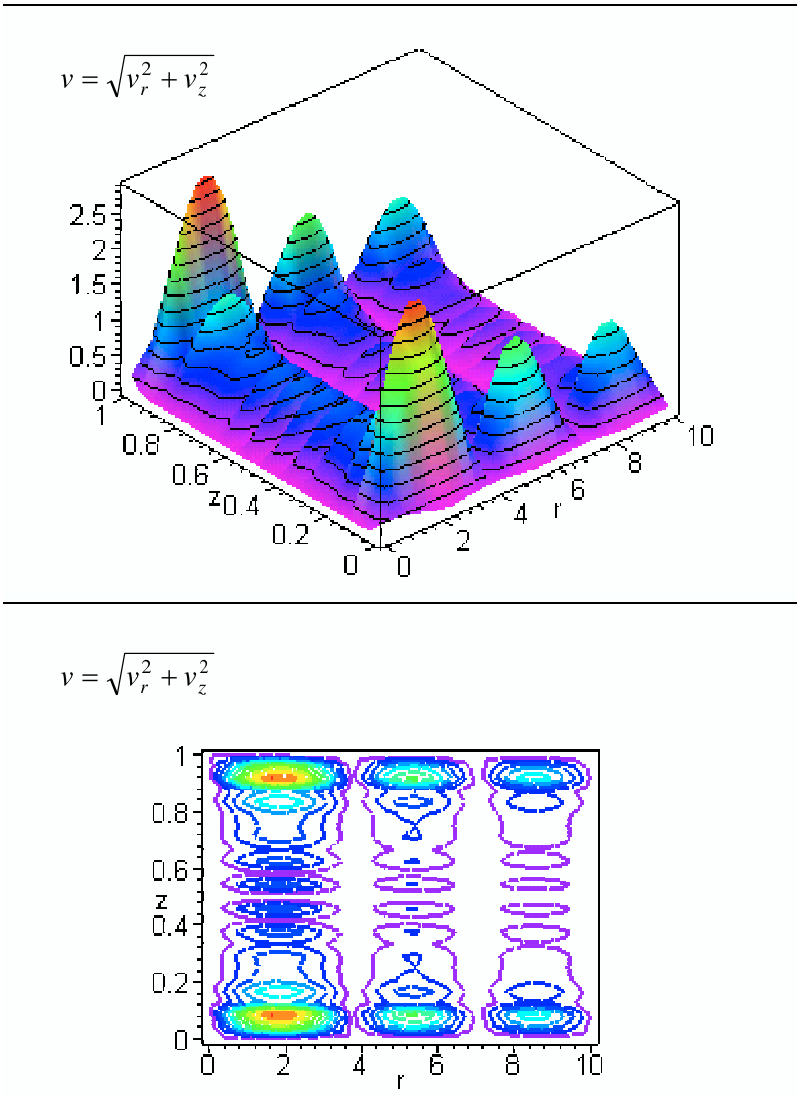

Figure 5.2: Velocity profile for non contact mode at $t = 1$. The distance of the particle to the interface of the liquid is $d = 0.42$ (All the distance dimensions are normalized to the film thickness $H_{0\Gamma}$; in these calculations $H_{0\Gamma} = 1$). This result shows that the velocity profile is distributed in peacks, with a main peak under the nanoparticle, at $r = 0$; for $r \to \infty$ the velocity profile is smaller, and eventualy tends to be zero. The velocity profile inside the bulk is smaller than the velocity near the interface.

Thus, the solution for $\overrightarrow{\chi}(t)$ is

$$\overrightarrow{\chi}(\bar{t}) = \widehat{M}\overrightarrow{G}(t). \tag{5.58}$$

Whit this transformation it is possible to make the computation of the functions $u_{nm}(t)$ and $A_{nm}(t)$ respectively as

$$\begin{aligned} u_{nm}(t) &= \alpha_{nm}(t) + \varpi_{nm}(t) \qquad (5.59)\\ &= \left(e^{\lambda_1 t}\alpha_0 + \frac{\lambda_1 B_{nm}\varepsilon_c\overline{H_0}\,(\pi^2n^2+m^2)}{(\lambda_1^2+\omega_c^2)\,(\lambda_2-\lambda_1)} \times [\omega_c\cos(t)+\lambda_1\sin(t)]\right) + \\ &\quad \left(e^{\lambda_2 t}\varpi_0 - \frac{\lambda_2 B_{nm}\varepsilon_c\overline{H_0}\,(\pi^2n^2+m^2)}{(\lambda_2^2+\omega_c^2)\,(\lambda_2-\lambda_1)}\,[\omega_c\cos(t)+\lambda_2\sin(t)]\right), \end{aligned}$$

$$\begin{aligned} A_{nm}(t) &= -\frac{\lambda_2}{p_{21}}\alpha_{nm}(t) - \frac{\lambda_2}{p_{21}}\varpi_{nm}(t) \qquad (5.60)\\ &= -\frac{\lambda_2}{p_{21}}\left(e^{\lambda_1 t}\alpha_0 + \frac{\lambda_1 B_{nm}\varepsilon_c\overline{H_0}\,(\pi^2n^2+m^2)}{(\lambda_1^2+\omega_c^2)\,(\lambda_2-\lambda_1)}\,[\omega_c\cos(t)+\lambda_1\sin(t)]\right) - \\ &\quad \frac{\lambda_2}{p_{21}}\left(e^{\lambda_2 t}\varpi_0 - \frac{\lambda_2 B_{nm}\varepsilon_c\overline{H_0}\,(\pi^2n^2+m^2)}{(\lambda_2^2+\omega_c^2)\,(\lambda_2-\lambda_1)}\,[\omega_c\cos(t)+\lambda_2\sin(t)]\right). \end{aligned}$$

Finally the functions $v_{nm}(t)$ and $u_{nm}(t)$ are linearly transformed into $f_{nm}(t)$ and $g_{nm}(t)$

$$f_{nm}(t) = \left(\frac{mu_{nm}(t) + n\pi v_{nm}(t)}{m^2 + (n\pi)^2}\right), \tag{5.61}$$

$$g_{nm}(t) = \left(\frac{mv_{nm}(t) - n\pi u_{nm}(t)}{m^2 + (n\pi)^2}\right); \tag{5.62}$$

These solutions must fulfill initial conditions and for this reason it is necessary to make correct definitions for the constants inside the previous expressions. The initial velocity fields as well as the pressure field are at the initial time equal to zero. For the time function of the pressure and the velocity fields one has

$$A_{nm}(0) = 0, \tag{5.63}$$

$$f_{nm}(0) = 0, \tag{5.64}$$

$$g_{nm}(0) = 0. \tag{5.65}$$

These last two conditions also imply

$$v_{nm}(0) = 0, \tag{5.66}$$

which yields $\beta_0 = 0$. For the other velocity field there is also a similar definition for the initial condition

$$u_{nm}(0) = 0 \tag{5.67}$$

Nevertheless, it is necessary to consider initial conditions for the $\alpha_{nm}(t)$ and $\varpi_{nm}(t)$ as

$$\alpha_{nm}(0) = 0, \tag{5.68}$$

$$\varpi_{nm}(0) = 0. \tag{5.69}$$

This last equations permits to fix the constants α_0 and ϖ_0

$$\alpha_0 = \frac{\lambda_1 B_{nm} \varepsilon_c \overline{H_0} \left(\pi^2 n^2 + m^2\right)}{\left(\lambda_1^2 + \omega_c^2\right)\left(\lambda_2 - \lambda_1\right)}, \tag{5.70}$$

$$\varpi_0 = \frac{\lambda_2 B_{nm} \varepsilon_c \overline{H_0} \left(\pi^2 n^2 + m^2\right)}{\left(\lambda_2^2 + \omega_c^2\right)\left(\lambda_2 - \lambda_1\right)}. \tag{5.71}$$

With the previous definitions given by equations (5.70) and (5.71) it is possible to deduce the corresponding field functions

$$\alpha_{nm}(t) = \alpha_0 \left[\cos(t) + \lambda_1 \sin(t) - e^{\lambda_1 t}\right], \tag{5.72}$$

$$\varpi_{nm}(t) = \varpi_0 \left[e^{\lambda_2 t} - \cos(t) - \lambda_2 \sin(t)\right]. \tag{5.73}$$

that means, the solutions are the composition of an oscillatory and a relaxation part. The complete solutions of the NS equations for a compressible fluid are

$$\begin{aligned} v^r(r,z,t) \;=\; & \sum_{n,m} \frac{m}{m^2 + (n\pi)^2} \times \Big(\frac{\lambda_1 B_{nm} \varepsilon_c \overline{H_0} \left(\pi^2 n^2 + m^2\right)}{\left(\lambda_1^2 + \omega_c^2\right)\left(\lambda_2 - \lambda_1\right)} \times \\ & \left(-\omega_c e^{\lambda_1 t} + \left[\omega_c \cos(t) + \lambda_1 \sin(t)\right]\right) + \\ & \frac{\lambda_2 B_{nm} \varepsilon_c \overline{H_0} \left(\pi^2 n^2 + m^2\right)}{\left(\lambda_2^2 + \omega_c^2\right)\left(\lambda_2 - \lambda_1\right)} \times \\ & \left(\omega_c e^{\lambda_2 t} - \left[\omega_c \cos(t) + \lambda_2 \sin(t)\right]\right)\Big) \times \\ & J_0(mr)\cos(nz), \end{aligned} \tag{5.74}$$

$$
\begin{aligned}
v^z(r,z,t) &= \sum_{n,m} \frac{-n\pi}{m^2+(n\pi)^2} \times \Big(\frac{\lambda_1 B_{nm}\varepsilon_c \overline{H_0}\,(\pi^2n^2+m^2)}{(\lambda_1^2+\omega_c^2)\,(\lambda_2-\lambda_1)} \times \\
&\quad (-\omega_c e^{\lambda_1 t} + [\omega_c\cos(t)+\lambda_1\sin(t)]) \\
&\quad + \frac{\lambda_2 B_{nm}\varepsilon_c \overline{H_0}\,(\pi^2n^2+m^2)}{(\lambda_2^2+\omega_c^2)\,(\lambda_2-\lambda_1)} \times \\
&\quad (\omega_c e^{\lambda_2 t} - [\omega_c\cos(t)+\lambda_2\sin(t)])) \times \\
&\quad J_1(mr)\sin(nz), \qquad (5.75)
\end{aligned}
$$

$$
\begin{aligned}
P(r,z,t) &= \sum_{n,m} (-\frac{\lambda_2}{p_{21}} \times \frac{\lambda_1 B_{nm}\varepsilon_c \overline{H_0}\,(\pi^2n^2+m^2)}{(\lambda_1^2+\omega_c)\,(\lambda_2-\lambda_1)} \times \\
&\quad (-\omega_c e^{\lambda_1 t} + [\omega_c\cos(t)+\lambda_1\sin(t)]) - \\
&\quad \frac{\lambda_1}{p_{21}} \frac{\lambda_2 B_{nm}\varepsilon_c \overline{H_0}\,(\pi^2n^2+m^2)}{(\lambda_2^2+\omega_c)\,(\lambda_2-\lambda_1)} \times \\
&\quad (\omega_c e^{\lambda_2 t} - [\omega_c\cos(t)+\lambda_2\sin(t)])) \times \\
&\quad J_0(mr)\cos(nz). \qquad (5.76)
\end{aligned}
$$

The previous solutions are a version that contain the coefficients λ_i and p_{ij} defined for the calculation of the uncoupled equations. Replacing the corresponding coefficients into λ_i one obtains

$$
\lambda_1 = \left[\pi^2n^2+m^2\right](K_\eta+K_\zeta)\,\frac{-1+\sqrt[2]{1-\frac{C_T}{[\pi^2n^2+m^2]\left(K_\eta+K_\zeta\right)}}}{2}, \qquad (5.77)
$$

$$
\lambda_2 = \left[\pi^2n^2+m^2\right](K_\eta+K_\zeta)\,\frac{-1-\sqrt[2]{1-\frac{C_T}{[\pi^2n^2+m^2]\left(K_\eta+K_\zeta\right)}}}{2}, \qquad (5.78)
$$

$$
\lambda_2-\lambda_1 = -\left[\pi^2n^2+m^2\right](K_\eta+K_\zeta)\,\sqrt[2]{1-\frac{C_T}{[\pi^2n^2+m^2]\,(K_\eta+K_\zeta)}}. \qquad (5.79)
$$

The explicit solutions for the pressure and velocity fields are

$$
\begin{aligned}
v^r(r,z,t) \;=\; & \sum_{n,m} \frac{mB_{nm}\varepsilon_c\overline{H_0}}{m^2+(n\pi)^2} \times \frac{\sqrt{\left[\pi^2n^2+m^2\right](K_\eta+K_\zeta)}}{2\sqrt{\left[\pi^2n^2+m^2\right](K_\eta+K_\zeta)-C_T}} \times \\
& \times([4\left(1-\sqrt[2]{1-\frac{C_T}{\left[\pi^2n^2+m^2\right](K_\eta+K_\zeta)}}\right) \div \\
& ((\left[\pi^2n^2+m^2\right](K_\eta+K_\zeta)(-1+ \\
& \sqrt[2]{1-\frac{C_T}{\left[\pi^2n^2+m^2\right](K_\eta+K_\zeta)}}))^2+4\omega_c^2)] \times \\
& (-\omega_c e^{\left(\left[\pi^2n^2+m^2\right]\left(K_\eta+K_\zeta\right)\frac{-1+\sqrt[2]{1-\frac{C_T}{\left[\pi^2n^2+m^2\right]\left(K_\eta+K_\zeta\right)}}}{2}\right)\overline{t}} + \\
& [\omega_c\cos(t)+(\left[\pi^2n^2+m^2\right](K_\eta+K_\zeta)\times \\
& \frac{-1+\sqrt[2]{1-\frac{C_T}{\left[\pi^2n^2+m^2\right]\left(K_\eta+K_\zeta\right)}}}{2})\sin(t)]) + \\
& [4\left(1-\sqrt[2]{1-\frac{C_T}{\left[\pi^2n^2+m^2\right](K_\eta+K_\zeta)}}\right) \div \\
& ((\left[\pi^2n^2+m^2\right](K_\eta+K_\zeta)(1+ \\
& \sqrt[2]{1-\frac{C_T}{\left[\pi^2n^2+m^2\right](K_\eta+K_\zeta)}}))^2+4\omega_c^2)] \times \\
& (\omega_c e^{\left(\left[\pi^2n^2+m^2\right]\left(K_\eta+K_\zeta\right)\frac{-1-\sqrt[2]{1-\frac{C_T}{\left[\pi^2n^2+m^2\right]\left(K_\eta+K_\zeta\right)}}}{2}\right)\overline{t}} - \\
& [\omega_c\cos(t)+(\left[\pi^2n^2+m^2\right](K_\eta+K_\zeta)\times \\
& \frac{-1-\sqrt[2]{1-\frac{C_T}{\left[\pi^2n^2+m^2\right]\left(K_\eta+K_\zeta\right)}}}{2})\sin(t)])) \times \\
& J_0(mr)\cos(nz), \qquad (5.80)
\end{aligned}
$$

$$
\begin{aligned}
v^z(r,z,t) \;=\; & \sum_{n,m} \frac{-n\pi\lambda_1 B_{nm}\varepsilon_c \overline{H_0}}{m^2+(n\pi)^2} \times \frac{\sqrt{\left[\pi^2n^2+m^2\right](K_\eta+K_\zeta)}}{2\sqrt{\left[\pi^2n^2+m^2\right](K_\eta+K_\zeta)-C_T}} \\
& ([4\left(1-\sqrt[2]{1-\frac{C_T}{\left[\pi^2n^2+m^2\right](K_\eta+K_\zeta)}}\right)\div \\
& ((\left[\pi^2n^2+m^2\right](K_\eta+K_\zeta)(-1+ \\
& \sqrt[2]{1-\frac{C_T}{\left[\pi^2n^2+m^2\right](K_\eta+K_\zeta)}}))^2+4\omega_c^2)]\times \\
& (-\omega_c e^{\left(\left[\pi^2n^2+m^2\right]\left(K_\eta+K_\zeta\right)\frac{-1+\sqrt[2]{1-\frac{C_T}{\left[\pi^2n^2+m^2\right]\left(K_\eta+K_\zeta\right)}}}{2}\right)\overline{t}}+ \\
& [\omega_c\cos(t)+(\left[\pi^2n^2+m^2\right](K_\eta+K_\zeta)\times \\
& \frac{-1+\sqrt[2]{1-\frac{C_T}{\left[\pi^2n^2+m^2\right]\left(K_\eta+K_\zeta\right)}}}{2})\sin(t)]) \\
& +[4\left(1-\sqrt[2]{1-\frac{C_T}{\left[\pi^2n^2+m^2\right](K_\eta+K_\zeta)}}\right)\div \\
& ((\left[\pi^2n^2+m^2\right](K_\eta+K_\zeta)(1+ \\
& \sqrt[2]{1-\frac{C_T}{\left[\pi^2n^2+m^2\right](K_\eta+K_\zeta)}}))^2+4\omega_c^2)]\times \\
& (\omega_c e^{\left(\left[\pi^2n^2+m^2\right]\left(K_\eta+K_\zeta\right)\frac{-1-\sqrt[2]{1-\frac{C_T}{\left[\pi^2n^2+m^2\right]\left(K_\eta+K_\zeta\right)}}}{2}\right)\overline{t}} \\
& -[\omega_c\cos(t)+(\left[\pi^2n^2+m^2\right](K_\eta+K_\zeta)\times \\
& \frac{-1-\sqrt[2]{1-\frac{C_T}{\left[\pi^2n^2+m^2\right]\left(K_\eta+K_\zeta\right)}}}{2})\sin(t)]))\times \\
& J_1(mr)\sin(nz), \qquad (5.81)
\end{aligned}
$$

$$
\begin{aligned}
P(r,z,t) \;=\; & \sum_{n,m} B_{nm}\varepsilon_c\overline{H_0}(-\left(K_\eta+K_\zeta\right)\frac{-1-\sqrt[2]{1-\frac{C_T}{\left[\pi^2n^2+m^2\right]\left(K_\eta+K_\zeta\right)}}}{2}\times \\
& [4\left(1-\sqrt[2]{1-\frac{C_T}{\left[\pi^2n^2+m^2\right]\left(K_\eta+K_\zeta\right)}}\right)\div \\
& ((\left[\pi^2n^2+m^2\right]\left(K_\eta+K_\zeta\right)(-1+ \\
& \sqrt[2]{1-\frac{C_T}{\left[\pi^2n^2+m^2\right]\left(K_\eta+K_\zeta\right)}}))^2+4\omega_c^2)]\times \\
& (-\omega_c e^{\left(\left[\pi^2n^2+m^2\right]\left(K_\eta+K_\zeta\right)\frac{-1+\sqrt[2]{1-\frac{C_T}{\left[\pi^2n^2+m^2\right]\left(K_\eta+K_\zeta\right)}}}{2}\right)t} \\
& +[\omega_c\cos(t)+\left[\pi^2n^2+m^2\right]\left(K_\eta+K_\zeta\right)\times \\
& \frac{-1+\sqrt[2]{1-\frac{C_T}{\left[\pi^2n^2+m^2\right]\left(K_\eta+K_\zeta\right)}}}{2}\sin(t))]- \\
& [4\left(1-\sqrt[2]{1-\frac{C_T}{\left[\pi^2n^2+m^2\right]\left(K_\eta+K_\zeta\right)}}\right)\div \\
& ((\left[\pi^2n^2+m^2\right]\left(K_\eta+K_\zeta\right)(1+ \\
& \sqrt[2]{1-\frac{C_T}{\left[\pi^2n^2+m^2\right]\left(K_\eta+K_\zeta\right)}}))^2+4\omega_c^2)]\times \\
& (\omega_c e^{\left(\left[\pi^2n^2+m^2\right]\left(K_\eta+K_\zeta\right)\frac{-1-\sqrt[2]{1-\frac{C_T}{\left[\pi^2n^2+m^2\right]\left(K_\eta+K_\zeta\right)}}}{2}\right)t} \\
& -[\omega_c\cos(t)+(\left[\pi^2n^2+m^2\right]\left(K_\eta+K_\zeta\right)\times \\
& \frac{-1-\sqrt[2]{1-\frac{C_T}{\left[\pi^2n^2+m^2\right]\left(K_\eta+K_\zeta\right)}}}{2})\sin(t)]))\times \\
& J_0(mr)\cos(nz). \qquad (5.82)
\end{aligned}
$$

These solutions are restricted in its domain to the boundary imposed by the liquid-vapor interface. In order to obtain all the boundary conditions it is neccesary to solve the NS equations in the gas phase and then correctely define the interface. The calculation of the solutions of the NS equations in the gas phase is presented in the next section.

5.3 Solutions in the gas phase

For the gas phase it is also possible to suppose that there are small perturbations of the mean velocity and pressure fields. The NS equations are formulated in this case , for the description of the small velocities and pressure, treating into the gas phase as a compressible non viscous liquid. A similar ansatz as presented for the liquid phase, is proposed for the small variation of the pressure and the two components of the velocity, i.e. the solutions are expressed as an expansion of orthonormal functions, with the function in the time as an unknown.

The velocity and pressure fields are calculated from the liquid-vapor interface to infinity; in this case $\lim_{z\to\infty} P_r(r,z,t) \to 0$ and also $\lim_{z\to\infty} v^i(r,z,t) \to 0$; both conditions allow the formulation of an exponential ansatz for the functions over the z axis. The proposed solutions are (in a similar way as the liquid phase, the small perturbations of each field δF will be noted simply as F)

$$v_D^r(r,z,t) = \sum_{n,m} f_{nm}^D(t) e^{-nz} J_1(mr), \tag{5.83}$$

$$v_D^z(r,z,t) = \sum_{n,m} g_{nm}^D(t) e^{-nz} J_0(mr), \tag{5.84}$$

$$P_r^D(r,z,t) = \sum_{n,m} A_{nm}^D(t) e^{-nz} J_0(mr), \tag{5.85}$$

$$\phi\prime_D(r,z,t) = \sum_{n,m} B_{nm}^D \overline{H_0} e^{-nz} J_0(mr). \tag{5.86}$$

The last equation require the estimation of the coefficients B_{nm}^D for the perturbation of the potential in the gas phase.

The gas above the liquid film is also a compressible liquid whose viscosity is extremely small; thus the only components of the stress tensor are the pressure on its diagonal. Therefore, from the NS equations and the continuity equation, three equations for each of those three fields are obtained:

$$\begin{aligned} \frac{d}{dt}\begin{pmatrix} f_{nm}^D(t) \\ g_{nm}^D(t) \\ A_{nm}^D(t) \end{pmatrix} &= \begin{pmatrix} 0 & 0 & m \\ 0 & 0 & n\pi \\ -C_T^D m & C_T^D 2\pi n & 0 \end{pmatrix} \begin{pmatrix} f_{nm}^D(t) \\ g_{nm}^D(t) \\ A_{nm}^D(t) \end{pmatrix} \\ &+ \begin{pmatrix} m \\ 2\pi n \\ 0 \end{pmatrix} \varepsilon_c B_{nm}^D \overline{H_0} \sin(\omega_c t), \end{aligned} \tag{5.87}$$

C_T^D is the isothermal compressibility constant for the gas phase (in this case a perfec gas will be considered).

From this equation

$$\frac{d}{dt}\left(\frac{1}{m}f_{nm}^{D}(t)-\frac{1}{n\pi}g_{nm}^{D}(t)\right)=0, \tag{5.88}$$

the integration of the previous equation gives:

$$f_{nm}^{D}(t)=\frac{m}{n\pi}g_{nm}^{D}(t)+\mathrm{Kte}_{f}. \tag{5.89}$$

For $t=0$ there are no velocity fields in the gas phase; therefore $g_{nm}^{D}(t)=0$ and $f_{nm}^{D}(t)=0$. This last condition implies that $\mathrm{Kte}_{f}=0$, making possible to stake the following relation:

$$f_{nm}^{D}(t)=\frac{m}{n\pi}g_{nm}^{D}(t). \tag{5.90}$$

Replacing this result into the eq. (5.87) one obtain

$$\frac{d}{dt}\begin{pmatrix} g_{nm}^{D}(t) \\ A_{nm}^{D}(t)\end{pmatrix}=\begin{pmatrix} 0 & m \\ D_{T} & 0\end{pmatrix}\begin{pmatrix} g_{nm}^{D}(t) \\ A_{nm}^{D}(t)\end{pmatrix}+\begin{pmatrix} \varepsilon_{c}B_{nm}^{D}\overline{H_{0}}\sin(\omega_{c}t) \\ 0\end{pmatrix}. \tag{5.91}$$

where $D_{T}=\frac{(n\pi)^{2}-m^{2}}{n\pi}C_{T}^{D}$. The equivalent vectorial form of the previous equation is

$$\frac{d}{dt}\overrightarrow{\chi^{D}}=\widehat{A^{D}}\overrightarrow{\chi^{D}}+\overrightarrow{h^{D}}, \tag{5.92}$$

which can be diagonalized in order to get an uncoupled differential equation; the elements in the previous equation are

$$\widehat{A^{D}}=\begin{pmatrix} 0 & m \\ D_{T} & 0\end{pmatrix}, \tag{5.93}$$

$$\overrightarrow{\chi^{D}}=\begin{pmatrix} g_{nm}^{D}(t) \\ A_{nm}^{D}(t)\end{pmatrix}, \tag{5.94}$$

$$\overrightarrow{h^{D}}\begin{pmatrix} \varepsilon_{c}B_{nm}^{D}\overline{H_{0}}\sin(\omega_{c}t) \\ 0\end{pmatrix}. \tag{5.95}$$

Diagonalizing the matrix $\widehat{A^{D}}$ gives the following spectral matrix:

$$\widehat{S^{D}}=\begin{pmatrix} \sqrt{D_{T}m} & 0 \\ 0 & -\sqrt{D_{T}m}\end{pmatrix}, \tag{5.96}$$

and using the same method applied for the liquid phase, uncoupled differential equations are obtained

$$\frac{d\alpha_{nm}^{D}(t)}{dt}=\frac{\sqrt{D_{T}m}}{2m}\left(2m\alpha_{nm}^{D}(t)+\varepsilon_{c}B_{nm}^{D}\overline{H_{0}}\sin(\omega_{c}t)\right), \tag{5.97}$$

$$\frac{d\varpi_{nm}^D(t)}{dt} = -\frac{\sqrt{D_T m}}{2m}\left(2m\alpha_{nm}^D(t) + \varepsilon_c B_{nm}^D \overline{H_0}\sin(\omega_c t)\right), \tag{5.98}$$

where[8]

$$\alpha_{nm}^D(t) = \frac{\sqrt{D_T m}}{2m} g_{nm}^D(t) + \frac{1}{2}A_{nm}^D(t), \tag{5.100}$$

$$\varpi_{nm}^D(t) = -\frac{\sqrt{D_T m}}{2m} g_{nm}^D(t) + \frac{1}{2}A_{nm}^D(t). \tag{5.101}$$

The solutions of the equations (5.97) and (5.98) are

$$\begin{aligned} \alpha_{nm}^D(t) &= C^\alpha e^{\sqrt{D_T m}t} - \frac{\varepsilon_c B_{nm}^D \overline{H_0}\sqrt{D_T m}}{2m(D_T m + \omega_c^2)} \times & (5.102)\\ & (\omega_c \cos(\omega_c t) - \sqrt{D_T m}\sin(\omega_c t)), & (5.103) \end{aligned}$$

$$\begin{aligned} \varpi_{nm}^D(t) &= -C^\varpi e^{-\sqrt{D_T m}t} + \frac{\varepsilon_c B_{nm}^D \overline{H_0}\sqrt{D_T m}}{2m(D_T m + \omega_c^2)} \times \\ & (\omega_c \cos(\omega_c t) - \sqrt{D_T m}\sin(\omega_c t)). & (5.104) \end{aligned}$$

Taking again into account that $g_{nm}^D(0) = 0$ and $A_{nm}^D(0) = 0$, it is possible to say that $\varpi_{nm}^D(0) = 0$ and $\alpha_{nm}^D(0) = 0$. This condition implies that the constants C^α and C^ϖ have the following values

$$C^\alpha = -C^\varpi = \frac{\varepsilon_c B_{nm}^D \overline{H_0}\omega_c\sqrt{D_T m}}{2m(D_T m + \omega_c^2)}; \tag{5.105}$$

transforming ϖ_{nm}^D and α_{nm}^D into g_{nm}^D and A_{nm}^D one obtains

$$\begin{aligned} g_{nm}^D(t) &= \frac{m}{\sqrt{D_T m}}\left(\alpha_{nm}^D(t) - \varpi_{nm}^D(t)\right) \\ &= \frac{\varepsilon_c B_{nm}^D \overline{H_0}\omega_c}{2(D_T m + \omega_c^2)}[e^{\sqrt{D_T m}t} + \\ & e^{-\sqrt{D_T m}t} + 2\cos(\omega_c t)] \end{aligned} \tag{5.106}$$

[8]The matrix of eigenvectors is in this case

$$\widehat{M^D} = \begin{pmatrix} \frac{m}{\sqrt{D_T m}} & \frac{-m}{\sqrt{D_T m}} \\ 1 & 1 \end{pmatrix} \tag{5.99}$$

$$
\begin{aligned}
A^D_{nm}(t) &= \alpha^D_{nm}(t) + \varpi^D_{nm}(t) \\
&= -\frac{\varepsilon_c B^D_{nm}\overline{H_0}\omega_c\sqrt{D_T m}}{2m(D_T m+\omega_c^2)}[e^{-\sqrt{D_T m}t} - \\
&\quad e^{\sqrt{D_T m}t} + 2D_T m\sin(\omega t)] \qquad (5.107)
\end{aligned}
$$

the two solutions for eq. (5.92). The complete solutions in the gas space are

$$
\begin{aligned}
v^r_D(r,z,t) &= \sum_{n,m}\frac{m}{n\pi}\frac{\varepsilon_c B^D_{nm}\overline{H_0}\omega_c}{2(\frac{(n\pi)^2-m^2}{n\pi}C^D_T m+\omega_c^2)}\times \\
&\quad [e^{\sqrt{\frac{(n\pi)^2-m^2}{n\pi}C^D_T m}t} + e^{-\sqrt{\frac{(n\pi)^2-m^2}{n\pi}C^D_T m}t} \\
&\quad +2\cos(\omega_c t)]\times e^{-nz}J_1(mr), \qquad (5.108)
\end{aligned}
$$

$$
\begin{aligned}
v^z_D(r,z,t) &= \sum_{n,m}\frac{\varepsilon_c B^D_{nm}\overline{H_0}\omega_c}{2(\frac{(n\pi)^2-m^2}{n\pi}C^D_T m+\omega_c^2)}\times \\
&\quad [e^{\sqrt{\frac{(n\pi)^2-m^2}{n\pi}C^D_T m}t} + e^{-\sqrt{\frac{(n\pi)^2-m^2}{n\pi}C^D_T m}t} \\
&\quad +2\cos(\omega_c t)]\times e^{-nz}J_0(mr), \qquad (5.109)
\end{aligned}
$$

$$
\begin{aligned}
P^D_r(r,z,t) &= \sum_{n,m}-\frac{\varepsilon_c B^D_{nm}\overline{H_0}\omega_c\sqrt{\frac{(n\pi)^2-m^2}{n\pi}C^D_T m}}{2m(\frac{(n\pi)^2-m^2}{n\pi}C^D_T m+\omega_c^2)}\times \\
&\quad [e^{-\sqrt{\frac{(n\pi)^2-m^2}{n\pi}C^D_T m}t} - e^{\sqrt{\frac{(n\pi)^2-m^2}{n\pi}C^D_T m}t} + \\
&\quad 2\frac{(n\pi)^2-m^2}{n\pi}C^D_T m\sin(\omega t)]\times e^{-nz}J_0(mr). \qquad (5.110)
\end{aligned}
$$

In the previous equation it is interesting to observe that there are imaginary values for $(n\pi)^2 < m^2$, implying that the exponetial functions are related only to a pure relaxatory but also to an oscillatory behavior(this result has origin in the definition of the ansatz on the z axis; in contrast, the solutions for the liquid phase are periodic and do not invert any sign in the continuity equation).

In the section about the results the calculation of the coefficients B^D_{nm} will be done. In the next section the calculation of the boundary conditions for the liquid-vapor phase will be presented.

5.4 Boundary conditions at the liquid-vapor interface

The perturbation of the liquid film by an external force induces not only deviations of the pressure and velocity, but also deviations of the interface. As was defined in the introduction of this chapter, the perturbation induced into the system imply also a perturbation of the vector normal to the interface

$$\overrightarrow{e}\prime_z = \varsigma(r,t)\overrightarrow{e}_r + \overrightarrow{e}_z, \tag{5.111}$$

where $\varsigma(r,t)$ is the perturbation of the normal vector, depending on the displacement of the interface. In the following points the general equations for the boundary conditions at the liquid-vapor interface are shown, considering conservation of mass and momentum.

1. Mass: The general equation for the mass conservation is

$$\rho_I\left(\overrightarrow{v}_I|_\Gamma - \overrightarrow{v}_\Gamma\right)\overrightarrow{e}\prime_z - \rho_{II}\left(\overrightarrow{v}_{II}|_\Gamma - \overrightarrow{v}_\Gamma\right)\overrightarrow{e}\prime_z = \left[-\frac{d\chi_m}{dt} + 2S_\Gamma\left|\overrightarrow{v_\Gamma}\right|\chi_m + \tau\right]. \tag{5.112}$$

   Because $\overrightarrow{v}_a$ and $\overrightarrow{v}_\Gamma$ are small velocities, the elements of second order involved in this formula will be reduced to first order therms.

   Then the following equation is obtained

$$\rho_I\left(\overrightarrow{v}_I|_\Gamma - \overrightarrow{v}_\Gamma\right)\overrightarrow{e}_z - \rho_{II}\left(\overrightarrow{v}_{II}|_\Gamma - \overrightarrow{v}_\Gamma\right)\overrightarrow{e}_z = \left[-\frac{d\chi_m}{dt} + 2S_\Gamma\left|\overrightarrow{v_\Gamma}\right|\chi_m + \tau\right]. \tag{5.113}$$

   where $\overrightarrow{v}_a$ are the velocities in the phases I or II, ρ_I is the density in the phase I and ρ_{II} is the density in the phase II; the velocity of the interface is in this equation given by $\overrightarrow{v}_\Gamma$. The left side is related to the rate of evaporation of the liquid, defined as:

$$\dot{m} = \rho_I\left(\overrightarrow{v}_I|_\Gamma - \overrightarrow{v}_\Gamma\right)\overrightarrow{e}_z - \rho_I\left(\overrightarrow{v}_{II} - \overrightarrow{v}_\Gamma\right)\overrightarrow{e}_z. \tag{5.114}$$

   On the right side χ_m represents the accumulation of mass at the interface, S_Γ represents the curvature of the interface, and τ is the surface density of mass production.

   In this problem there is no accumulation of mass at the interface and therefore there is no flux of mass inside of the system. Furthermore there is no production of mass at the interface. Then

$$\tau = 0, \tag{5.115}$$

$$\chi_m = 0 \tag{5.116}$$

and consequently the equation for the conservation of mass can be reduced to the following one (in the following equations $\overrightarrow{v}$ represents the velocity field in the fluid and $\overrightarrow{v_D}$ the velocity field in the gas phase)

$$\rho\,(\overrightarrow{v}|_\Gamma - \overrightarrow{v_\Gamma})\,\overrightarrow{e_z} - \rho_D\,(\overrightarrow{v_D}|_\Gamma - \overrightarrow{v_\Gamma})\,\overrightarrow{e_z} = 0, \tag{5.117}$$

which can be rewriten as the following equation, which describes the velocity field at the interface:

$$\overrightarrow{v_\Gamma}\overrightarrow{e_z} = \frac{(\rho\,\overrightarrow{v}|_\Gamma - \rho_D\overrightarrow{v_D}|_\Gamma)}{\rho - \rho_D}\overrightarrow{e_z}. \tag{5.118}$$

and completes the condition of mass conservation at the liquid-vapor interface. The boundary condition considered for the analysis of the conservation of momentum at the interface, will be presented in the following item.

2. Momentum: The most general equation for the conservation of momentum is given as

$$\left(\overleftrightarrow{T}_I - \overleftrightarrow{T}_{II}\right)|_\Gamma\,\overrightarrow{e}\prime_z - \dot{m}\,(\overrightarrow{p}_I - \overrightarrow{p}_{II})\,|_\Gamma = \left[-\frac{d\overrightarrow{\chi}_p}{dt} + 2S_\Gamma\,|\overrightarrow{v_\Gamma}|\,\overrightarrow{\chi}_p + \overleftrightarrow{\tau}\,\overrightarrow{e}\prime_z\right], \tag{5.119}$$

where $\overleftrightarrow{T}_a$ is the stress tensor in phase I or II and $\overrightarrow{p}_a$ is the momentum in phase I or II. On the right side of the equation $\overrightarrow{\chi}_p$ is the density flux at the interface

$$\overrightarrow{\chi}_p = \overrightarrow{v_\Gamma}\chi_m. \tag{5.120}$$

Using the fact that there is no accumulation of mass at the interface, given by (5.120), then

$$\overrightarrow{\chi}_p = 0, \tag{5.121}$$

$$2S_\Gamma\,|\overrightarrow{v_\Gamma}|\,\overrightarrow{\chi}_p = 0. \tag{5.122}$$

The last element of the right side of eq. (2) is given by

$$\overleftrightarrow{\tau}\,\overrightarrow{e}\prime_z = 2\gamma_\Gamma S_\Gamma\,\overrightarrow{e}\prime_z, \tag{5.123}$$

where γ_Γ is the surface tension of the interface. Therefore, considering that the rate of evaporation is equal to zero (eq. (5.124)) eq. (2) can be expressed in the following way

$$\left(\overleftrightarrow{T}_I - \overleftrightarrow{T}_{II}\right)|_\Gamma\,\overrightarrow{e}\prime_z = 2\gamma_\Gamma S_\Gamma\,\overrightarrow{e}\prime_z. \tag{5.124}$$

The solutions of this equation will be given in the next section.

5.4.1 Conservation of momentum at the interface: boundary conditions.

The equation (5.124) is valid for the present case where phase I is the liquid phase and the phase II is the vapor phase, i.e.

$$\left(\overleftrightarrow{T} - \overleftrightarrow{T}_D\right)|_\Gamma \overrightarrow{n} = 2\gamma_\Gamma S_\Gamma \overrightarrow{n}. \tag{5.125}$$

where $\overrightarrow{e}\prime_z = \varsigma(r,t)\overrightarrow{e}_r + \overrightarrow{e}_z$ is the normal vector to the interface, $\overleftrightarrow{T}_I = \overleftrightarrow{T_0}_0 + \delta\overleftrightarrow{T}$ ($\overleftrightarrow{T}_0$ is the stress tensor in equilibrium, whose diagonal elements are the pressure in equilibrium) and $S_\Gamma = S_{0\Gamma} + \delta S_\Gamma$ [9]; Considering that the perturbations of the system are very small, the previous equation can be derived into

$$\begin{aligned} 2\gamma_\Gamma\left(S_{0\Gamma} + \delta S_\Gamma\right)\left(\overrightarrow{e}\prime_z\right) &= \left(\overleftrightarrow{T}_0 + \delta\overleftrightarrow{T}\right)|_\Gamma\left(\overrightarrow{e}\prime_z\right) - \\ &\quad \left(\overleftrightarrow{T}_{0D} + \delta\overleftrightarrow{T}_D\right)|_\Gamma\left(\overrightarrow{e}\prime_z\right) \\ 2\gamma_\Gamma\left(S_{0\Gamma}\overrightarrow{e}\prime_z + \left(\delta S_\Gamma\right)\overrightarrow{e}_z\right) &= \overleftrightarrow{T}_0|_\Gamma\overrightarrow{e}\prime_z + \left(\delta\overleftrightarrow{T}|_\Gamma\right)\overrightarrow{e}_z - \\ &\quad \overleftrightarrow{T}_{0D}|_\Gamma\overrightarrow{e}\prime_z + \left(\delta\overleftrightarrow{T}_D|_\Gamma\right)\overrightarrow{e}_z \end{aligned} \tag{5.126}$$

In this last expression the perturbation of the equilibrium curvature at the interface is given by

$$S_\Gamma = \frac{1}{2}\nabla\frac{\nabla H_\Gamma}{\sqrt{1+\left(\nabla H_\Gamma\right)^2}}, \tag{5.127}$$

such that the linearized form of the surface curvature is given by

$$S_{0\Gamma} + \delta S_\Gamma = \frac{1}{2}\nabla\frac{\nabla H_{0\Gamma}}{\sqrt{1+\left(\nabla H_0\right)^2}} + \frac{1}{2}\nabla^2\delta H_\Gamma(r,t). \tag{5.128}$$

The perturbations of the system are small deviations from the equilibrium state. Aditionally the particle is placed far away from the interface where $S_{0\Gamma} \to 0$ (the surface tension is different to zero). Therefore for the film thickness

$$H_\Gamma(r,t) \to H_{0\Gamma} + \delta H_\Gamma(r,t), \tag{5.129}$$

where $H_{0\Gamma}$ is a constant. That means, the small perturbations introduce small deviations of the mean surface, where the curvature is absent. This result implies that the boundary will be evaluated at $H_{0\Gamma}$ (if this condition does not holds, i.e. for bigger perturbations of the system, the equations are again non linear). The

[9] It is interesting to observe that the equations in general relativity have the same form as the equations for this boundary condition. See for example[87]

conditions imposed for this equations have as principal implication that only non contact mode of AFM microscopy can be evaluated using linearized hydrodynamics.

In equilibrium a flat interface has the following implication for the equation for the boundary condition

$$\overleftrightarrow{T}_0|_\Gamma - \overleftrightarrow{T}_{0D}|_\Gamma = 0, \tag{5.130}$$

that means, in equilibrium the pressure of the gas phase is equal the pressure in the liquid phase. Therefore eq.(5.126) reduces to the following equation

$$\left(\delta\overleftrightarrow{T}|_\Gamma - \delta\overleftrightarrow{T}_D|_\Gamma\right)\overrightarrow{e}_z = 2\gamma_\Gamma\delta S_\Gamma\overrightarrow{e}_z \tag{5.131}$$

which describes the boundary conditions at the liquid-vapor interface under small external perturbations introduced by a nanoparticle (in the vapor phase), placed above the liquid-vapor interface.

In the present particular case the liquid and the vapor phase are compressible, with a viscous liquid phase. The problem is described in cylindrical coordinates and the system is symmetric on the radial coordinate. So the elements of the projected stress tensor[10] on the normal of the interface are:

$$\overleftrightarrow{T}_I\overrightarrow{e}_z = \begin{pmatrix} T^{rz} \\ T^{zz} \end{pmatrix} \tag{5.133}$$

where

$$T^{rz}(r,z,t) = K_\eta\left[\nabla_r v^z(r,z,t) + \nabla_z v^r(r,z,t)\right] \tag{5.134}$$

$$T^{zz}(r,z,t) = -\delta^{zz}P(r,z,t) + \left(K_\eta + \delta^{zz}K_\xi\right)\nabla_z v^z(r,z,t) + K_\xi\delta^{zz}\nabla_r v^r(r,z,t). \tag{5.135}$$

$$T^{zz}_D(r,z,t) = -\delta^{zz}P_D(r,z,t) \tag{5.136}$$

The equation eq. (5.131) is reduced to the following equations (In order to simply the notation $\delta S_{0\Gamma}$ will be writed as $S_\Gamma(r,t)$)

$$K_\eta\left[\nabla_r v^z + \nabla_z v^r\right]|_\Gamma = 0, \tag{5.137}$$

$$\begin{aligned} 2\gamma_\Gamma S_\Gamma(r,t) &= [-\delta^{zz}P(r,z,t) + \delta^{zz}P_D(r,z,t) - \phi\prime(r,z)\delta d(t) + \\ &\quad \left(K_\eta + \delta^{zz}K_\xi\right)\nabla_z v^z(r,H_{0\Gamma},t) + K_\xi\delta^{zz}\nabla_r v^r(r,H_{0\Gamma},t)]|_\Gamma \end{aligned} \tag{5.138}$$

[10]The stress tensor for compressible fluids is represented by means of the following expresion:

$$T^{ij} = P\delta^{ij} + K_\eta\delta^{ii}\nabla_i v^j + K_\xi\delta^{ij}\nabla_i v^i \tag{5.132}$$

The eq. (5.137) is a von Neuman like boundary condition for $v^z(r,z,t)$ at the interface and is one of the searched boundary conditions. This condition will be satisfied by the ansatz proposed for this velocity, because it is given by a sinus function whose complete period is defined inside the film

$$\begin{aligned}\nabla_r \sum_{n,m} v_0^z g_{nm}(t)\sin(nz)|_\Gamma J_1(mr) + \\ \nabla_z \sum_{n,m} v_0^r f_{nm}(t)\cos(nz)|_\Gamma J_0(mr) \quad = \\ \sum_{n,m}[v_0^z g_{nm}(t)\sin(2\pi n)|_\Gamma \nabla_r J_1(mr) + \\ v_0^r f_{nm}(t)\sin(2\pi n) J_0(mr)] = 0. \end{aligned} \tag{5.139}$$

This solution implyies that the boundary condition for mass conservation reduces into the following formula:

$$v_\Gamma^z = \frac{\rho_D v_D^z|_\Gamma}{\rho_D - \rho}. \tag{5.140}$$

Takig into account both, the ansatz proposed for the solutions of the presure and the velocity fields into the liquid film, and the definition of the gradient operator in cylindrical coordinates (right side of eq. (5.138)), the following expresion is obtained

$$\begin{aligned}\gamma_\Gamma \nabla^2 \delta H(r,t) \quad = \quad & \sum_{n,m}[A_{nm}^D(t)e^{-n\pi} + \{-A_{nm}(t) + (n\pi)\left(K_\eta + \delta^{zz}K_\xi\right) g_{nm}(t) \\ & + K_\xi \delta^{zz} m f_{nm}\}(t)\cos(2\pi n)]J_0(mr), \end{aligned} \tag{5.141}$$

which is a second order homogeneous differential equation. The following ansatz for $\delta H_\Gamma(r,t)$ is propossed

$$\delta H_\Gamma(r,t) = \sum_{n,m} W_{nm}^{0\Gamma}(t) J_0(mr), \tag{5.142}$$

with

$$\begin{aligned} W_{nm}^{0\Gamma}(t) \quad = \quad & \frac{e^{-2\pi n}}{\gamma_\Gamma m^2} A_{nm}^D(t) + \frac{\cos(2\pi n)}{\gamma_\Gamma m^2}[-A_{nm}(t) - B_{nm}\varepsilon_c \overline{H_0}\sin(\omega_c t) \\ & + (n\pi)\left(K_\eta + \delta^{zz}K_\xi\right) g_{nm}(t) + K_\xi \delta^{zz} m f_{nm}(t)]. \end{aligned} \tag{5.143}$$

In this equation it is possible to introduce the solutions for $A_{nm}(t)$, $A_{nm}^D(t)$, $g_{nm}(t)$ and $f_{nm}(t)$. Replacing this solutions into (5.143)and after some algebra

$$
\begin{aligned}
H_{nm}^{0\Gamma}(t) &= \frac{\varepsilon_c \overline{H_0}\omega_c}{\gamma_\Gamma}[-\frac{B_{nm}^D\sqrt{\frac{(n\pi)^2-m^2}{n\pi}C_T^D m}}{2m(\frac{(n\pi)^2-m^2}{n\pi}C_T^D m+\omega_c^2)}\times \\
&[e^{-\sqrt{\frac{(n\pi)^2-m^2}{n\pi}C_T^D mt}}-e^{\sqrt{\frac{(n\pi)^2-m^2}{n\pi}C_T^D mt}}+ \\
&2\frac{(n\pi)^2-m^2}{n\pi}C_T^D m\sin(\omega t)]\times e^{-2\pi n} \\
&-B_{nm}[\frac{(\lambda_2+(K_\xi(m^2-n\pi)^2)-K_\eta(n\pi)^2))\lambda_1}{(\lambda_1^2+\omega_c^2)(\lambda_2-\lambda_1)}\times \\
&(\cos(t)+\lambda_1\sin(t)-e^{\lambda_1 t})+ \\
&\frac{(\lambda_1+(K_\xi(m^2-(n\pi)^2)-K_\eta(n\pi)^2))\lambda_2}{(\lambda_2^2+\omega_c^2)(\lambda_2-\lambda_1)}\times \\
&(-\cos(t)-\lambda_2\sin(t)+e^{\lambda_2 t})]\cos(2\pi n)]. \qquad (5.144)
\end{aligned}
$$

which represents the function in the time of the small curvature of the interface; this set of equations complete the boundary conditions for the liquid and the vapor phase, giving information of its displacement.

The displacement of the interface can be projected over the r and z axis; as was shown in equation (5.140) the z component of the velocity at the interface is related to the component on the z axis of the velocity in the vapor phase. The total interfacial velocity is given by

$$v_\Gamma = \frac{\partial H(r,t)}{\partial t}, \qquad (5.145)$$

and therefore

$$v_\Gamma^r = \sqrt{(v_\Gamma)^2-(v_\Gamma^z)^2}, \qquad (5.146)$$

implying that the liquid at the interface suffers a normal and tangential displacement. The velocity of the liquid phase on the z axis at the interface is zero, implying condensation of the gas at the interface of the film; therefore the dynamics of the interface, in particular its velocity, is interpreted as the mechanical response of this gas condensation (i.e. the fluctuations of the interface can be found in the gas condensation at the interface).

5.4.2 Boundary conditions at substrate and radial boundary conditions

At the substrate there is a perfect mathematical boundary without curvature (in this particular problem a non structured substrate is considered). Additionally there is moreover no accumulation of mass and consequentely no density flux at this interface. Using the equation for the determination of the boundary conditions eq. (5.11) the following conditions are obtained:

1. Mass: the considered substrate is impermeable, i.e. there is no transport of mass through the solid-liquid interface. From the equation (5.11) for the conservation of mass the only therm that survive is the rate of transport of liquid through the substrate, given by:

$$\dot{m_f} = 0 \tag{5.147}$$

2. The substrate is non structured and admits slip boundary conditions. i.e. the tangential velocity at the surface of the solid-liquid interface is different to zero.

At infinite separation from the particle the solutions of the pressure and velocity fields must vanish. Then the following boundary conditions are imposed in the present system

$$\lim_{r\to\infty} v^i = 0, \tag{5.148}$$

$$\lim_{r\to\infty} P = 0, \tag{5.149}$$

The first condition is fulfilled by the expansion of v^z in terms of $sin(nz)$; the second condition is fulfilled by the Bessel expansion of all the solutions.

Remarks about the solutions In fig. 5.3 the pressure and the vertical component of the velocity are plotted as a function of the time, for $r = 0$ and $z = H_{0\Gamma}$; these results show (for the parameters employed in this numerical computations see the introduction) that the relaxation part only dominates for $t \to 0$; for $t > 0$ the solution is dominated by the harmonic functions.

The most significant result is the dependence of the velocity fields on the external potential, where the defect is imposed by an harmonic perturbation. In fig. 5.2 the velocity fields for a compressible simple liquid are represented for fixed time and for a fixed distance of the particle from the liquid film. In this case the density of the liquid is $\rho = 0.8$, the amplitude of the perturbation is about 6σ (the constants used in this calculation can be consulted in appendix I). In this solution a very fast relaxation of the velocity fields inside the liquid film is evident, where the velocity is particularly high at both interfaces of the liquid film.

The density and viscosity, as well as the film thickness and proper frequency, are quantities that permits to make the calculation of the Reynolds number of the system (see [78] [79]). If $Re_\eta < 30$ the fluid is laminar [79] [94]. So if this condition is not satisfied, then the liquid is turbulent. For thin films this condition is satisfied if both the proper velocity and the film thickness are small enough.

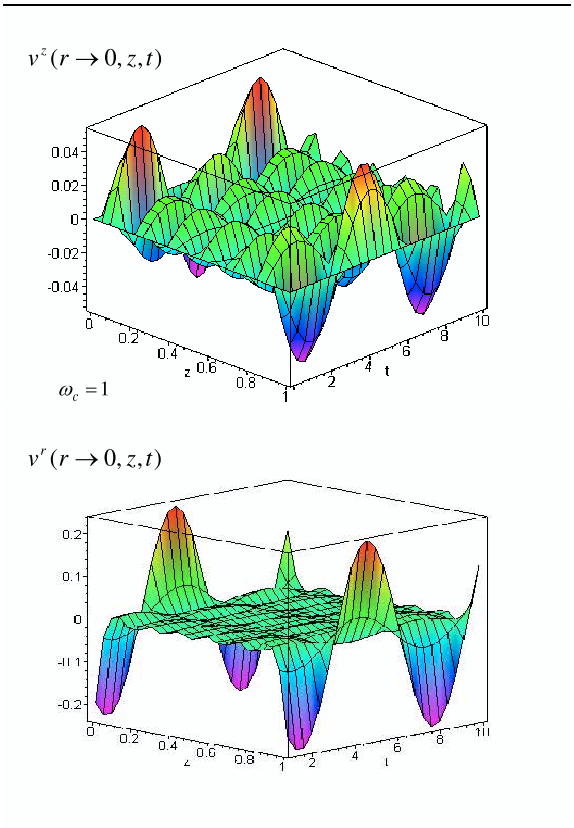

Figure 5.3: Time dependence of the solutions for velocity at a fixed frequency $\omega_c = 1.0$ (All the unities are normalized. See appendix I). From this results it is possible see that the oscillatory part have dominance in the solutions. In the first two figures above the components of the velocity field v_r and v_z are plotted as a function of the vertical distance and time.

5.5 Alternative potential and B_{nm} coefficients

The calculation of the solutions for the linearized hydrodynamics requires the expansion of the external potential in Bessel-Fourier-Bessel series. It was repeatedly shown that the particle interact with the liquid with a LJ potential; the main problem is that the transformation of such potential has no closed form, as is shown in appendix G. For this reason, an alternative potential, given as a functional of exponential functions, is introduced. This alternative function has a similar shape as the conventional potential and has a closed form after the Bessel-Fourier-Bessel transformation. This function is

$$\phi = \frac{1}{e^{\left(\frac{r-R-\sigma}{\gamma_1}\right)}} - \frac{1}{e^{\left(\frac{r-R-\sigma}{\gamma_2}\right)}}, \tag{5.150}$$

which is a superposition of an attractive and a repulsive part, in a similar way as a LJ potential. In this formula R is the radius of the particle and σ is the collision parameter.

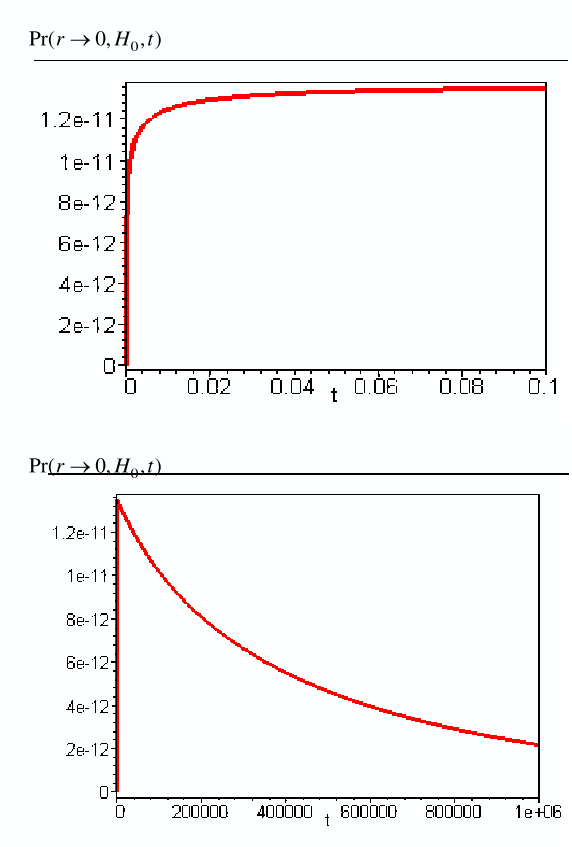

Figure 5.4: The solution for the pressure is shown in two different time regimes; this result suggest that the pressure has in such system a very slow relaxatory behavior.

The corresponding Fourier transform for this function is

$$B_{nm\_i} = \frac{1}{\pi}\int_0^h \sin(nz)dz \int_0^\infty drr\phi_i\prime J_0(mr), \tag{5.151}$$

where

$$\phi_i\prime = \frac{e^{\sigma_0}e^{-\frac{r}{\gamma_i}}(d-z)}{\sqrt{(d-z)^2+r^2}}, \tag{5.152}$$

with $\sigma_0 = \sigma + R$ and $i = 1, 2$. Then the complete transformation for the potential can be written as

$$B_{nm} = B_{nm\_1} + B_{nm\_2}. \tag{5.153}$$

After the calculation of the Hankel transform [91] of the potential with respect to the parameter d this function can be used to obtain the typical function

$$H_{\left[\frac{\partial\phi}{\partial d}\right]} = \frac{\sqrt{2\,(d-z)}\gamma_i^{\frac{1}{4}} e^{\sigma_0}\,(d-z)}{\sqrt{\pi}(1+\gamma_i m^2)^{\frac{1}{4}}} K_{1/2}\left[(d-z)\sqrt{(1+\gamma_i m^2)\,/\gamma_i}\right]. \tag{5.154}$$

Here the following equivalent function for the fractional Bessel function of third order is employed

$$K_{1/2}\left[(d-z)A\right] = \frac{\sqrt{2}\sqrt{\pi}e^{-A(d-z)}}{\sqrt{A(d-z)}}, \tag{5.155}$$

where $A = \sqrt{(1+\gamma_i m^2)\,/\gamma_i}$. Using this transformation, the second integral over z is obtained as

$$\begin{aligned} B_{nm\_i} &= \frac{2\gamma_i^{\frac{1}{4}} e^{\sigma_0 - Ad}}{\sqrt{A}(1+\gamma_i m^2)^{\frac{1}{4}}} \int_0^{2\pi} e^{Az}(d-z)\sin(nz)dz \\ &= \frac{2\gamma_i^{\frac{1}{4}} e^{\sigma_0 - Ad}}{\sqrt{A}(1+\gamma_i m^2)^{\frac{1}{4}}} \frac{1}{\left(A^2+n^2\right)^2} \times \\ &\quad [\cos(nz)\left(n^3 z - ndA^2 - n^3 d - 2nA + nzA^2\right) + \\ &\quad \sin(nz)\left(A^3 d + Adn^2 + A^2 - n^2 - A^3 z - Azn^2\right)]_0^{2\pi} \end{aligned} \tag{5.156}$$

$$B_{nm\_i} = \frac{2\gamma_i^{\frac{1}{4}} e^{\sigma_0 - A\overline{d}}}{\sqrt{A}(1+\gamma_i m^2)^{\frac{1}{4}}} \frac{1}{\left(A^2+n^2\right)^2} \times \tag{5.157}$$

$$[\cos(2\pi n)\begin{pmatrix} 2\pi n^3 - ndA^2 \\ -n^3 d - 2nA + 2\pi nA^2 \end{pmatrix} - \tag{5.158}$$

$$\left(-ndA^2 - n^3 d - 2nA\right) + \tag{5.159}$$

$$\sin(2\pi n)\begin{pmatrix} A^3 d + Adn^2 + A^2 \\ -n^2 - 2\pi A^3 - 2\pi An^2 \end{pmatrix}]. \tag{5.160}$$

With this potential it is possible to obtain analytical results for the Fourier -Bessel-Fourier coefficients. Given that $n \in N$, is recommended to express the expansion coefficient of the potential of the nanoparticle as

$$\begin{aligned} B_{nm\_i} &= \frac{2\gamma_i^{\frac{1}{4}} e^{\sigma_0 - A\overline{d}}}{\sqrt{A}(1+\gamma_i m^2)^{\frac{1}{4}}} \frac{1}{\left(A^2+n^2\right)^2} \times \\ &\quad [\cos(2\pi n)\left(2\pi n^3 - ndA^2 - n^3 d - 2nA + 2\pi nA^2\right) \\ &\quad - \left(-ndA^2 - n^3 d - 2nA\right)]. \end{aligned} \tag{5.161}$$

This potential, and its transform, will be used along the present chapter for the calculation of the corresponding results. For the parameters employed in the present

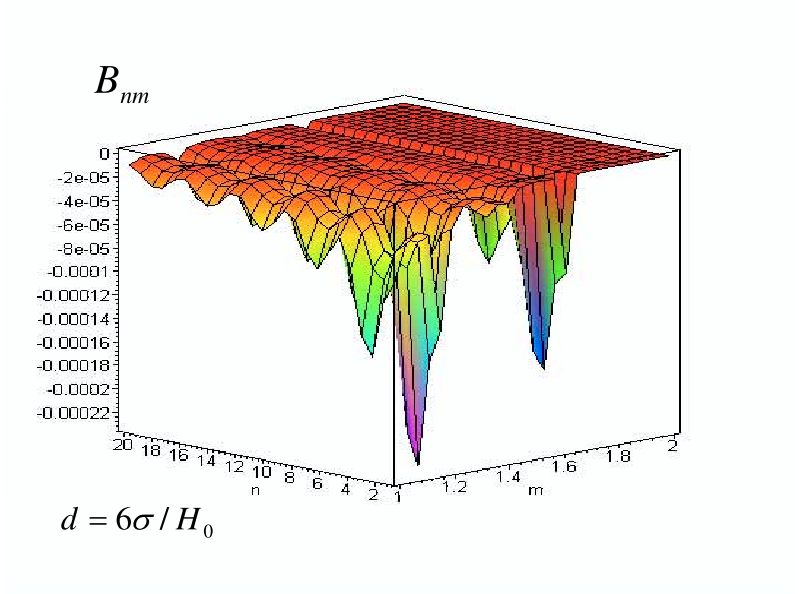

Figure 5.5: Fourier-Bessel-fourier transform of the modified LJ potential, for a particle with $R_{eff} = 4$, as a function of m and n.

problem (see appendix I), the dependence of the transform B_{nm} on n and m is shown in the figure 5.5.

On the other hand the expansion coefficients in the gas phase B^D_{nm} can be expressed as

$$B^D_{nm} = \int_{H_0}^{\infty} dz e^{-nz} \int_0^{\infty} drr\phi\prime(r,z) J_0(mr); \tag{5.162}$$

in such case the Fourier-Bessel transformation can be done; using the same expression for the Kummer function defined above in eq. (5.162), the following equation for each coefficient $B^D_{nm\_i}$ is obtained

$$\begin{aligned} B^D_{nm\_i} &= \frac{2\gamma_i^{1/4} e^{\sigma_0 - Ad}}{\sqrt{A}(1+\gamma_i m^2)^{1/4}} \lim_{z\to\infty} [e^{-(A+n)z}(-Ad - n\pi d + Az + n\pi z + 1) + \\ &\quad e^{-(A+n)H_0}(Ad + n\pi d - AH_0 - n\pi H_0 - 1)] \end{aligned} \tag{5.163}$$

due that $A > 0$, then the previous expression reduces to

$$B^D_{nm\_i} = \frac{2\gamma_i^{1/4} e^{\sigma_0 - Ad}}{\sqrt{A}(1+\gamma_i m^2)^{1/4}} e^{-(A+n)H_0}(Ad + n\pi d - AH_0 - n\pi H_0 - 1) \tag{5.164}$$

completing the expressions necessary for the expansion coefficients of the external potential.

5.6 Results

The presented results in this section were performed using periodic perturbations, given by the function $sin(\omega_c t)$. The size of the film and the nanoparticle in this calculations are not different as those used for the simulations; the effective radius of the particle is in this case $R_{eff} = 10$ and the thickness of the liquid is $H_{0\Gamma} = 14$, all quantities given in LJ unities. In appendix I the constants and main quantities used in this computations are shown

The solutions for the time domain show, as very interesting feature, two main peaks, one at the substrate and the other at the interface; at intermediary positions the pressure fluctuates around a mean value (see fig. 5.6 and fig. 5.7). In compressible fluids it was considered that the pressure is connected to the density through the isothermal bulk modulus; so the plots for the pressure are related to the density of the fluid.

The maximum pressure in the profile lies under the particle surrounded by small pressure maxima for $r > r_0$, where r_0 is the position of the particle. When $r \to \infty$ the pressure tends to zero. The pressure profile shows also a dramatic relaxation of the pressure in the bulk of the film.

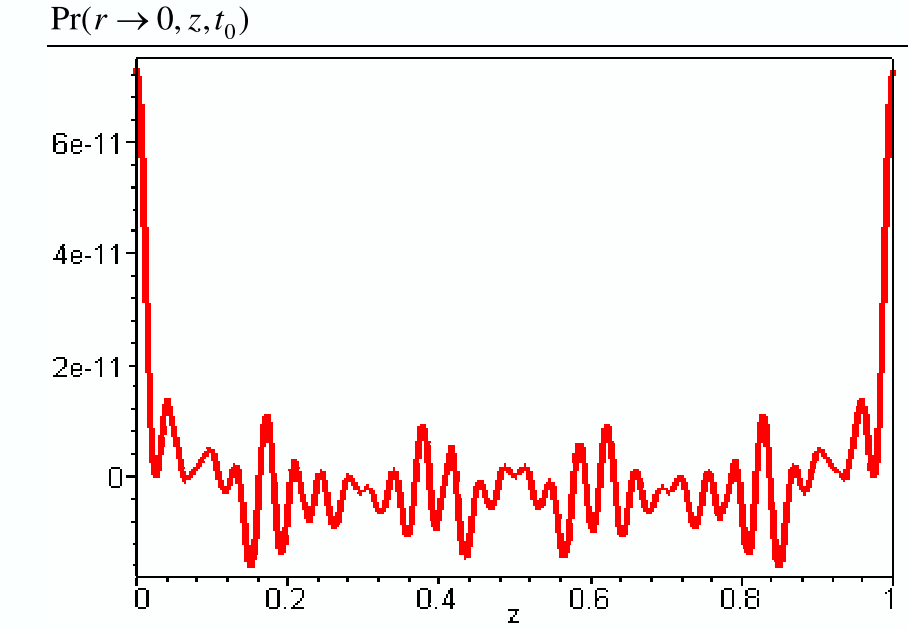

Figure 5.6: Small perturbation of the pressure for a compressible simple liquid with harmonic perturbations introduced by a nanoparticle at a fixed time and at $r = 0$. In this case, a big pressure peak close to the substrate-liquid and liquid-vapor interfaces is evident; in bulk the pressure profile has a small oscillatory behavior just bellow zero. As in the present case, the liquid is compressible, this pressure profile is related to a density profile.

The boundary conditions restricts the present problem to non contact modes (the so called non typing mode in AFM microscopy), where the position of the particle is given by $z_p = H_{0\Gamma} + d$. In the present calculations $d = 6$, which is large enough in order to avoid a curvature at the interface (See chapter 3). An analysis of the z component of the velocity is made in order to verify the boundary conditions: the solution fluctuates around a mean function that shows that the movement of the liquid at the substrate is compensated by the motion of the liquid at the interface, where the velocity produces compression lines (according to the theory, the present solutions do not admit vorticity).

All the plots presented in this chapter were computed for a fixed time, where the system is in an oscillatory regime. The solutions in the time domain are composed by a relaxatory and an oscillatory part; the relaxation obtained in this calculations was very fast. The plot of the solutions allows also to observe that near any of both interfaces the response of the liquid is bigger than inside the film, making possible to observe only small perturbations inside the film.

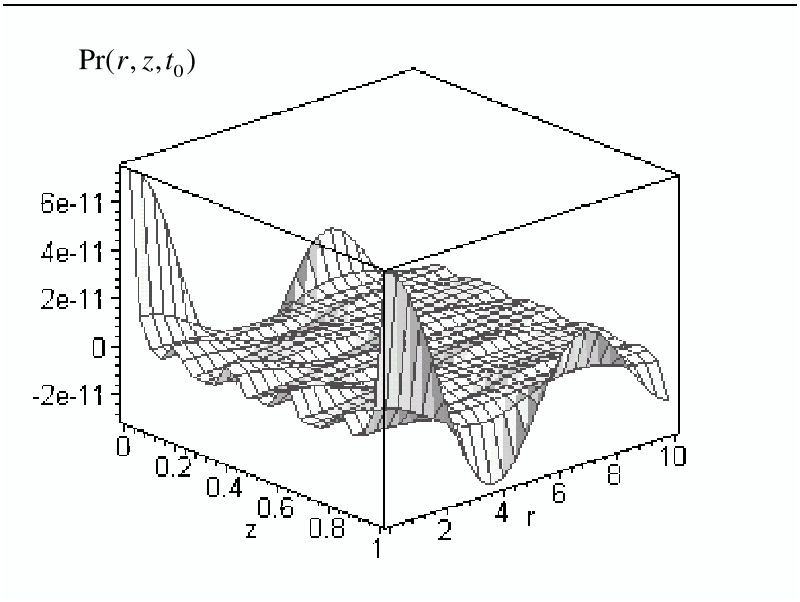

Figure 5.7: Pressure of a compressible simple liquid under load in the time domain, for a fixed time as a function of r and z. The nanoparticle is placed at $r = 0$. It is quite evident that at bulk the pressure dissipates faster than at both interfaces, where the maximal pressure is situated below the nanoparticle. Furthermore the intensity decreases as the distance to the nanoparticle increases.

5.7 Conclusions

In this section the calculation of the NS equations was shown for a liquid confined between a substrate and a single nanoparticle, for compressible and incompressible liquids, restricted to a single frequency $\omega_c = 1$. The most interesting result is the qualitative agreement with the results of simulations of fluids between two plates. It was observed that slip boundary conditions permits the existence of symmetric velocity and pressure profiles at the interface and at the substrate. The solutions for the velocity do not show vorticity; this result is clear because there are only small perturbations on the system. Aditionally the velocity shows small localized perturbations; the modulus of the velocity at the interface is bigger than the modulus of the velocity inside the liquid film.

The present results are only valid for a particle situated at a relative large distance to the interface in order to avoid its curvature. This restriction implies small deviations of the flat interface. It is important to take into account the limitations of this model, if it is used for the interpretation of experimental results, like, for example, non typing mode in AFM microscopy. The modelation of typing mode imply a curved interface that makes, through the boundary conditions, the NS equations be no more linear; therefore this calculation is useful for films with interfaces that, in equilibrium, are flat. An other restriction is the nature of the liquid: the results presented are valid only for simple liquids; in the appendix J a short calculation in the frequency domain for a complex liquid (using the so called Maxwell model for the viscosity) is shown.

A The effect of the interface on the dynamics of the particle

A.1 Short times

In this work there are two fundamental problems to be analyzed: one is related to the statics of the system (chapter 3), which was useful for the detection of the glass transition at the interface of the liquid film, and the other is related to the dynamics of the probe and its coupling with the dynamics of the particles in the melt (chapter 4). The present appendix is placed between both analysis. The question to be answered is: has the liquid-vapor interface as well as the probe-liquid interface some influence on the dynamics of the tracking particle? This question is closely related with the definition of the interaction potential of the particle: is there some difference in the dynamics of a particle that interacts with a simple LJ potential or with a modified LJ potential with the monomers?

In this case observations in the bulk are contrasted with observations at the polymer film. Moreover in the present section a comparison between the VCF and the FCF for a simple LJ particle and the modified LJ particle is shown. The relation between the MSD and the VCF of a modified LJ particle at different temperatures helps to do an analysis of the behavior of the dynamics of the tracking particle and, together with the analysis of the embedding of the particle, to obtain information on the interplay between interface and displacement.

In contrast with the results shown in chapter 4, the VCF for a LJ particle does not have the same damped oscillation behavior as that of the modified LJ particle (see fig. A.1); instead the behavior of this function shows a relaxation, similar to the typical behavior of Ornstein-Uhlenbeck process [33]. In particular this function fits to an exponential function. For $T = 0.8$ the function $\Psi(t)$ has also a negative tail that relaxes to zero; this result suggests that correlated collisions between the probe and liquid particles dominate the dynamics of the tracking particle. [1]. For $T = 1.4$ the relaxation character and a very small negative tail of the VCF is evident; this result insinuates that the dynamics of the LJ nanoparticle at this temperature is dominated by binary collisions, whereas in the first case the total force acting on

[1] The conventional theories for self diffusion in liquids are based on the Boltzmann equation, where binary collisions between particles are take into account. Such picture is applicable only for low densities; but it will be used in this section for the interpretation of the dynamics of the particles in the fluid [56][63] [64]

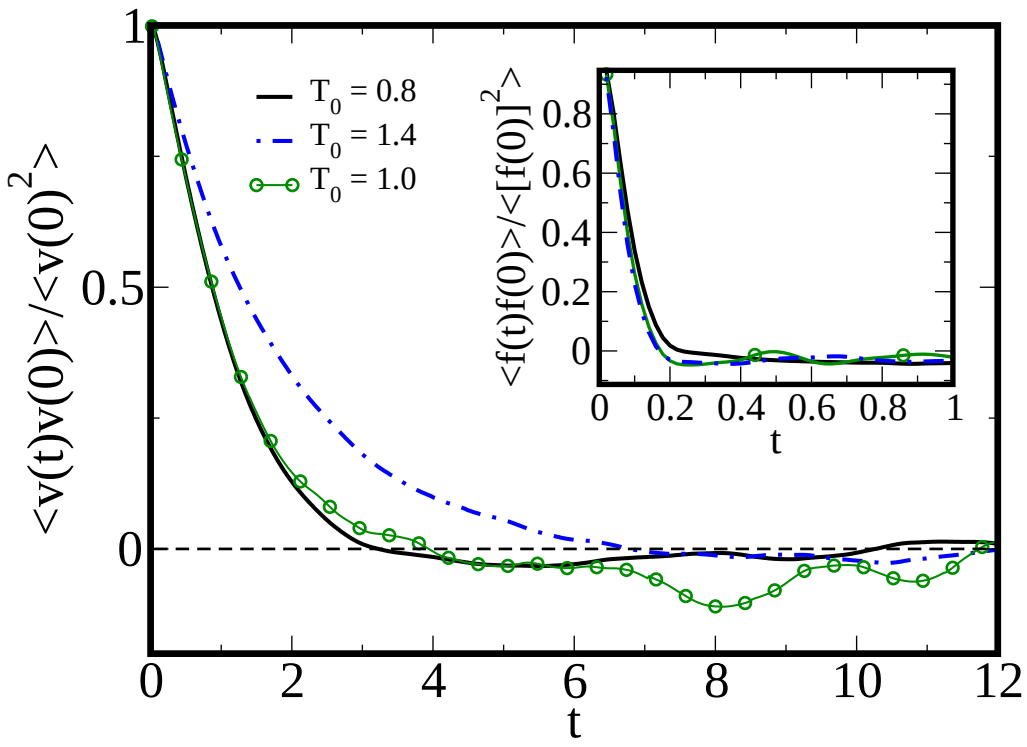

Figure A.1: VCF for a simple LJ particle at short times and three different temperatures above T_g. For $T = 1.4$ is possible to observe a long decay and a very small negative tail of the function. In contrast with the results obtained in chapter 4, at $T >> T_g$ the VCF in this case do not shows the damped oscillatory behavior but the conventional behavior of VCF of LJ liquids [Yip].

the particle has origin in the collisions between the particle and all the neighboring particles.

This result explains again the stability of the vertical position of the particle, as was shown in the analysis of the statics of the system, and permits to understand why the modified LJ potential is more stable for the simulation of tracking particles than simple LJ potentials: the persistence of negative tails in the VCF of the modified LJ particle at very short times, shown in the chapter 4, has origin in the persistence of correlated collisions, even for $T >> T_g$, which are also responsible to 'trap' the particle in the melt. The results of the VCF for simulations with LJ particles at short times is plotted in fig. A.1. [2]

As was shown in the previous section, on the nanoparticle there is not only a

[2]For $T \sim T_g$ the negative part of the VCF is related to the diffusion of the cage on the particle [63], where independent correlated collisions lead to a negative tail of the VCF. For fluids with continuous interactions -for example polymer liquids- independent binary collisions leads to damped oscillations of the VCF. Such result can be interpreted as oscillations of the particle in its solvation shell [63] which is in this time regime at rest; in the next order the cage is allowed to move. After this time the particle can diffuse, making the self diffusion coefficient different to zero.

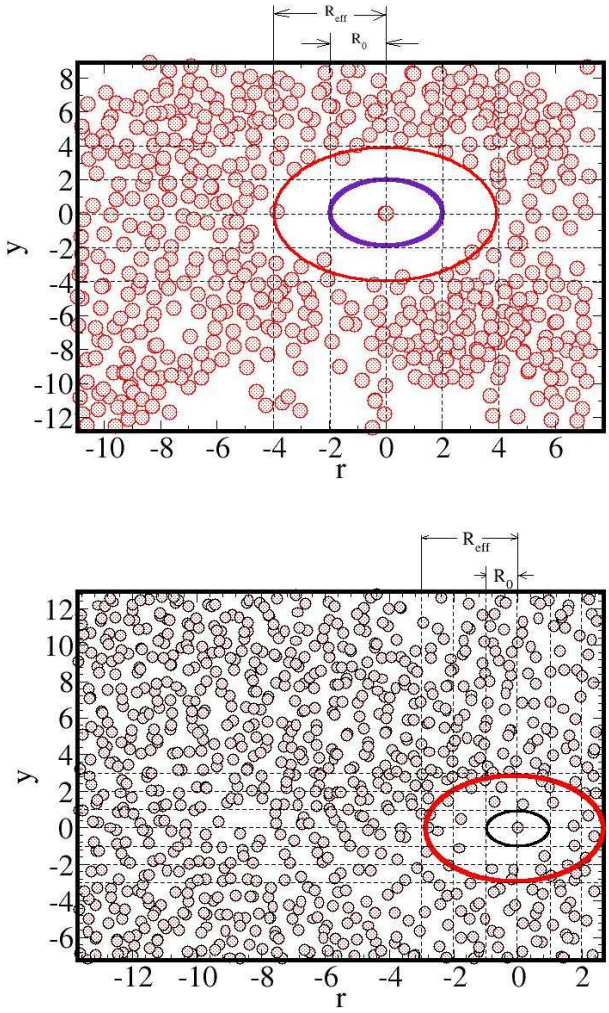

Figure A.2: Cut snapshots with different interaction potentials of the tracking particle for $T = 0.8$; the fluid has $N = 2250$, with $N_p = 10$. In this plot two different situations was tested: $R_0 = 1.0$, for $R_{eff} = 3.0$ and $R_{eff} = 4.0$, and $R_0 = 2.0$ with. For $R_0 = 2.0$ with $R_{eff} = 4.0$ the effective radius of the layer of the monomers is similar to R_{eff}, whereas for $R_0 = 1.0$, with $R_{eff} = 3.0$, this layer is smaller than $R_{eff} = 3.0$. This analysis probes whether the hard core of the particle interacts with the monomers in the film.

solvation shell but also a layer of particles around the core of the tracking particle; this fact is confirmed in the density profiles close to the particle and the qualitative calculations of the hydrostatics of the liquid: as was discussed in a previous chapter, for $T \sim T_g$ the particle produces at the interface an indentation, whereas for $T > T_g$ the particle sinks inside the melt and permits the formation of a layer at its interface (as was demonstrated in the results of the density profile close to the particle and the qualitative results for hydrostatics). In both extremes the tracking particle is strongly coupled to the monomers in the neighborhood by means of the strongly

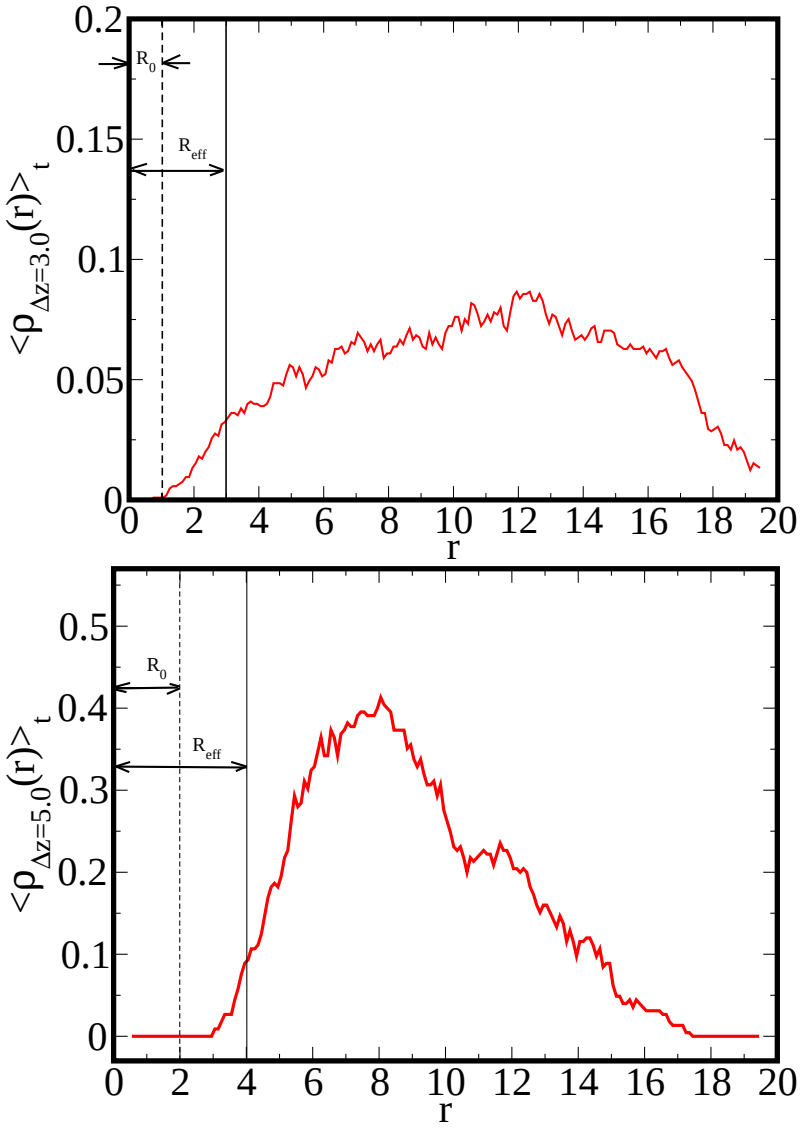

Figure A.3: Density profile for $N = 2250$, with $N_p = 10$ at $T = 0.8$. In the first panel $R_0 < \sigma$ (this result is not normalized); in the second one $R_0 \sim \sigma$. In the first case it is quite obvious that the nanoparticle is part of the other bulk particles, whereas the second density profile shows that the particle produces an excluded density and modifies the bulk density near the particle.

attractive character of the potential at the interface of the particle.

Therefore the layer of monomers on the particle induces additional effects in its dynamics by means of the increase of correlated collisions. Making a variation of the size of the hard core it is fundamental to observe the variation of the layer of particles on the nanoparticle and therefore to control different effects on the MSD of the probe. So, if $R_0 \to R_{eff}$ the area of the hard core is similar to the effective area and therefore the area of the layer of particles is similar to the effective size

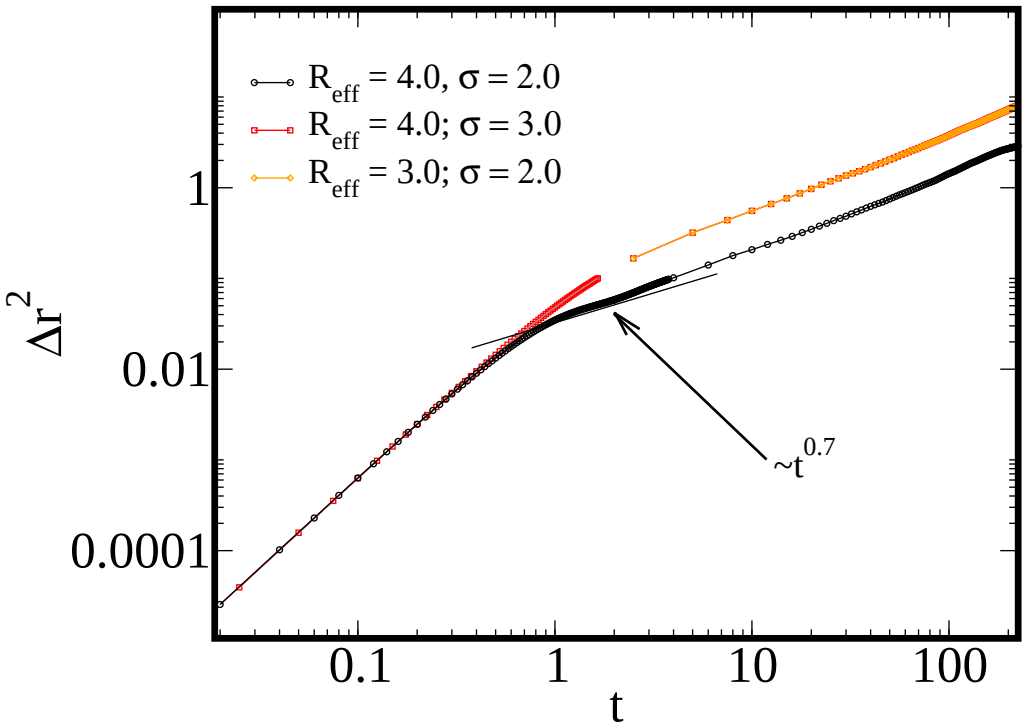

Figure A.4: DS for $N = 2250$, with $N_p = 10$ at $T = 0.8$. For $R_0 < \sigma$ it is evident that the particle evolves directly from a ballistic into a diffusive regime; in the curve below the MAD for a particle with $R_0 \sim \sigma$. In this last case the particle has a subdiffusive regime before the particle reaches a r=diffusive behavior, showing that the particle does not diffuses like a conventional LJ particle.

of the particle; a particle interacting with a simple LJ potential represents in this case a particle with a simple hard core, without a layer of particles, i.e $R_0 = R_{eff}$ and, therefore, the particle is not trapped by the neighboring monomers . On the other hand if $R_0 << R_{eff}$ the size of the layer on the particle decreases; if $R_0 \to \sigma$ the tracking particle has the same behavior as the monomers in the melt. In fig. A.2 a cut of 1σ in the polymer melt, at the equatorial line of the tracking particle, is shown; in this case the system consists of 2250 monomers, the particle has $R_{eff} = 3.0$, $R_0 = 1.0$, and $R_{eff} = 4.0$, $R_0 = 2.0$ respectively. In this snapshot the variation of the size of the layer of particles on the tracking particle is evident. The density profile as a function of this variation is shown in fig. A.3. In bot cases the MSD was computed at $T = 0.8$; the result is shown in fig. A.4. For $R_0 \to R_{eff}$ the particle shows a subdiffusive behavior, whereas for the smaller hard core particle (for $R_0 = 1.0$, $R_{eff} = 3.0$ and $R_{eff} = 4.0$) there is a direct transition from a ballistic into a diffusive regime . This result shows very clearly the effect of the layer on the tracking particle, even for $T >> T_g$, i.e. the effective covering layer of monomers on the tracking particle has a similar role as a solvation shell[3] [4].

[3] A solvation shell is similar as the cage on the particle. See [63]

[4] At temperatures close to the glass transition temperature the MSD shows very short subdifusive

An other question is, why the duration time of the plateau of the MSD in the present simulations is so short? [5] In contrast with the monomers in the melt, the hard core of the particle is able to diffuse inside the effective radius R_{eff}, where the density of particles is much smaller than outside of the particle. This affirmation has support in fig. A.3, where the density of the melt in the cut, as a function of r, is plotted from the center of the particle to $r = 40$.

crossovers. In the film this effect is reflected by a characteristic plateau (caging of the particle) followed by a very short subdiffusive regime with a characteristic slope x_1 and then either the formation of a second short plateau in bulk (Please refer to the corresponding plots for the MSD of the particle in bulk discussed in chapter 4) or the transition into an other subdiffusive regime with an other characteristic slope x_2. The described result can be again interpreted as the effect of the coupling between the particles at the layer on the nanoparticle; therefore the particles at the layer suffer also caging (which is detected in the MSD of the tracking particle).

[5] F. Varnik, personal conversation.

B D(t) in film and in bulk at $T \sim T_g$

For low temperatures the nanoparticle remains close to the interface of the film, when in the initial configuration the particle is placed above the film[1]; in this case, observing the snapshots for the system melt-particle fig. 3.10, is possible to observe that the particle produces a curvature of the interface, which is not totally flat. Is it possible that this defect at the interface has some influence on the dynamics of nanoparticles? In this case the temperature is close to T_g; fluctuations of the interface at such temperature are very slow and therefore insignificant for short times. For very long times the system reaches an ergodic limit and therefore it is possible to account for an averaged interface, which means an averaged curvature. In the present case after intermediary to long relaxation times such curvature is soft, affecting the diffusion of the particle [83]. Making an analysis of the MSD of the tracking particle it is possible to observe that at low temperatures there is a persistence of the subdiffusive behavior. After this regime the system relaxes into a diffusive regime. If the curvature of the interface plays a role in the dynamics of the particle (in this case the interface is a fluctuating surface, the so called capillary waves) then it is reasonable to think that this fact must have influence in the computation of the transport coefficients: the diffusion constant of the particle and the viscosity of the liquid close to the particle. So the diffusion constant in bulk must be different than the diffusion constant of the particle close to the interface of the film

$$\Delta D(t) = D_{Bulk}(t) - D_{Film}(t) \tag{B.1}$$

For this reason simulations in the bulk including a simple and a complex liquid are crucial in order to understand the influence of the interface. The test simulations show that there is a difference between the diffusion coefficient at short and intermediary times: in bulk this coefficient is slightly bigger than on the film. In fig. B.1 the diffusion coefficient, measured as $\Delta r^2/t$ is shown for a nanoparticle in a complex liquid in bulk and in the polymer film; an additional simulation shows the results for the diffusion coefficient of a particle inside a simple LJ liquid. In this results is possible to observe that for short times $\Delta D(t) > 0$, showing that the interface has influence on the particle at short time regimes. In intermediary to long time

[1] Like a hockey player on a frozen lake: at the interface the monomers have a very low mobility and therefore (and for the happiness of the player) he remains at the interface. The seasons convert the hokey player into a swimmer.

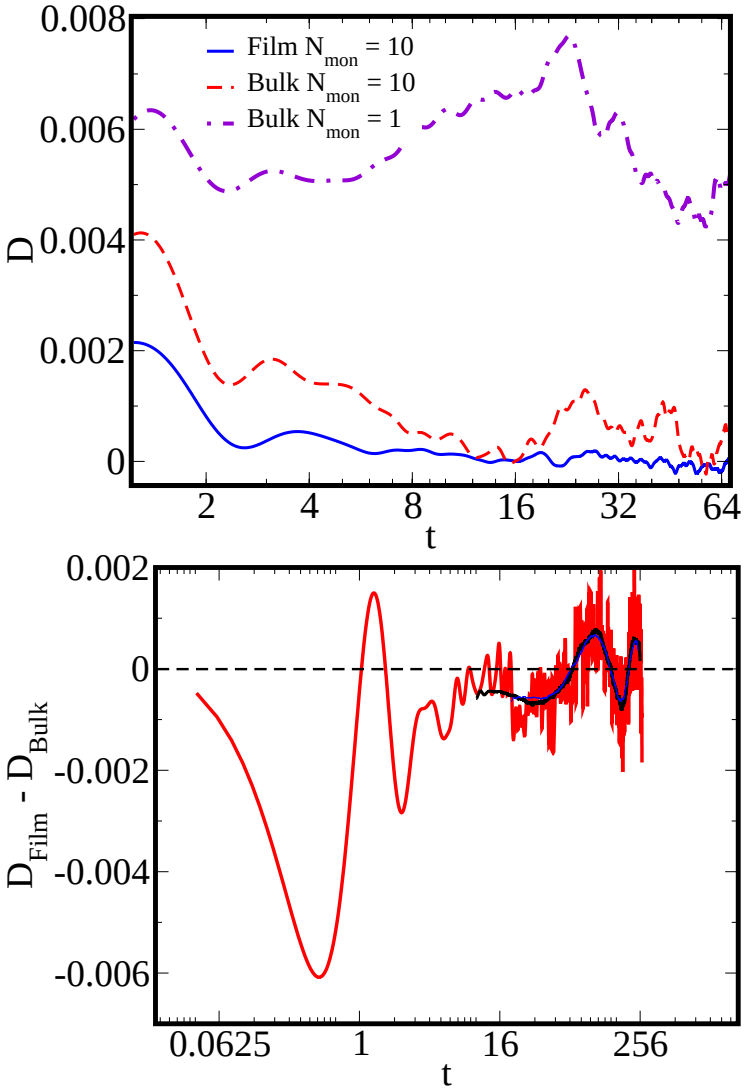

Figure B.1: Difference of the Self diffusion coefficient as a function of time of the particle in bulk and on the polymer film, with $N = 10$. In the first panel the different diffusion functions are shown; in the panel below the difference of the diffusion coefficients in bulk and to film is shown. In short and intermediary times there is no convergence of D_{bulk} to D_{film}; this result shows the influence of interfacial effects in short time regimes. In long times an oscillation around zero is observed (but with lot of statistical errors).

regimes, $\Delta D(t)$ fluctuates around zero. In this case, an improvement of the statistics is neccesary.

The test done with a simple liquid shows that at intermediary times this coefficient is bigger than the previous computed coefficients. Thus the complexity of the fluid as well as the presence of the particle at the interface (only for small temperatures and intermediary times) has influence on the diffusion of the particle.

C Method for the computation of the shear module using the time dependent diffusion coefficient

C.1 Relation between $D(t)$ and VCF

In the long time limit the integral of the VCF, $D_{VCF}(t)$, converges to the time derivative of the MSD, $D_{MSD}(t)$, and the convergence value is equal to the self diffusion constant. Such constant is a functional of the viscosity of the system. From the results of the present simulations there is accurate information for both $D_{VCF}(t)$ and $D_{MSD}(t)$. The idea is to use both expressions for the computation of the shear modulus in the philosophy of microrheology.

The intermediary times of both functions represents the intermediary time of a function that depends of a non constant viscosity. The expression leading to the diffusion coefficient can be expressed as

$$\lim_{t\to\infty} D(t) = \frac{1}{d}\left[\int_0^t \phi(t\prime)dt\prime + \int_t^\infty \phi(t\prime)dt\prime\right], \tag{C.1}$$

where $D(t)$ is a time dependent function that determines the diffusion coefficient and d is the dimension of the system; in the simulations there is a finite computation time where $D(t_a) \to D$, i.e.

$$\int_t^{t_a} \phi(t\prime)dt\prime = D, \tag{C.2}$$

so, applying the Laplace transform in the first equation it is necessary to make the computation of the VCF using the time dependent diffusion coefficient:

$$\phi(s) = dsD(s) - dD. \tag{C.3}$$

The Laplace transform can be expressed as a Fourier transform, in such a way that the previous expression for the VCF can be writen as

$$D(\omega) = -i\omega\frac{1}{d}\phi(\omega) - i\omega D \tag{C.4}$$

and hence:

$$\phi(\omega) = d\omega D(\omega) - dD. \tag{C.5}$$

Any expression in the frequency domain can be expressed as the superposition of a real and imaginary part. So the function related to the diffusion coefficient can be expressed as

$$D(\omega) = D(\omega) - iIm[D(\omega)], \tag{C.6}$$

Using this expression, the real part of the VCF in frequency domain is given by

$$\Re[\phi(\omega)] = d\omega Im[D(\omega)] - dD, \tag{C.7}$$

and the imaginary part can be expressed as:

$$\Im[\phi(\omega)] = d\omega Re[D(\omega)]. \tag{C.8}$$

As both $D_{VCF}(t)$and $D_{MSD}(t)$ converges in some time regime then

$$\Re[\phi(\omega)] = d\omega Im[D_{VCF}(\omega)] - dD_{VCF} \approx d\omega Im[D_{MSD}(\omega)] - dD_{MSD} \tag{C.9}$$

$$\Im[\phi(\omega)] = d\omega Re[D_{VCF}(\omega)] = d\omega Re[D_{MSD}(\omega)] \tag{C.10}$$

this result shows two alternative ways to make the computation of the shear module using the VCF.

C.2 Computation of the viscosity

Using the Stokes-Einstein law it is possible to express the viscosity in the liquid as a function of the diffusion coefficient as

$$\eta = \lim_{t\to\infty} \frac{k_B T}{6\pi D(t) R_{part}}. \tag{C.11}$$

The objection to use this expression for the computation of the frequency dependent viscosity is that the Stokes-Einstein relation is only valid for very long times. But this expression, together with the equivalence of both the memory function of the VCF and of the viscosity in bulk, is just the starting point for any measurement in microrheology [44] (somewhere else it was shown that $G^*_{Diff}(s) = \eta_0 = \frac{1}{4\pi R}\frac{k_B T}{s\Delta r^2}$). Therefore it is imperative to express the Fourier transform of this expression in the following way

$$F[\eta](\omega) = \frac{k_B T}{6\pi R_{part}} F[(D(t))^{-1}](\omega) \tag{C.12}$$

and hence the shear modulus as:

$$G(\omega) = i\omega F[\eta](\omega) \tag{C.13}$$

In repeated computations, using the conventional methods for microrheology, where a Laplace transform is involved, has shown inaccuracy: the introduction of two transformations in the analysis is probably related with the appearance of numerical imprecisions So, the real part of the shear modulus can be expressed as

$$G\prime(\omega) = -\omega Im[F[\eta](\omega)] = -\omega \frac{k_B T}{6\pi R_{part}} Im[F[(D(t))^{-1}](\omega)] \tag{C.14}$$

and the imaginary part is given by

$$G"(\omega) = -\omega Re[F[\eta](\omega)] = -\omega \frac{k_B T}{6\pi R_{part}} Re[F[(D(t))^{-1}](\omega)], \tag{C.15}$$

Due that in the present simulation there is enough information of $D(t)$, and $D^{-1}(t)$ has no singularity, it is allowed to use this function in the place of the VCF in order to compute the shear modulus.

D Rouse modes

The fundamental idea behind the Rouse model is the solution of the equations of motion of a system composed of beads and springs. The equation governing such system is similar to the Langevin equation and has the following form

$$\frac{\partial \overrightarrow{R}_n}{\partial t} = \sum_m H_{mn} \left(-\frac{\partial U}{\partial \overrightarrow{R}_m} + \overrightarrow{f}_m \right) + \frac{1}{2} k_B T \sum_m \frac{\partial}{\partial \overrightarrow{R}_m} H_{mn}, \tag{D.1}$$

where U is the potential between the beads defined as:

$$U = \frac{3k_B T}{2b^2} \sum_{n=2}^{N} \left(\overrightarrow{R_n} - \overrightarrow{R_{n-1}} \right)^2, \tag{D.2}$$

and $H_{mn} = \frac{g_{mn}}{\xi}$ is the mobility matrix and R_n represents the position of the n'th bead. From these positions it is possible to make the following definitions: The mean square of the end-to end distance is defined as

$$R_e = \left\langle (r_N - r_1)^2 \right\rangle, \tag{D.3}$$

and the gyration Radius as

$$R_G = \frac{1}{N} \sum_{i=1}^{N} \left\langle (r_i - R_{CM})^2 \right\rangle; \tag{D.4}$$

moreover the mean square displacement of the center of mass is

$$\left\langle (R_G(t) - R_G(0))^2 \right\rangle = 6 \frac{k_B T}{N\zeta} t. \tag{D.5}$$

Considering:

$$P(t) = R_N(t) - R_0(t), \tag{D.6}$$

the end to end vector one can derive

$$\langle P(t) P(0) \rangle = N b^2 \sum_{p=1,2..} \frac{8}{p^2 \pi^2} e^{-\frac{t p^2}{\tau_1}}, \tag{D.7}$$

where the relaxation time is given by

$$\tau_1 = \frac{\zeta N^2 b^2}{3\pi^2 k_B T} \tag{D.8}$$

A basic assumption of the Rouse model is that every monomer experiences a local random force which is Gaussian distributed. If $R = r_i(t) - r_j(0)$ represent the displacement of two particles, then R is also Gaussian distributed. Such displacements can be expressed using the Rouse modes, given by

$$X_p = \frac{1}{N}\sum_{i=1}^{N} r_i(t) \cos\left[\frac{p\pi(i-1/2)}{N}\right], \tag{D.9}$$

where p denotes the mode index. In the present work the rouse modes were analyzed and it is shown that the modes correlation functions are orthogonal,

$$\langle X_p(t) X_q(t)\rangle = \delta_{pq} \tag{D.10}$$

using this characteristic we are able to make the computation of the displacements of the monomers.

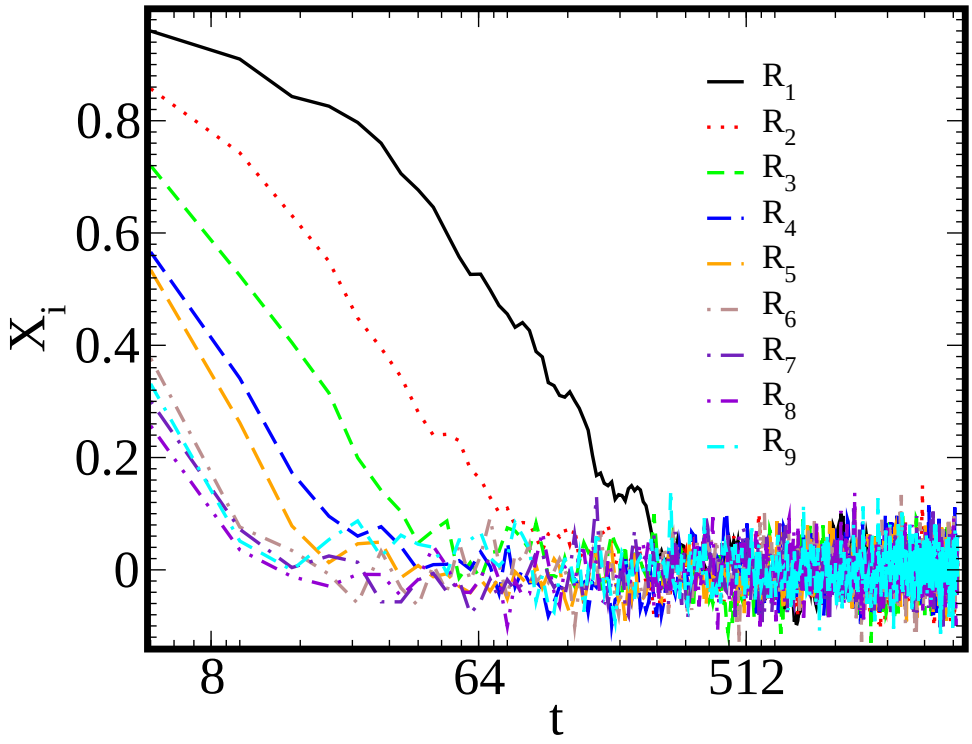

Figure D.1: Rouse modes for a polymer melt with $N_p = 2250$ and $N = 10$. The temperature of this system is $T = 0.8$.

$(\overrightarrow{r}_1, \overrightarrow{r}_2, ...)$ the position of the beads; moreover, using this modes, it is possible to get an uncoupled differential equation by making a transformation of the equation

(D.1) for $\overrightarrow{r}_1$into an equation for $X_p(t)$. The mean square amplitude of each mode is given by

$$\left\langle X_p^2(t)\right\rangle = \frac{b^2}{4\sin^2(p\pi/2N)}, \tag{D.11}$$

and the relaxation function is given by

$$\langle X_p(t)X_q(0)\rangle = \left\langle X_p^2(t)\right\rangle e^{t/\tau_p}, \tag{D.12}$$

where

$$\tau_p = \frac{12kT}{\zeta b^2}\sin^2\left(\frac{p\pi}{2N}\right) \tag{D.13}$$

for long chains and small mode number $\tau_p \sim (N/p)^2$. In fig. D.1 the Rouse modes for a film consisting of $N_p = 2250$ monomers, each chain with $N = 10$, are shown.

E Formulation of the Navier Stokes equations in cylindrical coordinates with rotational symmetry

The equations for the hydrostatics describe an equilibrium between the pressure of the liquid and the force induced by an external field. If such a field is represented by a potential ϕ the following equation is obtained

$$\nabla_i P = -\rho \nabla_i \phi. \tag{E.1}$$

Using this formula we get the following expressions for the divergence of the stress tensors is obtained

$$\nabla_r t^{rr} = -\nabla_r g^{rr} \delta P - \rho \nabla_r g^{rr} \delta \phi, \tag{E.2}$$

$$\nabla_z t^{zz} = -\nabla_z g^{zz} \delta P - \rho \nabla_z g^{zz} \delta \phi; \tag{E.3}$$

These formulas express the diagonal elements of the stress tensor, which are related to the external force and the pressure in the liquid.

The viscosity tensor is related to the strain rate. Implicitly, it was included a compressional stress in addition to shear. This tensor must be invariant under rotation or translation of the reference frame, implying isotropy of the stress. If $p^b_a = \partial_a v^b$, then the stress tensor can be written as a sum of p^{ab} in the following way[1]

$$p^{ab} = \frac{1}{2}\left(p^{ab} + p^{ba}\right) + \frac{1}{2}\left(p^{ab} - p^{ba}\right), \tag{E.4}$$

where the second term is related to a rigid body rotation (or vorticity). For an incompressible fluid this viscosity tensor is given only in terms of the symmetrical combinations of g^{ab} [2]

$$t^{rz} = -\eta\left[\nabla_r g^{rr} \delta v^z + \nabla_z g^{zz} \delta v^r\right], \tag{E.5}$$

[1] Landau, Lehrbuch der Theoretischen Physik VI [32]

[2] See for example Rothman and Zalensky. In this case it is supposed that the metric tensor is self symmetric [79].

where $g^{rr} = g^{zz} = 1$ and η is the shear viscosity.

The general formula for the divergence of the Viscous-stress tensor - with zero compressibility- in tree dimensions is

$$\sum_{j=1}^{3} \frac{\partial t^{ij}}{\partial x^j} = \sum_{j=1}^{3} \frac{\partial}{\partial x^j} \left[\frac{\partial v^i}{\partial x^j} + \frac{\partial v^j}{\partial x^i} \right] = \Delta v^i + \frac{\partial \left(\nabla_j \cdot v^j \right)}{\partial x^i} = \Delta v^i, \tag{E.6}$$

where Δ is the Laplacian operator on a vector field, which can be expressed in cylindrical coordinates in the following way

$$\nabla_r t^{rz} = -\eta \left[\nabla_r^2 \delta v^r + \nabla_z^2 \delta v^r \right], \tag{E.7}$$

$$\nabla_z t^{rz} = -\eta \left[\nabla_r^2 \delta v^z + \nabla_z^2 \delta v^z \right]. \tag{E.8}$$

Combining all the equations (E.5), (E.7) and (E.8), the following Navier Stokes equations for the velocity fields with shear viscosity are obtained

$$\begin{aligned} \rho \partial_t \delta v^r &= \nabla_r t^{rr} + \nabla_z t^{rz} \\ &= -\nabla_r \delta P - \rho \nabla_r \left(\frac{\partial \phi}{\partial d} \right) \delta d - \eta \Delta \delta v^r, \end{aligned} \tag{E.9}$$

$$\begin{aligned} \rho \partial_t \delta v^z &= \nabla_z t^{zz} + \nabla_r t^{rz} \\ &= -\nabla_z \delta P - \rho \nabla_z \left(\frac{\partial \phi}{\partial d} \right) \delta d - \eta \Delta \delta v^z. \end{aligned} \tag{E.10}$$

these equations are valid for incompressible fluids.

F Differential operators and cylindrical coordinates

F.1 Appendix 5-2: Laplacian in cylindrical coordinates

In cylindrical coordinates the vector Laplacian has the following form [1]:

$$\Delta\left(v^r, v^\theta, v^z\right) = \begin{bmatrix} \frac{\partial^2 v^r}{\partial r^2} + \frac{1}{r^2}\frac{\partial^2 v^r}{\partial \theta^2} + \frac{\partial^2 v^r}{\partial z^2} + \frac{1}{r}\frac{\partial v^r}{\partial r} - \frac{2}{r^2}\frac{\partial v^\theta}{\partial \theta} - \frac{v^r}{r^2} \\ \frac{\partial^2 v^\theta}{\partial r^2} + \frac{1}{r^2}\frac{\partial^2 v^\theta}{\partial \theta^2} + \frac{\partial^2 v^\theta}{\partial z^2} + \frac{1}{r}\frac{\partial v^\theta}{\partial r} + \frac{2}{r^2}\frac{\partial v^r}{\partial \theta} - \frac{v^\theta}{r^2} \\ \frac{\partial^2 v^z}{\partial r^2} + \frac{1}{r^2}\frac{\partial^2 v^z}{\partial \theta^2} + \frac{\partial^2 v^z}{\partial z^2} + \frac{1}{r}\frac{\partial v^z}{\partial r} \end{bmatrix} \tag{F.1}$$

This expression, derived from the differential geometry [87], is applied along this work for the expression of the differential operators in the NS equations.

F.2 Main operations with Bessel functions

The solution of the NS equations is in the present solutions based on the concept of eigenfunctions. In particular the Bessel functions are eigenfunctions of differential operators, i.e. the gradient and the Laplacian. In this short appendix this fundamental characteristic is shown:

$$\nabla_r^2 J_1(mr)\widehat{e_r} = \left[\frac{\partial^2 J_1(mr)}{\partial r^2} + \frac{1}{r}\frac{\partial J_1(mr)}{\partial r} - \frac{J_1(mr)}{r^2}\right]\widehat{e_r} = -m^2 J_1(mr)\widehat{e_r} \tag{F.2}$$

$$\nabla_z^2 J_0(mr)\widehat{e_z} = \left[\frac{\partial^2 J_0(mr)}{\partial r^2} + \frac{1}{r}\frac{\partial J_0(mr)}{\partial r}\right]\widehat{e_z} = -m^2 J_0(mr)\widehat{e_z} \tag{F.3}$$

$$\nabla_r J_1(mr)\widehat{e_r} = \frac{1}{r}\partial_r r J_1(mr)\widehat{e_r} = m J_0(mr) \tag{F.4}$$

$$\partial_r J_0(mr) = -m J_1(mr) \tag{F.5}$$

[1] In this case the Laplacian must be refereed to a covariant derivative For general operations in cylindrical coordinates [95] [87]

G Determination of the coefficients B_{nm} for the expansion in Fourier-Bessel-Fourier series for $\left(\frac{\partial \phi}{\partial d}\right)$ assuming a flat interface

The variation of the potential ϕ is a function of the derivative of the external function with respect to the distance d. In the present case, there is also a small perturbation of the potential which is related to the potential of the particle. Therefore, the expansion must only be done for the potential of the particle. Along this work it is considered that the particle interacts through a LJ potential with the liquid. Such a potential can be defined as

$$\widehat{\phi\prime} = \frac{-12\left(d-\frac{z}{2\pi}\right)\overline{\sigma}^{12}}{\left(\left(d-\frac{z}{\pi}\right)^2+r^2\right)^7} + \frac{6\left(d-\frac{z}{2\pi}\right)\overline{\sigma}^{6}}{\left(\left(d-\frac{z}{\pi}\right)^2+r^2\right)^4}. \tag{G.1}$$

This potential can be expanded in a Fourier-Bessel-Fourier series; this implies

$$\widehat{\phi\prime} = \sum_{n;m} B_{nm}\sin(nz)J_0(mr), \tag{G.2}$$

where $n = 1, 2, 3, ...$ and $m = 1, 2, 3, ...$

In the present case

$$B_{nm} = \frac{1}{\pi}\int_0^{2\pi} B_{0m}(z)\sin(nz)dz, \tag{G.3}$$

are the coefficients for the Fourier series. In this case $B_{0m}(z)$ are the coefficients calculated from the Fourier-Bessel series. [1] The integral over r has an infinite domain; it ables us to write the Fourier-Bessel coefficients as Hankel-transforms, which are defined as

[1] See "Advanced Engineering Mathematics", Kryzig, [89] for a complete discussion of the mathematical properties of this series.

$$B_{0m}(z) = \int_0^\infty \widehat{\phi\prime} J_0(mr) r dr. \tag{G.4}$$

The original description for a Hankel transform is: [2]

$$H_\nu[f(r); m] = \int_0^\infty f(r) J_\upsilon(mr)(mr)^{\frac{1}{2}} dr. \tag{G.5}$$

Thus, in this point the problem is to find the right formula that could give the equivalence between the integral and the Hankel transformation. If there is an equivalence, and the Hankel transform is known, one has resolved this integral.

The strategy used is to redefine the potential in convenient functions and rewrite this integrals as known formulas. The potential is in general a sum of functions of the form

$$\varpi_1(\overline{r}, \overline{z}) = a\left(a^2 + r^2\right)^{-7} \overline{\sigma}^{12}, \tag{G.6}$$

$$\varpi_2(\overline{r}, \overline{z}) = a\left(a^2 + r^2\right)^{-3} \overline{\sigma}^{6}, \tag{G.7}$$

where

$$a = \left(d - \frac{z}{\pi}\right), \tag{G.8}$$

such that

$$\widehat{\phi\prime} = -12\varpi_1(r, z) + 6\varpi_2(r, z). \tag{G.9}$$

The solution of the integral for the coefficients is thus reduced to the numerical evaluation of the two integrals

$$b_{0m}(z)_1 = \int_0^\infty \varpi_1 J_0(mr) r dr, \tag{G.10}$$

$$b_{0m}(z)_2 = \int_0^\infty \varpi_2 J_0(mr) r dr \tag{G.11}$$

This integral can be solved as a Hankel transform if and only if the function $f(r)$ is expressed as

$$f_1(r) = a\left(a^2 + r^2\right)^{-\mu\prime_1} r^{\frac{1}{2}}, \tag{G.12}$$

$$f_2(\overline{r}) = a\left(a^2 + r^2\right)^{-\mu\prime_2} r^{\frac{1}{2}}. \tag{G.13}$$

[2] The definition of the following Hankel Transformations is taken from "The Bateman Project". [91]

Thus

$$b_{0m}(\overline{z})_1 = \int_0^\infty \varpi_1(r,z) J_0(mr) r dr = \frac{1}{\sqrt[2]{m}} H_0[f_1(r);m], \tag{G.14}$$

$$b_{0m}(\overline{z})_2 = \int_0^\infty \varpi_2(r,z) J_0(mr) r dr = \frac{1}{\sqrt[2]{m}} H_0[f_2(r);m], \tag{G.15}$$

Following the 'Bateman project' [91] it is possible to write

$$H_\nu[a\left(a^2+r^2\right)^{-\mu-1}\overline{r}^{\frac{1}{2}};m] = \frac{a^{\nu-\mu+1}m^{\mu+\frac{1}{2}}K_{\nu-\mu}(am)}{2^\mu\Gamma(\mu+1)}, \tag{G.16}$$

where $\mu\prime = \mu + 1$ and $K_{\nu-\mu}$ is the modified Bessel function. This formula is valid only if

$$\Re(a) > 0, \tag{G.17}$$

and

$$-1 < \Re(\nu) < 2\Re(\mu) + \frac{3}{2}. \tag{G.18}$$

In the previous equations $\Re(a)$ symbolizes the real part of a.

In this case $\nu = 0$. For $\mu = 3$ are obtained

$$H_0[a\left(a^2+\overline{r}^2\right)^{-4}\overline{r}^{\frac{1}{2}};m] = \frac{a^{-2}m^{3+\frac{1}{2}}K_{-3}(am)\overline{\sigma}^6}{8\Gamma(4)}. \tag{G.19}$$

For $\mu = 6$

$$H_0[a\left(a^2+\overline{r}^2\right)^{-7}\overline{r}^{\frac{1}{2}};m] = \frac{a^{-5}m^{6+\frac{1}{2}}K_{-6}(am)\overline{\sigma}^{12}}{2^6\Gamma(7)}; \tag{G.20}$$

since[3]

$$K_{-\nu}(w) = K_\nu(w), \tag{G.21}$$

it is allowed to write

$$H_0[a\left(a^2+\overline{r}^2\right)^{-4}\overline{r}^{\frac{1}{2}};m] = -\frac{a^{-2}m^{3+\frac{1}{2}}K_3(am)\overline{\sigma}^6}{8\Gamma(4)}, \tag{G.22}$$

$$H_0[a\left(a^2+\overline{r}^2\right)^{-7}\overline{r}^{\frac{1}{2}};m] = -\frac{a^{-5}m^{6+\frac{1}{2}}K_6(am)\overline{\sigma}^{12}}{2^6\Gamma(7)}. \tag{G.23}$$

Here it importnat to make the reconstruction of the formula for the coefficients of

[3]This property can be observed in Abramowitz and Stegun [90]

the potential. The relation between the coefficients and the Hankel transformations is

$$b_{0m}(\overline{z})_1 = \frac{1}{\sqrt[2]{m}} H_0[f_1(\overline{r}); m], \tag{G.24}$$

$$b_{0m}(\overline{z})_2 = \frac{1}{\sqrt[2]{m}} H_0[f_2(\overline{r}); m], \tag{G.25}$$

and from both formulas it is essential to rewrite the expansion coefficient as

$$\begin{aligned} B_{0m}(\overline{z}) &= -12 b_{0m}(\overline{z})_1 + 6 b_{0m}(\overline{z})_2 \\ &= 12 \frac{a^{-5} m^6 K_6(am) \overline{\sigma}^{12}}{2^6 \Gamma(7)} - 6 \frac{a^{-2} m^{3+\frac{1}{2}} K_3(am) \overline{\sigma}^6}{8\Gamma(4)}. \end{aligned} \tag{G.26}$$

The integral over z is between the substrate and the interface, with a position H_Γ on z axis, where H_Γ represents the film thickness. This thickness is independent of the coordinates for a flat interface. Thus

$$B_{nm} = \frac{1}{\pi} \int_0^{2\pi} \left[12 \frac{a^{-4} m^6 K_6(am) \overline{\sigma}^{12}}{2^6 \Gamma(7)} - 6 \frac{a^{-2} m^{3+\frac{1}{2}} K_3(am) \overline{\sigma}^6}{8\Gamma(4)} \right] \sin(nz) dz. \tag{G.27}$$

This integral is not analytic and can be solved with numerical methods. But the tarjet is to have a closed analytical formula for this transformation. For this reason an alternative function with the same chape as the -modified- LJ potential was used in chapter 5.

H Solutions of the NS equations for an incompressible fluid

The present system is axisymmetric around the position of the particle above the film; moreover the liquid in this first approximation has a constant density. This condition for incompressibility implies

$$\nabla_r \delta v^r + \nabla_z \delta v^z = 0. \tag{5}$$

In the former case the velocity fields are very small, such that the Navier stokes equations are reduced in to the following equations [32]

$$\rho \partial_t \delta v^r = -\nabla_r \delta P - \rho \nabla_r \left(\frac{\partial \phi}{\partial d} \right) \delta d + \eta \left[\nabla_r^2 \delta v^r + \nabla_z^2 \delta v^r \right], \tag{6-a}$$

for the r component of the velocity field, and

$$\rho \partial_t \delta v^z = -\nabla_z \delta P - \rho \nabla_z \left(\frac{\partial \phi}{\partial d} \right) \delta d + \eta \left[\nabla_r^2 \delta v^z + \nabla_z^2 \delta v^z \right], \tag{6-b}$$

for the component z of the corresponding field.

Using the definition of the Laplacian in cylindrical coordinates and taking in account that the velocities in the fluid are symmetric on z, one can rewrite the linear Navier-Stokes equation in cylindrical coordinates for the corresponding fields as [79]

$$\partial_{\overline{t}} v^r = \partial_{\overline{r}} \overline{P} - \varepsilon_c \partial_{\overline{r}} \widehat{\phi \prime} \overline{\delta d} + K_\eta \left[\frac{1}{\overline{r}} \partial_{\overline{r}} \left(\overline{r} \partial_{\overline{r}} v^r \right) - \frac{v^r}{\overline{r}^2} + \pi^2 \frac{\partial^2 v^r}{\partial \overline{z}^2} \right], \tag{H.1}$$

$$\partial_t v^z = \pi \partial_{\overline{z}} P - \pi \varepsilon_c \partial_{\overline{z}} \phi \prime \delta d + K_\eta \left[\frac{1}{r} \partial_r \left(r \partial_r v^z \right) + \pi^2 \frac{\partial^2 v^z}{\partial z^2} \right]. \tag{H.2}$$

Since this equation is linear, the sum of two or more individual solutions is also a solution. That permit us to write the solution as a sum of harmonic solutions.

From this frontier conditions and the from of the differential equations the solution for v^i as well as P can be expressed thus as a Fourier-Bessel-Fourier series in r and z.

$$v^r = \sum_{n,m} f_{nm}(t) \cos(nz) J_1(mr), \tag{H.3}$$

$$v^z = \sum_{n,m} g_{nm}(t)\sin(nz)J_0(mr), \tag{H.4}$$

$$\delta P = \sum_{n,m} A_{nm}(t)\cos(nz)J_0(mr), \tag{H.5}$$

$$\widehat{\phi\prime} = \sum_{n,m} B_{nm}(t)\cos(nz)J_0(mr). \tag{H.6}$$

Using the last ansatz for the potential

$$\partial_{\overline{r}}\phi\prime = -\sum_{n;m} mB_{nm}\cos(nz)J_1(mr), \tag{H.7}$$

$$\partial_z\phi\prime = -\sum_{n;m} nB_{nm}\sin(nz)J_0(mr). \tag{H.8}$$

The Laplacian of the solutions for the velocities gives:

$$\Delta v^r = -(m^2+\pi^2n^2)v^r, \tag{H.9}$$

$$\Delta v^z = -(m^2+\pi^2n^2)v^z, \tag{H.10}$$

More over using the condition $\nabla_{\overline{r}}v^r = -\nabla_{\overline{z}}v^z$ and from the incompressibility the following identity is obtained

$$mf_{mn}(\overline{t}) = ng_{nm}(\overline{t}) \tag{H.11}$$

Inserting this last condition and the proposed solutions into the Navier Stokes equations one obtains the following equations in the time

$$\frac{df_{mn}(t)}{dt} = mA_{nm}(t) + m\varepsilon_c B_{nm}\overline{H_0}\sin(\omega t) + K_\eta(m^2+\pi^2n^2)f_{nm}(t), \tag{H.12}$$

$$\frac{m}{n}\frac{df_{mn}(t)}{dt} = \pi nA_{nm}(t) + \pi n\varepsilon_c B_{nm}\overline{H_0}\sin(\omega\overline{t}) + K_\eta(m^2+\pi^2n^2)\frac{m}{n}f_{nm}(t). \tag{H.13}$$

Both equations, after some algebraic manipulation, can be reduced into a single one if

$$A_{nm}(t) = -B_{nm}\varepsilon_c\overline{H_0}\sin(t). \tag{H.14}$$

That means that the small perturbations in the pressure are in mechanical equilibrium with the small perturbations in the potential. Replacing this equation in the equation one gets a differential equation in time for the function $f(t)$

$$\frac{df_{mn}(t)}{dt} = -(\pi^2 n^2 + m^2) K_\eta f_{nm}(t) \tag{H.15}$$

with the following solution

$$f_{nm}(t) = e^{-\tau_{nm} t} \tag{H.16}$$

f_0 is given by the initial conditions. The field at $t = 0$ is $f_{nm}(t = 0) = 0$. Then the solution for the time dependent part of the field $f_{nm}(\overline{t})$ is trivial!

This last result shows that the approximation of the liquid film into an incompressible one does not allow the transmission of mechanical load into the liquid. For this reason it is necessary to consider compressible fluids.

I Table of conversions

The solutions given in chapter 5 are given in LJ units. In this short appendix some typical unitis for polymer liquids and the conversion in LJ unities are given [88]. In the present case the energy unit is the strength of the LJ potential ϵ_0 and the distance unit σ is the radius of a single monomer. The main convertion of unities are

$$1Pa = N/m^2 \tag{I.1}$$

$$1N = J/m \tag{I.2}$$

$$1Pa = J/m^3 \tag{I.3}$$

For the pressent problem the following convertions of energy, force, distance, pressure in LJ unities can be maid (All unities taked from the handbook of polymers, IFF school about soft condensed matter)

$$1J = 6.03 \times 10^{20}\varepsilon, \tag{I.4}$$

$$1N = 6.03 \times 10^{11}\varepsilon/\sigma, \tag{I.5}$$

$$1m = 1 \times 10^{9}\sigma, \tag{I.6}$$

$$1Pa = 6.03 \times 10^{-7}\varepsilon/\sigma^3. \tag{I.7}$$

The surface tension of a typical polymer film is [83]

$$\gamma_\Gamma = 0.01N/m = 6.03\varepsilon/\sigma^2, \tag{I.8}$$

the typicall dynamic viscosity for a polymer is

$$K_\eta = 10^6 MPa, \tag{I.9}$$

which can be expressed as

$$K_\eta = 1 \times 10^{12}Pa = 7.53 \times 10^5\varepsilon/\sigma^3. \tag{I.10}$$

On the other hand the bulk viscosity is given by

$$k_\xi = \frac{1}{2(1+\nu)}E. \tag{I.11}$$

and the isothermal coefficient by

$$k_T = \frac{1}{3(2\nu-1)}E, \tag{I.12}$$

where E is the Young modulus. For typical polymers

$$\nu = 0.3, \tag{I.13}$$

and

$$E = 1MPa. \tag{I.14}$$

Therefore

$$K_\xi = \frac{1}{8}MPa = 7.53 \times 10^{-2}\varepsilon/\sigma^3, \tag{I.15}$$

$$K_T = \frac{1}{15}MPa = 4.03 \times 10^{-2}\varepsilon/\sigma^3, \tag{I.16}$$

and the isothermal bulk modulus in the liquid film is

$$C_T = \frac{k_\xi}{P_0} = 3.3 \times 10^{-3}\varepsilon/\sigma^3. \tag{I.17}$$

For the computation of the solutions in the chapter 5 all the coordinates are normilized to the film thickness H_0.

J Solutions of the NS equations for complex fluids in the frequency domain

J.1 Non-Newtonian fluids: Maxwell model.

J.1.1 Viscoelastic fluids

In the viscoelastic fluids the stress tensor has some dependence on a memory function, that means, very slow relaxation process take place in the system. One possible way to model such relaxation process is through the so called generalized Maxwell model: here the pressure tensor is related to the composition of a strain tensor with a function describing a relaxation process:

$$T^{ij} = \int G\left(t - t'\right) \overset{\bullet}{\Upsilon}{}^{ij} d\tau, \tag{J.1}$$

where $\overset{\bullet}{\Upsilon}{}^{ij}$ is the derivative strain tensor with the time, and $G\left(t - t'\right)$ is the memory function. This function is related to the strain tensor in the following way [78] [84]

$$\overset{\bullet}{\Upsilon}{}^{ij} = \nabla_i \nabla_j \delta v^i(r_i, \tau). \tag{J.2}$$

In the linear Maxwell model the memory function can be expressed as an exponential function

$$T^{ij} = \sum_k \int_{-\infty}^{t} \frac{\eta_k}{\lambda_k} e^{-(t-\tau)\lambda_k} \overset{\bullet}{\Upsilon}{}^{ij}(r_i, \tau) d\tau, \tag{J.3}$$

where τ is the relaxation time. In this case, the viscosity is not constant any more and is the result of the integration over the relaxation modulus [86]. Moreover the sum is infinite allowing an infinite spectrum of relaxation times and viscosities. The previous expression represents a convolution of the strain with the relaxation function; in a general form this means

$$T^{ij} = e^{t\lambda_k} \otimes \overset{\bullet}{\Upsilon}{}^{ij}(r_i, \tau). \tag{J.4}$$

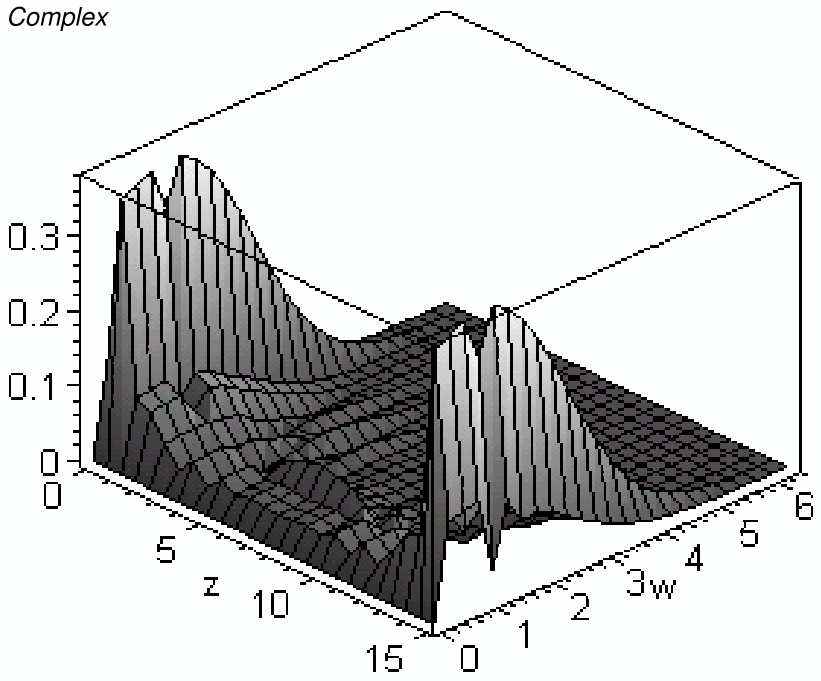

Figure J.1: Magnitude of the total velocity in the complex liquid film as a function of z and ω, the frequency of perturbation. This magnitude was computed for $r \to 0$, i.e. under the nanoparticle. It is allowed to observe the characteristic oscillation of the pressure in the bulk, together with the peaks of pressure at the interfaces substrate-liquid and liquid-vapor.

In the present calculation only few relaxation times are considered; this simplifies the sum to only few terms.

J.2 Solution of the linear hydrodynamics for non-Newtonian liquids

The Maxwell model for complex fluids is based on a convolution of the strain tensor with a function expressing the relaxation of the fluid. The Fourier transform of a convolution is

$$F[f(t) \otimes g(t)] = F[\int_{-\infty}^{\infty} f(t-\tau)g(\tau)d\tau] = F[f(t)]F[g(t)]. \tag{J.5}$$

A Fourier transform is performed in order to find a solution of the NS equations. In

this sense it is also neccesary to make a Fourier transform of the Maxwell formula for viscoelastic fluids

$$F[\sum_k \int_{-\infty}^{\infty} \frac{\eta_k}{\lambda_k} e^{-(t-\tau)\lambda_k} \overset{\bullet}{\Upsilon}^{ij}(r_i,\tau)d\tau] = \sum_k \frac{\eta_k}{\lambda_k} F[e^{-\lambda_k t}] * F[\overset{\bullet}{\Upsilon}^{ij}(r_i,t)]. \quad \text{(J.6)}$$

Therefore the Fourier transform of the stress tensor is in this case

$$T^{ij}(\omega,r,z) = -\frac{1}{2\pi^2}\left[\frac{\lambda_k}{\omega^2+(\lambda_k/2\pi)^2}\right]\overset{\bullet}{\Upsilon}^{ij}(r,z,\omega); \quad \text{(J.7)}$$

as effect of this transformation a viscosity is obtained that depends on the internal relaxation times of the complex fluid and in the frequency: $K_\eta \rightarrow K(\lambda_k,\omega)$

$$K_\eta = -\frac{1}{2\pi^2}\left[\frac{\lambda_k}{\omega^2+(\lambda_k/2\pi)^2}\right]; \quad \text{(J.8)}$$

this condition implies that K_η is replaced for $K(\lambda_k,\omega)$. In this sense it is convenient to express the solutions of the NS equations in a frequency space, rather than time space. This option allows to make a direct comparison with experiments performed also in frequency space. The definition of this memory function is only one of many possible definitions that can be explored using the previous solutions.

Other alternative approaches could express the complex relaxation processes in the liquid; but in this work the representation of the complex fluid is restricted to the Maxwell model. In fig. J.1 and fig. J.2 the solutions of the velocities in the frequency domain (Fourier space) are plotted, when the system has a Gaussian perturbation and the nanoparticle has contact with the fluid. This value was computed under the nanoparticle. Such kind of perturbation implies sensitivity for low frequencies. In the simple liquid it is necessary to observe fast dissipation of the velocity as a function of the frequency, whereas the complex fluid preserves a complex velocity patron for $\omega > 0$. For $\omega \rightarrow \infty$ the velocity tends to zero .The proper frequency of the system was $\omega_0 = 1.0$ in LJ units.

J.2.1 solution in the frequency space

The matrix equation (5.35) can be rewritten as a vectorial one

$$\frac{d}{d\overline{t}}\overrightarrow{A}_{fl}(t) = \widehat{M_p}\overrightarrow{A}_{fl}(t) + \overrightarrow{\Omega}_{ex}(t), \quad \text{(J.9)}$$

with:

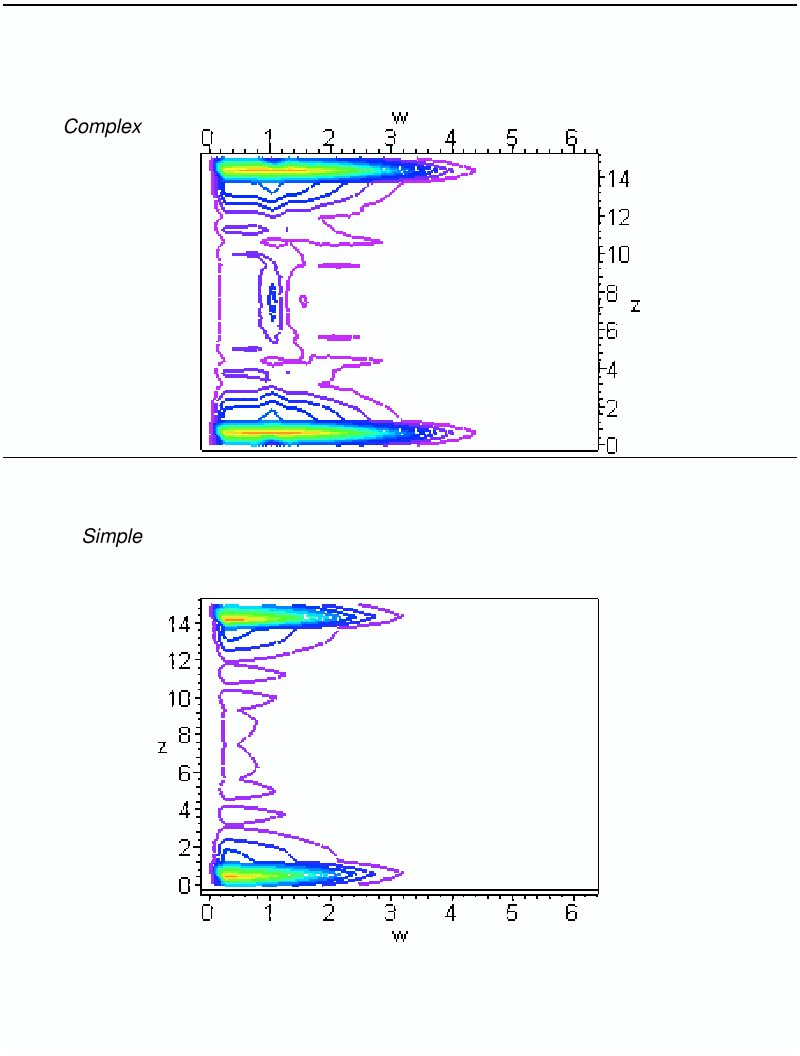

Figure J.2: Total velocity of a complex and simple compressible liquid as a function of z and of the frequency ω under Gaussian perturbation and tapping mode. In the first panel the magnitude of the velocity is shown; in the two panels a comparison of the velocity profiles for the complex and the simple liquids is shown. From this plots it is evident the fast relaxation of the velocity in the simple liquid. With a Gaussian perturbation the liquid has no sensitivity at high frequencies; for $\omega > 0$ there is a persistence of the velocity at both interfaces of the liquid film.

$$\overrightarrow{A}_{fl}(t) = \begin{pmatrix} A_{nm}(\overline{t}) \\ g_{nm}(\overline{t}) \\ f_{nm}(\overline{t}) \end{pmatrix}, \tag{J.10}$$

$$\widehat{M}_p = \begin{pmatrix} 0 & -C_T\pi n & -C_T m \\ \pi n & -B_2 & -\pi n m K_\zeta \\ m & -\pi n m K_\zeta & -B_1 \end{pmatrix}, \tag{J.11}$$

$$\overrightarrow{\Omega}_{ex}(t) = \begin{pmatrix} 0 \\ \pi n \varepsilon_c B_{nm} \overline{H_0} \sin(\omega_c \bar{t}) \\ m \varepsilon_c B_{nm} \overline{H_0} \sin(\omega_c \bar{t}) \end{pmatrix}. \tag{J.12}$$

Applying the Fourier transform on the vectorial differential equation yields the following algebraic equation

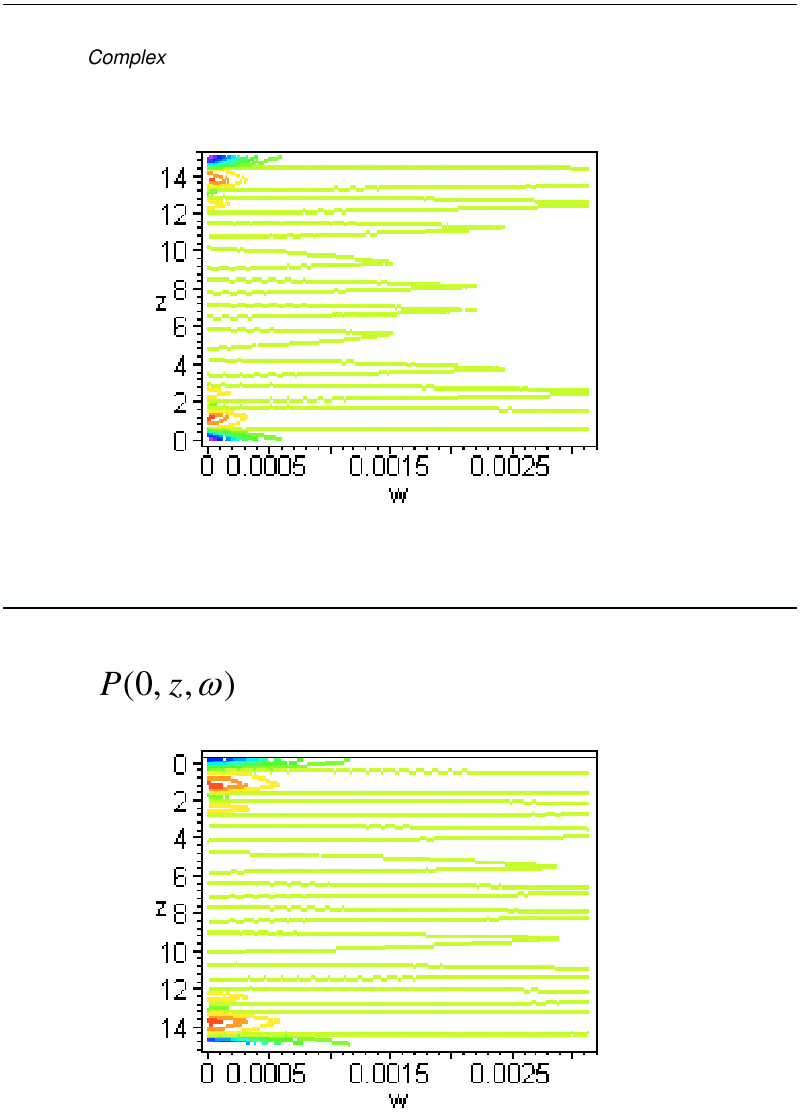

Figure J.3: Pressure profile in the Fourier space: in the first panel the pressure function for a complex fluid is presented, whereas in the second panel the pressure for a simple liquid is show. Both profiles are functions of ω and z and were computed for $r = 0$, i.e. under the particle. Given that the fluid is incompressible it is imperative to say that the pressure fluctuations correspond to density fluctuations. For $\omega \sim> 0$ there is some persistence of density fluctuations for the simple liquid in bulk. In comparison with this result, the density fluctuations in the complex fluid slows in the bulk agreement with the frequency grow. For $\omega \to \infty$, $Pr \to 0$.

$$i\omega \overrightarrow{A}_{fl}(\omega) = \widehat{M_p} \overrightarrow{A}_{fl}(\omega) + \overrightarrow{\Omega}_{ex}(\omega), \tag{J.13}$$

and solving for $\overrightarrow{A}_{fl}(\omega)$ the following expression is obtained

$$\overrightarrow{A}_{fl}(\omega) = \left(\widehat{I}i\omega - \widehat{M_p}\right)^{-1} \overrightarrow{\Omega}_{ex}(\omega), \tag{J.14}$$

The function $\left(\widehat{I}i\omega - \widehat{M_p}\right)$ matrix is 3×3 and its inverse can be easily computed by conventional methods. This matrix is a functional of both the shear and bulk viscosities, which are explained in the section 4 of this chapter; its solution makes possible to introduce the Maxwell expression for both viscosities and find the solutions of the dynamics of a complex fluid in frequency domain.[1] The corresponding results will be discussed in the section called 'results'.

[1] In such calculations it is introduced a Gaussian perturbation with the form

$$F[e^{-\omega_1 t^2}](\omega) = \sqrt{\frac{\pi}{\omega_1}} e^{-\pi^2\omega^2/\omega_1}, \tag{J.15}$$

where ω_1 is the proper perturbation frequency.

Bibliography

[1] Mamin J. H., Terris B. D., Fan L. S. , Hoen S., Barret R.C., Rugar D. *High density data storage using proximal probe techniques* IBM Journal of research and development, **39**, 6 (1995)

[2] Wangsness R. *Introductory topics in theoretical physics* John Wiley and Sons. (1963)

[3] Stewart P. S., Costerton B. *How biofils form and how to attack them*, Scientific Ammerican, July (2001)

[4] Stoodley P. *Biofilms: does signaling really matter?* Center of Biofilm Engineering, News Update, Vol. 5, 9 (2002)

[5] news.bbc.co.uk/1/hi/sci/tech/4421867.stm

[6] http://www-lmr.usc.edu/ lmr

[7] Smolin L. *Matrix models and non-local hidden veriables theories* 'Quovdis Quantum mechanics', Springer (2005)

[8] http://microfluids.engin.brown.edu

[9] Giessbl F.J. *Forces and shifts in the atomic resolution dynamic force mycroscopy*, Phys. Rev. B, **54**, Nr 24, pp.56 (1997.)

[10] Chaterji A., Horbach J. *Combining Molecular Dynamics with Lattice-Boltzmann: A Hybrid Method for the Simulation of (Charged) Colloidal Systems* cond-mat/0505276

[11] Resch R., Bugacov A., Baur C., Madhukar A., Koeal B.E., Requicha A.A.G., P.Will *Manipulation of nanoparticles using dynamic force microscopy: simulation and experiments*, Appl. Phys. A, **67**, 265-271 (1998)

[12] Milchev , Binder K. *Nanodroplets adsorbed on nanocylinders: a montecarlo study* J. Chem. Phys. **117**, 6852 (2002)

[13] Rapaport D. C. *The art of molecular dynamics simulation*, Cambridge University press (1995)

[14] Aichele M. *Simulation studies of correlation functions and relaxation in polymeric systems*, Dissertation, Mainz, (2004)

[15] Müller M. *Personal comunication*

[16] Müller M. and Macdowell L. *Wetting of polymer liquids: Montecarlo simulations and self consistent field calculations*, J. Phys.Condens. Matter, **15**, 610, (2003)

[17] Kremer K., Grest S. *Dynamics of entagled lynear polymer melts: A molecular-dynamics simulation*, J. Chem. Phys., **92**, 5057 (1990)

[18] Benneman C., Paul W., Binder K., Dünweg B. *Molecular dynamics simulations of the thermal glass transition in polymer melts: α relaxation behavior*, Phys. Rev. E., **57**, 843 (1998).

[19] Frenkel D., Smit B. *Understanding molecular simulation*, Academic Press, (1996)

[20] Haile J. M. *Molecular dynamics simulations: elementary methods*, John Wiley and sons. (1992)

[21] Sedgewick R. *Algorithms in C*, Addison Wesley (1990)

[22] Press W., Flannery B. P., Teukolsky S. A., Vetterling W. T. *Nummerical recipes*, Cambridge University press (1989)

[23] Allen M. P. *Introduction to molecular dynamics simulation*, Winter school, computational soft matter: from syntetic polymers to proteins (2004)

[24] Kremer K. *Computer simulations in soft matter science* 33 IFF Ferienkurs 'Soft matter:complex materials in mesoscopic scales' (2002)

[25] Baschnagel J., Wittmer P. J., Meyer H. *Montecarlo simulations of polymers: coarse grained models* Winterschool, computational soft matter: from syntetic polymers to proteins (2004)

[26] Binder K. *Montecarlo and molecular dynamics simulations of amorphous polymers* Computational modeling of polymers, Marcel Dekker inc. (1992)

[27] Binder K. *Personal comunication*

[28] Dünweg B *Advanced simulations for hydrodynamic problems: Lattice Boltzman and dissipative particle dynamics* Winterschool, computational soft matter: from syntetic polymers to proteins (2004)

[29] Rasmusen S., Smith J. *Lattice polymer automata* Ber. Bunsenges. Phys. Chem. **98**, 1185 (1994)

[30] Boon, Yip S. *Molecular Hydrodynamics*, Dover (1991)

[31] Feynman R., *Lectures on Physics, Vol II*,

[32] Landau L. *Theoretische Physik (Vol VI)*, Akademie Verlag, Berlin (1974)

[33] Paul W., Baschnagel G. *Stochastic process* Springer Verlag (1999)

[34] Haken H. *Synergetics: an introduction*, Springer Verlag (1983)

[35] Mason T.G., Weitz D.A. *Optical measurement of frequency-Dependent Linear Viscoelastic Moduli of complex fluids*, Phys. Rev. Lett. **74**, 1250 (1995)

[36] Dünweg B., personal conversation.

[37] Einstein A. *Über die von molecularkinnetischen Theorie der Wärme geforderte Bewegung von in ruhenden Flüssigkeiten suspendierten Teilchen* Ann. d. Physik **17**, 549 (1905)

[38] Saxton M. J. *Single particle tracking: effects of corrals* Biophys. J. **69**, 389 (1995).

[39] Qian Biophis Journal, **79**, 137 (2009)

[40] Gellman M. *The Quark and the Jaguar* Tus Quets (1995)

[41] Martin J., Rakotomala N, Salin D. *Hydrodynamics dispersion of non colloidal suspensions: Measurement from Einstein's argument* Phys. Rev. Lett **74**, pp 1347 (1995)

[42] Zwanzig R. *Non equilibrium Statistical Mechanics*, Oxford University Press, (1983)

[43] van Zanten J.H., Rufender, K.P. *Brownian motion in single relaxation time maxwell fluid*, Phis. Rev. E **62**, 5389 (2000)

[44] Mason T.G., Ganesan K., van Zanten J.H., Wirz D., Kuo S.C. *Particle tracking microrheology of complex fluids* Phys. Rev. Lett. **79**, 3282 (1997)

[45] Varnik F., personal conversation.

[46] Kob W. *The Mode coupling theory of the glass transition*

[47] Moreno A. J., Kob W. *Dynamics of a rigidrod in a glassy medium*, Europhysics Lett. (Preprint)

[48] Abdulwahab S. A., Sholl D. S., *Brownian dynamics study of polymer-Stabilized Nanoparticles*, Nanothecnology, preprint (2004)

[49] Lewis L.J., Wanström G., *Molecular Dynamics of supercooled ortho-therphenil*, Phys. Rev. E **50**, 3865 (1994)

[50] Gisler T., Weitz D.A. *Scaling of the Microrheology of semidilute F-Actin solutions*, Phys. Re. Lett. **82**, 1606 (1999)

[51] Horbach J. Kob W., Binder K., Angell A. A. *Finite size effects in simulations of glass dynamics*, Phys. Rev. E **54**, 5897 (1996)

[52] Schnurr D., Gittes F., MacKintosh F.C, Schmidt C.F. *Determining microscopic viscoelasticity in flexible and semiflexible polymer networks from thermal fluctuations*, Macromol., **30**, 7781 (1997).

[53] Levine A. J., Lubensky T. C., *One and two particle microrheology*, Phys. Rev. Lett **85**, 1774 (2000)

[54] Byutner O., Smith G. D., *Prediction of the Linear viscoelastic shear modulus of an entangled polybutadiene melts from simulation and theory*, Macromol **34**, 134 (2001)

[55] Raganathan S. *Binary collisions in fluids: II: velocity autocorrelation function* Can. J. Phys. **61**, 1655 (1983)

[56] Cohen E.D.G. *Fifty years of kinetik theory* Physica A **194**, 229 (1993)

[57] Gittes F., Mackintosh *Dynamic shear modulus of semiflexible polymer network* Phys. Rev. E **58**, 1241 (1997)

[58] Doi M., Edwards S. F. *The theory of polymer dynamics* Claredon Press, Oxford (1989)

[59] Paul W. Personal conversation.

[60] Lipowski R., Gomper G., *Interface delocalization transitions in finite systems*, Phys. Rev. B, **29**, 5213 (1984)

[61] Bartsch H. J *Mathematische Formeln* Buch und Zeit Verlagsgessellschaft (1969)

[62] de Gennes P. G. *Wetting: statistics and dynamics*, Rev. of Mod. Phys. **57**, 827 (1985)

[63] Vergeles M., Szamel G. *A theory for self diffusion in liquids* J. Chem. Phys. **110**, 3009 (1990)

[64] Leegwater J. A. *Velocity autocorrelation function of lennar jones fluids* J. Chem Phys., **94**, 7402 (1991)

[65] Becker J., Grün G., Seeman R., Mantz H., Jacobs K., Mecke K. R., Blossey R. *Complex dewetting scenarios captured by thin film models*, Nature Materials, **2**, 59, (2003)

[66] Ansari A., *Langevin modes analysis of myoglobin*, J. Chem. Phys., **110**, 1774 (1999)

[67] Weber R., Grottkopp I., Stettner J., Tolan M., Press W. *Embedding of gold nanoclusters on polyestyrene surfaces: the surface modification on the glass transition*, Macromol. **36**, 9100 (2003)

[68] Lipowski R., Gompper G. *Interface delocalization transitions in finite systems*, Phys. Rev. B. **29**, 5213 (1983)

[69] Gelfand M., Lipowski R. *Wetting on cylinders and spheres*, Phys. Rev. B **36**, 8725 (1987)

[70] Zaporojtchenko V., Strunkus T., Erichsen J., Faupel F., *Embedding of noble metal Nanoclusters into polymers as a potential probe of the surface glass transition*, Macromol **34**, 1125 (2001)

[71] Goldenfeld N. *Lectures on phase transitions and the renormalization group* Perseus Books (1992)

[72] Perry A. *Personal conversation*

[73] Santer S., Rühe J. *Motion of nano objects on polymer brushes* Polymer **45**, 8279 (2004)

[74] huntchenson S. A., Mckenna G. B. *Nanosphere embedding into polymer surfaces: a viscoelastic contact analysis* Phys. Rev. Lett. **94**, 075103 (2005)

[75] Teichoeb J. H., Forrest J. A. *Direct imaging of nanoparticle embedding to probe viscoelasticity of olymer surfaces* Phys. Rev. Lett. **91**, 016104 (2003)

[76] Meinhold-Heerlein L. *Surface conditions for the liquid vapor system, taking into account entropy production caused by mass and energy transport across the interface*, Phys. Rev. A **8**, 2574 (1973)

[77] Roters A., Johannsman D., *Distance dependent noise measureme nts in scaning force microscopy*, J. Phys.: Condens. Matter **8**, 7561 (1996)

[78] Byrd R. B., Curtiss C. F., Armstrong R. C., Hassanger O. *Dynamics of polymeric liquids, Vol I and II* Whyley-interscience (1987)

[79] Rothman D. H., Zaleski S. *Lattice-Gas Cellular Automata (simple models of complex Hydrodynamics)* Cambridge University Press (1997)

[80] Varnik F. *Molekulardynamik simulationen zum Glasübergang in Makromolekularen Filmen*, Dissertation (2000)

[81] Paul W. *Eigenschaften eines Helium II-Films unter dem Einfluss verschiedenartiger Wärmeströme*, Diplomarbeit (1986)

[82] Pleiner H. *Komplexe fluide- ein überblick* 28 IFF Ferienkurs 1997, Dynamik und strukturbildung in kondensierter materie (1997)

[83] Seek O. H. *Capillary wave on polymer thin films* 33 IFF Ferienkurs, 'Soft matter: complex materials in mesoscopic materials' (2002)

[84] Zimmerman N. *Hydrodynamics of complex fluids* 33 IFF Ferienkurs, 'Soft matter: complex materials in mesoscopic materials' (2002)

[85] Gomper G. *Statistical mechanics of membranes* 33 IFF Ferienkurs, 'Soft matter: complex materials in mesoscopic materials' (2002)

[86] Rathgeber S. *Some topics about rheology* 33 IFF Ferienkurs, 'Soft matter: complex materials in mesoscopic materials' (2002)

[87] Tolman R. C. *Relativity, thermodynamics and cosmology* Oxford university press (1934)

[88] Alger M.S.M. *Polymer science dictionary* Elsevier (1990)

[89] Kreyszig E. *Advanced engineering mathematics* Wiley (1964)

[90] Abramowitz M., Stegun I. A. *Handbook of mathematical functions* Dover (1965)

[91] Bateman M. *Higher Transcendental Functions*

[92] *Drainage of a thin liquid film confined between hydrophobic surfaces* Langmuir, **11**, 2213 (1995)

[93] Perez R., Payne M. *Role of covalent Tip surface interactions in noncontact atomic force microscopy on reactive surfaces* , Phys. Rev. Lett **78**, 678 (1997)

[94] Weisstein *Scienceworld.com* http://scienceworld.wolfram.com/physics/

[95] *Mathworld* http://mathworld.wolfram.com

[96] *Elementos del calculo tensorial* Lichnerowitz, Salvat (1962)